SOLVING SIMPLE QUANTUM SYSTEMS USING BOOTSTRAPPING

A THESIS SUBMITTED TO
THE GRADUATE SCHOOL OF NATURAL AND APPLIED SCIENCES
OF
MIDDLE EAST TECHNICAL UNIVERSITY

BY

ALI ULVI NOHUTÇU

IN PARTIAL FULFILLMENT OF THE REQUIREMENTS
FOR
THE DEGREE OF MASTER OF SCIENCE
IN
PHYSICS

AUGUST 2024

Approval of the thesis:

SOLVING SIMPLE QUANTUM SYSTEMS USING BOOTSTRAPPING

submitted by **ALI ULVI NOHUTÇU** in partial fulfillment of the requirements for the degree of **Master of Science in Physics Department, Middle East Technical University** by,

Prof. Dr. Naci Emre Altun
Dean, Graduate School of **Natural and Applied Sciences** _____

Prof. Dr. Seçkin Kürkcüoğlu
Head of Department, **Physics** _____

Assoc. Prof. Dr. Yusuf İpekoğlu
Supervisor, **Physics, METU** _____

Examining Committee Members:

Prof. Dr. Sadi Turgut
Physics, METU _____

Assoc. Prof. Dr. Yusuf İpekoğlu
Physics, METU _____

Prof. Dr. Tahmasib Aliyev
Mathematics, Hacettepe University _____

Prof. Dr. İsmet Yurduşen
Physics, METU _____

Prof. Dr. Seçkin Kürkcüoğlu
Physics, METU _____

Date:22.08.2024

I hereby declare that all information in this document has been obtained and presented in accordance with academic rules and ethical conduct. I also declare that, as required by these rules and conduct, I have fully cited and referenced all material and results that are not original to this work.

Name, Surname: Ali Ulvi Nohutçu

Signature :

ABSTRACT

SOLVING SIMPLE QUANTUM SYSTEMS USING BOOTSTRAPPING

Nohutçu, Ali Ulvi
M.S., Department of Physics
Supervisor: Assoc. Prof. Dr. Yusuf İpekoğlu

August 2024, 106 pages

In this thesis, we investigate the application of the bootstrap method, which is a numerical approach for identifying energy eigenstates in quantum systems developed in a series of recent articles in the literature, to solve several quantum mechanical systems. First, we establish the theoretical background of the bootstrap method, focusing on the Hamburger moment problem and how it can be related to quantum mechanical systems. We obtain the generalized moment recursion relation and discuss the parameters needed to initialize it. We discuss possible problems with the algorithm and offer optimizations that use the bootstrapping method combined with numerical methods. As examples, we apply the method to the Simple Harmonic Oscillator, the Anharmonic Oscillator, and the Hydrogen atom, then compare the results to theoretical values and evaluate the effectiveness of the method.

Keywords: Bootstrap Method, Moment Problems, Simple Harmonic Oscillator, Anharmonic Oscillator, Hydrogen Atom

ÖZ

BASİT KUANTUM SİSTEMLERİN ÖZYÜKSELTİM İLE ÇÖZÜLMESİ

Nohutçu, Ali Ulvi
Yüksek Lisans, Fizik Bölümü
Tez Yöneticisi: Doç. Dr. Yusuf İpekoğlu

Ağustos 2024 , 106 sayfa

Bu tezde, kuantum sistemlerindeki enerji özdurumlarını belirlemeye yönelik, literatürde son dönemde geliştirilen nümerik bir yaklaşım olan Özyükseltim metodunun çeşitli kuantum mekanik sistemlere uygulanması incelenmektedir. İlk olarak, Özyükseltim metodunun teorik temelleri ele alınarak, bu bağlamda, Hamburger moment probleminin kuantum mekanik sistemlerle nasıl ilişkilendirilebileceği gösterildi. Genel moment yineleme ilişkisi elde edilerek, bu ilişkinin başlatılabilmesi için gerekli parametreler tartışıldı. Algoritma ile ilgili olası sorunlar ele alındı ve Özyükseltim metodunu nümerik yöntemlerle birleştirerek iyileştirmeler önerildi. Yöntem, Basit Harmonik Osilatör, Anharmonik Osilatör ve Hidrojen atomuna uygulanarak, sonuçlar teorik değerlerle karşılaştırılarak metodun etkinliği değerlendirildi.

Anahtar Kelimeler: Özyükseltim Metodu, Moment Problemleri, Basit Harmonik Osilatör, Anharmonik Osilatör, Hidrojen Atomu

To whom who have gone, so I have found the motivation to push myself a step further.

ACKNOWLEDGMENTS

I would like to express my sincere appreciation to Seçkin Kürkcüoğlu and Yusuf İpekoğlu for their guidance and support throughout my research. Their feedback and suggestions were crucial in refining my approach to conducting research in physics. I am also grateful to Tahmasib Aliyev for his assistance with any physics related questions that arose during my graduate studies in physics, and for our walks around the campus.

I am thankful to my friend Serkan Kaskan for his encouragement and motivation during the initial stages of my thesis. His support was crucial in helping me stay focused and productive.

I would like to thank TÜBİTAK for providing financial support to me for 2 years through the 2210 – A General Domestic Graduate Grant, which allowed me to pursue my master's education without financial concerns.

Finally, last but not least, during the whole time I have studied physics, I have made promises to many baristas that I would thank them in my acknowledgments once I completed my thesis. So, here is that part where I express my gratitude to countless number of baristas working in numerous different cafes for boosting my motivation for physics through pouring me another cup of coffee.

TABLE OF CONTENTS

LIST OF TABLES

TABLES

LIST OF FIGURES

FIGURES

LIST OF ABBREVIATIONS

1D	1-Dimensional
SDPA	Semidefinite Programming Algorithm
SHO	Simple Harmonic Oscillator
NPD	Non Positive Definite
MSE	Mean Square Error

LIST OF SYMBOLS

$\langle \hat{x}^n \rangle$	Moments
$\mathcal{M}$	Bootstrap Matrix
K	Depth of the Bootstrap
S	Search Space
S^i	Element of the Search Space
S_B	Boundaries of the Search Space
τ_a	Precision of the Bootstrap
K_i	Initial Depth of the Bootstrap
K_f	Final Depth of the Bootstrap
ϵ	Convergence Limit
P_μ	Search Point
I	Search Interval
τ_a'	Increased Precision of the Bootstrap
Γ	Minimum Number of Required Non-Positive Definite Points
ϵ_i	Initial Convergence Limit
Υ	Maximum Value of Mean Squared Error
ρ	Number of Trials for Forced Convergence
$A(r)$	Auxiliary Extrapolation Function
$\tilde{\mathcal{M}}$	Half-Line Bootstrap Matrix
A	Search Area

CHAPTER 1

INTRODUCTION

Bootstrapping techniques were first developed in the 1960s and 1970s [1, 2], in exploring strongly interacting particles and the S-matrix approach, but after that, they received relatively less attention until their revival in recent years. In the past decade or so, these methods have been revived in the context of conformal field theories [3], have been increasingly applied to large N matrix models [4, 5]. Han, Hartnoll, and Kruthoff initiated the application of bootstrapping ideas to quantum mechanics [6], applying the bootstrap method to the Anharmonic Oscillator system which is a polynomial potential, and extending the application to matrix models. Moreover, Berenstein and Hulsey further extended the bootstrap method to the Harmonic Oscillator and the Hydrogen atom, which involve potentials in the form of a polynomial or power function [7]. These studies made bootstrapping quantum mechanics a promising area of research since this approach may prove particularly useful in determining the spectrum of quantum systems that are challenging to solve analytically. The method has been widely applied to Harmonic Oscillators [8, 9], Anharmonic Oscillators [9–12], and Double-Well Potentials [9, 11–14]. The method has also been applied to solve for the spectrum of more complex 1-Dimensional (1D) Schrödinger equations such as periodic potentials [15, 16], Calabi-Yau model [17], Poschl-Teller potential [18] and many more complex systems [14, 19–23].

The bootstrap method has been adapted to accommodate boundary conditions in various 1D quantum mechanical systems [24]. With the integration of Semidefinite Programming Algorithm (SDPA) solvers [25, 26], it has allowed for the precise calculations of the spectrum especially the lower level energy eigenstates and other observables.

In this thesis, we follow the articles [6] and [7] and apply the bootstrap method to the Simple Harmonic Oscillator (SHO), the Hydrogen atom and the Anharmonic Oscillator systems. Our aim is to test the reliability and effectiveness of the bootstrap method in providing accurate results for lower level energy eigenstates and other observables within these quantum systems.

This thesis is organized as follows:

In Chapter 2, we give the theoretical background of the bootstrap method and discuss related numerical algorithms for the application of the method. We will first review the moment problems, specifically focusing on the Hamburger moment problem which covers the real domain $\mathbb{R}$ [27]. We discuss the necessary conditions for a sequence to be called a moment sequence in the Hamburger moment problem and then elaborate on the positivity constraints on the Hankel matrices generated through these moment sequences. We follow this review by relating the moment problem to quantum mechanics in 1D and show that for any Hermitian operator $\hat{\mathcal{O}}$ the sequence generated through the expectation values of powers of $\hat{\mathcal{O}}$ is in fact a moment sequence and the Hankel matrices generated from this moment sequence, are positive semidefinite. Following this, we derive a generalized moment recursion relation which depend on the energy eigenvalues E of any Hamiltonian $\hat{H}$ and discuss the minimum requirements necessary to initialize this recursion relation, which we call the search space. After presenting this theoretical background of the method, we continue with providing a detailed algorithmic structure of the "original bootstrap" algorithm [7] and discuss the possible computational problems that can be addressed with it. We first suggest an optimized version of the algorithm which we call the "one split bootstrap" algorithm. Subsequently, we introduce a new algorithm which we call the "guided bootstrap" algorithm, that works with the bootstrapping method and uses numerical methods to improve the accuracy and reliability of the final results.

In Chapter 3, we apply the bootstrap method to the SHO system, following the footsteps of previous works [7–9]. The SHO system is the simplest example among the systems we study, primarily because its search space contains only a single element, namely the energy, and the system is defined in 1D Cartesian coordinates over the entire domain, $(-\infty, +\infty)$. In this chapter, we first derive the specific moment re-

cursion relation for the SHO and then explore the corresponding search space. We proceed by showing examples of how the bootstrap matrix is constructed for this system through detailed examples. Finally, we apply the original bootstrap algorithm, the one split bootstrap algorithm, and the guided bootstrap algorithm to the system, to analyze how these methods perform in obtaining the lower energy eigenstates and qualitatively discuss the applicability of these algorithms to potentials with unknown energy spectra.

In Chapter 4, we apply the bootstrap method to the Hydrogen atom, following the works of Berenstein and Hulsey in [7, 24]. The Hydrogen atom system is one of the most important examples to demonstrate the usefulness of the bootstrap method. Unlike the SHO system, the potential in the Hydrogen atom is a power function defined on the half-line $\mathbb{R}_+$, allowing us to analyze how the method operates in a different domain. To handle the change in the domain of the problem we introduce the Stieltjes moment problem [27] where we discuss the necessary conditions for a sequence to be called a moment sequence on the half-line and then discuss the positivity constraints over the Hankel matrices generated through these moment sequences. Another reason the Hydrogen problem is an important example is due to the centrifugal barrier term, within the effective potential, which we must consider when deriving the recursion relation for the problem. In this chapter, we first derive the generalized recursion relation for spherically symmetric potentials, which we then use to derive the specific recursion relation for the Hydrogen atom system. We proceed by discussing the search space for the system, demonstrating that the obtained recursion relation can be initiated using only an initial prediction space for the energy of the system. Finally, we apply the original bootstrap algorithm, the one split bootstrap algorithm, and the guided bootstrap algorithm to evaluate their effectiveness in determining the lower energy eigenstates, particularly for different values of the angular momentum quantum number ℓ.

In Chapter 5, we apply the bootstrap method to the Anharmonic Oscillator system

$$V(\hat{x}) = \hat{x}^2 + \lambda \hat{x}^4, \tag{1.0.1}$$

following the previous studies in [9–12]. Unlike the SHO and Hydrogen atom systems, the Anharmonic Oscillator has two elements in its search space, making it a

more suitable example for us to examine how the method performs with search spaces with more than one element. In this chapter, we first derive the specific moment recursion relation for the Anharmonic Oscillator. We keep the coupling constant λ in the recursion relation so that we can analyze how the bootstrap method performs with the varying values of the coupling constant λ. Finally, we apply the original bootstrap algorithm, to the system, to analyze how the bootstrap method performs in obtaining the lower energy eigenstates of a system with more than one element in its search space, and how the results get affected for different values of the coupling constant.

CHAPTER 2

METHOD

2.1 Definitions

We focus our investigations on 1D systems with polynomial potentials therefore in the most general case, the Hamiltonian for these system can be written as

$$\hat{H} = \frac{\hat{p}^2}{2m} + V(\hat{x}) \tag{2.1.1}$$

where $V(\hat{x})$ is a polynomial in $\hat{x}$.

Most generally we seek to determine the solutions of the time independent Schrödinger equation defined as

$$\hat{H}|\psi\rangle = E|\psi\rangle. \tag{2.1.2}$$

Through out this thesis we will use $m = 1$, $\hbar = 1$ so; then equation (2.1.1) becomes

$$\hat{H} = \frac{1}{2}\hat{p}^2 + V(\hat{x}), \tag{2.1.3}$$

where the operators $\hat{x}$ and $\hat{p}$ are defined in the configuration space as

$$\hat{x} = x\,, \quad \hat{p} = -i\partial_x. \tag{2.1.4}$$

The canonical commutation relations between the operators $\hat{x}$ and $\hat{p}$ are given as usual

$$[\hat{x}, \hat{p}] = i\,, \quad [\hat{x}^n, \hat{x}^m] = 0\,, \quad [\hat{p}^n, \hat{p}^m] = 0. \tag{2.1.5}$$

where $n, m \in \mathbb{Z}_+$.

During our calculations we also make frequent use of the following expression [28]

$$[F(\hat{x}), \hat{p}] = iF'(\hat{x}), \tag{2.1.6}$$

where F' denotes the derivative of F with respect to its argument. A simple derivation for this expression can be shown as

$$\begin{aligned}
[F(\hat{x}), \hat{p}]\phi(x) &= F(\hat{x})\left(\hat{p}\phi(x)\right) - \hat{p}\left(F(\hat{x})\phi(x)\right), \\
&= F(\hat{x})\left((-i\partial_x)\phi(x)\right) - (-i\partial_x)\left(F(\hat{x})\phi(x)\right), \\
&= -iF(\hat{x})\left(\partial_x\phi(x)\right) + i(\partial_x)\left(F(\hat{x})\phi(x)\right), \\
&= -iF(\hat{x})\left(\partial_x\phi(x)\right) + iF(\hat{x})\left(\partial_x\phi(x)\right) + i\phi(x)\left(\partial_x F(\hat{x})\right), \\
&= i\partial_x F(\hat{x})\phi(x), \\
&= iF'(\hat{x})\phi(x).
\end{aligned} \tag{2.1.7}$$

2.2 The Moment Problem

In this thesis, we are going to make use of ideas from the so called theory of "moment problem" [29] to formulate the bootstrap method for 1D quantum mechanics problems. Mainly, there are three types of moment problems, which are the Hamburger moment problem, which investigates the domain $\mathbb{R}$, the Stieltjes moment problem which investigates the domain $\mathbb{R}_+$ and the Hausdorff moment problem which investigates the domain $(0, 1)$ [27]. We want to establish the bootstrap method over the entire domain $\mathbb{R}$ hence, we ground the theoretical framework of this thesis over the Hamburger moment problem.

Hamburger moment problem searches for a positive integration measure μ on the domain $\mathbb{R}$, given an infinite sequence of real numbers $\{s_n\}$ where $n \geq 0$ that converges and satisfies the integral [29]

$$s_n = \int_{-\infty}^{+\infty} x^n d\mu. \tag{2.2.1}$$

If there exists a measure μ such that $\mu > 0$ then, the real sequence $\{s_n\}$ is called a moment sequence and satisfies the condition explained below:

Let us define some linear functional L on the polynomial algebra $\mathbb{C}[x]$ as

$$L(x^n) = s_n, \tag{2.2.2}$$

and a polynomial $P(x)$ of the form

$$P(x) = \sum_{i=0}^{n} c_i x^i, \tag{2.2.3}$$

where $c_i \in \mathbb{C}$. The Hamburger moment problem states that for a positive integration measure μ and the moment sequence s_n, the functional L satisfies

$$\begin{aligned} L(|P|^2) &= \int P(x)P^*(x)d\mu, \\ &= \int \left(\sum_{i,j=0}^{n} c_i c_j^* x^{i+j} \right) d\mu, \\ &= \sum_{i,j=0}^{n} c_i c_j^* s_{i+j} \geq 0. \end{aligned} \tag{2.2.4}$$

Then we conclude that $L(|P|^2) \geq 0\,, \forall P \in \mathbb{C}[x]$. An $(n+1) \times (n+1)$ Hankel matrix, H_n, generated through $L(|P|^2)$ can be defined as

$$H_n(s) := (s_{i+j}), \tag{2.2.5}$$

where $0 \leq i\,, j \leq n$. From equation (2.2.4) we see that the Hankel matrix $H_n(s)$ is positive semidefinite for each $n \geq 0$. Note also that any Hankel matrix is a symmetric matrix, which is readily observed for H_n given in equation (2.2.5)

An important aspect of the Hamburger moment problem is determining the uniqueness of the measure μ for a given moment sequence s_n. If a measure μ is unique for a moment sequence s_n, the equation

$$\int_{-a}^{a} P(x)d\mu = \int_{-a}^{a} P(x)d\tilde{\mu}, \tag{2.2.6}$$

is satisfied if and only if $\mu = \tilde{\mu}$ on any bounded interval $[a, -a]$, where $a > 0$.

A sufficient criterion to check the uniqueness of μ is the so called "Carleman condition" which states that the integration measure μ is unique if the moment sequence s_n satisfies the relation [29]

$$\sum_{n=1}^{\infty} (s_{2n})^{-\frac{1}{2n}} = +\infty. \tag{2.2.7}$$

We are not going to go into the details of this as it is not necessary to do so for our purposes. However, interested readers may consult [29].

2.3 Bootstrapping Quantum Mechanics

To apply the Hamburger moment problem techniques to quantum mechanics, we start by assuming any Hermitian operator $\hat{\mathcal{O}}$ defined as a polynomial in $\mathbb{C}[x]$ as

$$\hat{\mathcal{O}} = \sum_n c_n \hat{\mathcal{O}}_n, \tag{2.3.1}$$

where $n \geq 0$. We choose the real sequence s_n to be the expectation values of the Hermitian operators $\hat{\mathcal{O}}_n$ where the expectation value is calculated over an energy eigenket $|\psi\rangle$ defined as

$$\begin{aligned} \langle \hat{\mathcal{O}}_n \rangle &= \langle \psi | \hat{\mathcal{O}}_n | \psi \rangle, \\ &= \int \psi^* \hat{\mathcal{O}}_n \psi dx, \end{aligned} \tag{2.3.2}$$

and provide sufficient conditions for the existence of an integral measure $\mu > 0$ so that $s_n := \langle \hat{\mathcal{O}}_n \rangle$ is in fact a moment sequence and the Hankel matrix H_n generated through the expectation values of $\hat{\mathcal{O}}$ is positive semidefinite.

In this thesis, we are only interested in applying the bootstrap method to 1D quantum mechanical problems with potentials in the form of a polynomial and therefore, we focus our attention to operators of the form

$$\hat{\mathcal{O}} \sim \hat{x}^n, \tag{2.3.3}$$

the reasons for which will become evident as we proceed. (In Chapter 4, we will generalize these ideas to Hydrogen atom problem, by exploiting the rotational symmetry of the problem). It is worth noting that other choices of operators $\hat{\mathcal{O}}$ can be applied in different systems with various potentials, which the examples can be found in [15–17, 19].

Since all expectation values of hermitian operators are real, $\langle \hat{x}^n \rangle$ form a real and infinite sequence as

$$s_n := \{ \langle \hat{x}^n \rangle \}. \tag{2.3.4}$$

Then the moment problem given in equation (2.2.1) becomes

$$\begin{aligned} s_n &= \int_{-\infty}^{+\infty} x^n d\mu, \\ &= \int_{-\infty}^{+\infty} \psi^* \hat{x}^n \psi dx, \\ &= \int_{-\infty}^{+\infty} |\psi|^2 \hat{x}^n dx = \langle \hat{x}^n \rangle, \end{aligned} \tag{2.3.5}$$

so the differential on integration measure μ is given as

$$d\mu = |\psi|^2 dx. \tag{2.3.6}$$

If we integrate equation (2.3.6) we obtain

$$\mu = \int |\psi|^2 dx, \tag{2.3.7}$$

which is a norm in Hilbert space, this imposes two important conditions on μ as

$$0 \leq \mu = \int |\psi|^2 dx < \infty. \tag{2.3.8}$$

Therefore, we conclude that there exists a finite and positive real valued integration measure μ that satisfies the equation (2.2.1) for the real sequence $\{\langle \hat{x}^n \rangle\}$, thereby confirming that the sequence is indeed a moment sequence. From this point on, we will call the expectation values of the powers of the position operator $\langle \hat{x}^n \rangle$ as "moments".

If we check the uniqueness of the integration measure μ through the equation (2.2.7) we have

$$\sum_{n=1}^{\infty} \left(\int_{-\infty}^{+\infty} |\psi|^2 \hat{x}^{2n} dx \right)^{-\frac{1}{2n}}, \tag{2.3.9}$$

which is dependent on the characteristic behaviour of the wave function, thereby preventing a direct proof of uniqueness. A typical, bound state wave function decays sufficiently fast as $x \to \infty$, causing $\langle \hat{x}^{2n} \rangle$ to increase slowly as $n \to \infty$, possibly resulting in the summation above to diverge to $+\infty$ [24]. Therefore, we expect that the integration measure μ is unique [4, 7].

Since the infinite set generated through $\langle \hat{x}^n \rangle$ form a moment sequence they should satisfy the identity obtained in equation (2.2.4) and the Hankel matrix H_n defined

in equation (2.2.5) should be positive semidefinite. We will call the Hankel matrix H_n generated through the moment sequence $\{\langle\hat{x}^n\rangle\}$ as the "bootstrap matrix" and denote it as $\mathcal{M}$. The dimension of the bootstrap matrix will be called the "depth of the bootstrap" and will be denoted as K. We have

$$K = n + 1. \tag{2.3.10}$$

The elements of the bootstrap matrix $\mathcal{M}$ are given by

$$\mathcal{M}_{ij} = \langle\hat{x}^{i+j}\rangle, \tag{2.3.11}$$

where $0 \leq i\,, j \leq K-1$ and the matrix $\mathcal{M}$ at depth K is

$$\mathcal{M} := \begin{bmatrix} \langle\hat{x}^0\rangle & \langle\hat{x}\rangle & \langle\hat{x}^2\rangle & \cdots & \langle\hat{x}^{K-1}\rangle \\ \langle\hat{x}\rangle & \langle\hat{x}^2\rangle & \langle\hat{x}^3\rangle & \cdots & \langle\hat{x}^{K}\rangle \\ \langle\hat{x}^2\rangle & \langle\hat{x}^3\rangle & \langle\hat{x}^4\rangle & \cdots & \langle\hat{x}^{K+1}\rangle \\ \vdots & \vdots & \vdots & \ddots & \vdots \\ \langle\hat{x}^{K-1}\rangle & \langle\hat{x}^{K}\rangle & \langle\hat{x}^{K+1}\rangle & \cdots & \langle\hat{x}^{2K-2}\rangle \end{bmatrix}. \tag{2.3.12}$$

The generated matrix $\mathcal{M}$ is symmetric, $\mathcal{M}^T = \mathcal{M}$, as expected for all Hankel matrices.

We also note that the operator $\hat{x}^0$ is the identity operator $\mathbb{1}$. Then

$$\begin{aligned} \langle\psi|\hat{x}^0|\phi\rangle &= \langle\psi|\mathbb{1}|\phi\rangle, \\ &= \langle\psi|\phi\rangle, \\ &= \delta_{\psi\phi}. \end{aligned} \tag{2.3.13}$$

Then for the energy eigenket $|\psi\rangle$ we have

$$\langle\hat{x}^0\rangle = 1. \tag{2.3.14}$$

The fundamental concept underlying bootstrapping quantum mechanics is based on the bootstrap matrix $\mathcal{M}$ being positive semidefinite. In this thesis, we follow a stronger constraint such that $\mathcal{M}$ is positive definite, which is previously used by Berenstein and Hulsey in [7] to enforce the validity of the moment sequence.

The bootstrap method proceeds as follows. We make some guesses over some initial parameters, which always includes the energy E, to create a minimal search space

and generate the moment sequence $\{\langle \hat{x}^n \rangle\}$ using the dynamical properties for a given Hamiltonian. We construct the bootstrap matrix $\mathcal{M}$ for a given initial depth K, for each point within the minimal search space and check the positive definiteness of $\mathcal{M}$. For the points that yield a positive definite bootstrap matrix, we increase the depth of the bootstrap and generate the next order bootstrap matrix as $K \to (K+1)$. We perform this operation only for the points that yield a positive definite matrix since the matrix with depth K will be a principal submatrix of the higher order bootstrap matrix with depth $K+1$. The fact that the positive definiteness of the higher order bootstrap matrix depends on that of the principal submatrix which can be proven as follows:

Let A be a $K \times K$ Hankel matrix and let B be a $(K+1) \times (K+1)$ Hankel matrix which is formed by adding a row and column to A. The matrix B can be shown as

$$B = \begin{bmatrix} A & v \\ v^T & \alpha \end{bmatrix}, \tag{2.3.15}$$

where v, v^T are K dimensional column and row vectors and α is a real number. For invertible matrices A such that there exists no vanishing eigenvalue ($\lambda = 0$) that satisfies the eigenvalue equation

$$|A - \lambda I| = 0, \tag{2.3.16}$$

the eigenvalues of the matrix B are determined by the characteristic equation [30]

$$\begin{aligned} |B - \lambda I| &= \begin{vmatrix} |A - \lambda I| & v \\ v^T & \alpha - \lambda \end{vmatrix} \\ &= |A - \lambda I| \, (\alpha - \lambda) - v^T v \\ &= |A - \lambda I| \, (\alpha - \lambda - v^T \, |A - \lambda I|^{-1} \, v) \\ &= 0 \end{aligned} \tag{2.3.17}$$

where we have used Schur complement passing from the second line to the third line [30]. Notice that all solutions of the equation in (2.3.16) are also should be the solutions of equation (2.3.17) with a new eigenvalue being generated from the term $(\alpha - \lambda - v^T \, |A - \lambda I|^{-1} \, v)$. Therefore the definiteness property of any matrix B depends on its invertible principle submatrices.

As we increase the order of the bootstrap, only a narrower set of points will yield a positive definite matrix $\mathcal{M}$. Since we expect that the integration measure μ is unique for the moment sequence $\langle \hat{x}^n \rangle$ associated with each Hamiltonian, we also expect these points will successively approach closer to the true observables of the given Hamiltonian.

2.4 Derivation of Moment Recursion

Since we are only interested in the operators $\hat{\mathcal{O}} \sim \hat{x}^t$, we seek to connect the energy eigenstates E to the moments $\langle \hat{x}^t \rangle$ in the form of a recursion relation. For this, we use the identity [6]

$$\langle \hat{\mathcal{O}} \hat{H} \rangle = E \langle \hat{\mathcal{O}} \rangle, \tag{2.4.1}$$

where the expectation value "$\langle\ \rangle$" is taken on energy eigenstate. The proof for the identity is quiet straightforward. The action of the Hamiltonian $\hat{H}$ on an energy eigenket $|\psi_n\rangle$ is given by;

$$\hat{H}|\psi_n\rangle = E_n|\psi_n\rangle, \tag{2.4.2}$$

then, if we evaluate the expression in the the left hand side of the equation (2.4.1), we have

$$\begin{aligned} \langle \psi_n | \hat{\mathcal{O}} \hat{H} | \psi_n \rangle &= \langle \psi_n | \hat{\mathcal{O}} E_n | \psi_n \rangle, \\ &= E_n \langle \psi_n | \hat{\mathcal{O}} | \psi_n \rangle, \\ &= E \langle \hat{\mathcal{O}} \rangle. \end{aligned} \tag{2.4.3}$$

In order not to clutter the notation in what follows, we suppress the subscript n of E_n.

To obtain the anticipated recursion relation; we examine the equation (2.4.1) with the operator $\hat{\mathcal{O}}$ such that; $\hat{\mathcal{O}} = \hat{x}^{t-1}$. Then, we have

$$\begin{aligned} \langle \hat{\mathcal{O}} \hat{H} \rangle &= \langle \hat{x}^{t-1} (\frac{1}{2}\hat{p}^2 + V(\hat{x})) \rangle, \\ &= \langle \frac{1}{2}\hat{x}^{t-1}\hat{p}^2 + \hat{x}^{t-1} V(\hat{x}) \rangle, \\ &= \frac{1}{2}\langle \hat{x}^{t-1}\hat{p}^2 \rangle + \langle \hat{x}^{t-1} V(\hat{x}) \rangle, \\ &= E \langle \hat{\mathcal{O}} \rangle, \\ &= E \langle \hat{x}^{t-1} \rangle. \end{aligned} \tag{2.4.4}$$

Rearranging the terms of the third and fifth lines of the equation (2.4.4) we obtain,

$$E\langle\hat{x}^{t-1}\rangle = \frac{1}{2}\langle\hat{x}^{t-1}\hat{p}^2\rangle + \langle\hat{x}^{t-1}V(\hat{x})\rangle. \tag{2.4.5}$$

Notice that in equation (2.4.5) there is a term $\langle\hat{x}^{t-1}\hat{p}^2\rangle$ which depends on the momentum operator $\hat{p}$. Therefore, we need to find an expression of the form

$$\langle\hat{x}^{t-1}\hat{p}^2\rangle = \sum_t c_t\langle\hat{x}^t\rangle, \tag{2.4.6}$$

where $c_t \in \mathbb{C}$ are constant coefficients to be determined. This form of a mixed operator expectation value can be expressed in terms of position moments by exploiting the identity [6]

$$\langle[\hat{H}, \hat{\mathcal{O}}]\rangle = 0. \tag{2.4.7}$$

A simple proof of this identity can be given as

$$\begin{aligned}\langle[\hat{H}, \hat{\mathcal{O}}]\rangle &= \langle\psi_n|[\hat{H}, \hat{\mathcal{O}}]|\psi_n\rangle, \\ &= \langle\psi_n|\hat{H}\hat{\mathcal{O}} - \hat{\mathcal{O}}\hat{H}|\psi_n\rangle, \\ &= \langle\psi_n|\hat{H}\hat{\mathcal{O}}|\psi_n\rangle - \langle\psi_n|\hat{\mathcal{O}}\hat{H}|\psi_n\rangle,\end{aligned} \tag{2.4.8}$$

where $|\psi_n\rangle$ is the energy eigenstates of the Hamiltonian $\hat{H}$. Then; considering equation (2.4.2) we can also obtain a relation for the action of Hamiltonian $\hat{H}$ over $\langle\psi_n|$ as

$$\langle\psi_n|\hat{H} = \langle\psi_n|\hat{H}^\dagger = (\hat{H}|\psi_n\rangle)^\dagger = E_n\langle\psi_n|, \tag{2.4.9}$$

If we re write equations (2.4.2) and (2.4.9) back into the equation (2.4.8) we obtain

$$\begin{aligned}\langle[\hat{H}, \hat{\mathcal{O}}]\rangle &= E\langle\psi_n|\hat{\mathcal{O}}|\psi_n\rangle - E\langle\psi_n|\hat{\mathcal{O}}|\psi_n\rangle, \\ &= (E - E)\langle\psi_n|\hat{\mathcal{O}}|\psi_n\rangle, \\ &= 0.\end{aligned} \tag{2.4.10}$$

We now evaluate the identity in (2.4.7) for the operator $\hat{\mathcal{O}} = \hat{x}^s$. It reads

$$\begin{aligned}
\langle[\hat{H}, \hat{\mathcal{O}}]\rangle &= \langle[\hat{H}, \hat{x}^s]\rangle, \\
&= \langle[\frac{1}{2}\hat{p}^2 + V(\hat{x}), \hat{x}^s]\rangle, \\
&= \frac{1}{2}\langle[\hat{p}^2, \hat{x}^s]\rangle + \langle[V(\hat{x}), \hat{x}^s]\rangle, \\
&= \frac{1}{2}\langle[\hat{p}^2, \hat{x}^s]\rangle, \\
&= \frac{1}{2}\langle\hat{p}[\hat{p}, \hat{x}^s] + [\hat{p}, \hat{x}^s]\hat{p}\rangle, \\
&= \frac{1}{2}\langle\hat{p}(-is\hat{x}^{s-1}) + (-is\hat{x}^{s-1})\hat{p}\rangle, \\
&= \frac{1}{2}\langle-is(\hat{p}\hat{x}^{s-1}) + (-is\hat{x}^{s-1})\hat{p}\rangle.
\end{aligned} \tag{2.4.11}$$

We can determine the first term $\hat{p}\hat{x}^{s-1}$ in the last line of equation (2.4.11) by equation (2.1.6). For this purpose; we take $F(\hat{x}) = \hat{x}^{s-1}$, then we have

$$\begin{aligned}
[\hat{x}^{s-1}, \hat{p}] &= \hat{x}^{s-1}\hat{p} - \hat{p}\hat{x}^{s-1}, \\
&= i(s-1)\hat{x}^{s-2}.
\end{aligned} \tag{2.4.12}$$

Rearranging the above relation yields

$$\hat{p}\hat{x}^{s-1} = \hat{x}^{s-1}\hat{p} - i(s-1)\hat{x}^{s-2}. \tag{2.4.13}$$

Inserting the result we have obtained in equation (2.4.13) back into equation (2.4.11) we have;

$$\begin{aligned}
\frac{1}{2}\langle[\hat{H}, \hat{\mathcal{O}}]\rangle &= \langle-s(s-1)(\hat{x}^{s-2}) - is\hat{x}^{s-1}\hat{p} - is\hat{x}^{s-1}\hat{p}\rangle, \\
&= \frac{1}{2}\langle-s(s-1)\hat{x}^{s-2} - 2is\hat{x}^{s-1}\hat{p}\rangle, \\
&= -\frac{1}{2}s(s-1)\langle\hat{x}^{s-2}\rangle - is\langle\hat{x}^{s-1}\hat{p}\rangle,
\end{aligned} \tag{2.4.14}$$

Due to equation (2.4.7) this expression should be equal to zero, therefore we have

$$s\langle\hat{x}^{s-1}\hat{p}\rangle = \frac{i}{2}s(s-1)\langle\hat{x}^{s-2}\rangle. \tag{2.4.15}$$

Next we consider the operator $\hat{\mathcal{O}} = \hat{x}^t p$ and solve the identity in (2.4.7) for this $\hat{\mathcal{O}}$. Then we have

$$\begin{aligned}
\langle[\hat{H}, \hat{\mathcal{O}}]\rangle &= \langle[\hat{H}, \hat{x}^t\hat{p}]\rangle, \\
&= \langle[\frac{1}{2}\hat{p}^2 + V(\hat{x}), \hat{x}^t\hat{p}]\rangle, \\
&= \frac{1}{2}\langle[\hat{p}^2, \hat{x}^t\hat{p}]\rangle + \langle[V(\hat{x}), \hat{x}^t\hat{p}]\rangle.
\end{aligned} \tag{2.4.16}$$

Let's call the first summand the "kinetic" and the second summand the "potential" terms of the commutation relation. We now evaluate the kinetic and the potential commutators one by one. We start by evaluating the commutation relation for the kinetic term. We have

$$\begin{aligned}
\langle[\hat{p}^2, \hat{x}^t\hat{p}]\rangle &= \langle\hat{x}^t[\hat{p}^2, \hat{p}]\rangle + \langle[\hat{p}^2, \hat{x}^t]\hat{p}\rangle, \\
&= \langle\hat{p}[\hat{p}, \hat{x}^t]\hat{p}\rangle + \langle[\hat{p}, \hat{x}^t]\hat{p}^2\rangle, \\
&= \langle -it(\hat{p}\hat{x}^{t-1})\hat{p}\rangle + \langle(-it\hat{x}^{t-1})\hat{p}^2\rangle, \\
&= \langle -it(\hat{x}^{t-1}\hat{p} - i(t-1)\hat{x}^{t-2})\hat{p}\rangle + \langle(-it\hat{x}^{t-1})\hat{p}^2\rangle, \\
&= \langle -t(t-1)\hat{x}^{t-2}\hat{p}\rangle - 2ti\langle\hat{x}^{t-1}\hat{p}^2\rangle, \\
&= -t(t-1)\langle\hat{x}^{t-2}\hat{p}\rangle - 2ti\langle\hat{x}^{t-1}\hat{p}^2\rangle, \\
&= -\frac{i}{2}t(t-1)(t-2)\langle\hat{x}^{t-3}\rangle - 2ti\langle\hat{x}^{t-1}\hat{p}^2\rangle.
\end{aligned} \tag{2.4.17}$$

When passing from third line to fourth line of the equation above, we use the relation in equation (2.4.13) to express $\hat{p}\hat{x}^{t-1}$, through the substitution $s \to t$ and while passing from the penultimate to the last line we have used the identity obtained for $s\langle\hat{x}^{s-1}\hat{p}\rangle$ in equation (2.4.15) with the substitution $s \to t-1$.

We now tackle the commutation relation for the potential part of the Hamiltonian. We have

$$\begin{aligned}
\langle[V(\hat{x}), \hat{x}^t\hat{p}]\rangle &= \langle\hat{x}^t[V(\hat{x}), \hat{p}]\rangle + \langle[V(\hat{x}), \hat{x}^t]\hat{p}\rangle, \\
&= \langle\hat{x}^t[V(\hat{x}), \hat{p}]\rangle, \\
&= i\langle\hat{x}^tV'(\hat{x})\rangle,
\end{aligned} \tag{2.4.18}$$

where we have used equation (2.1.6) to compute the commutator $[V(\hat{x}), \hat{p}]$.

If we rewrite the commutator identities obtained in equations (2.4.17) and (2.4.18) into the equation (2.4.16) we obtain

$$\begin{aligned}
\langle[\hat{H}, \hat{\mathcal{O}}]\rangle &= \frac{1}{2}\langle[\hat{p}^2, \hat{x}^t\hat{p}]\rangle + \langle[V(\hat{x}), \hat{x}^t\hat{p}]\rangle, \\
&= -\frac{i}{4}t(t-1)(t-2)\langle\hat{x}^{t-3}\rangle - it\langle\hat{x}^{t-1}\hat{p}^2\rangle + i\langle\hat{x}^tV'(\hat{x})\rangle.
\end{aligned} \tag{2.4.19}$$

Since this expression should vanish identically due to relation in equation (2.4.7), we obtain

$$t\langle\hat{x}^{t-1}\hat{p}^2\rangle = -\frac{1}{4}t(t-1)(t-2)\langle\hat{x}^{t-3}\rangle + \langle\hat{x}^tV'(\hat{x})\rangle. \tag{2.4.20}$$

Finally if we rewrite the identity found for $\langle \hat{x}^{t-1}\hat{p}^2 \rangle$ in equation (2.4.20) into equation (2.4.5) we obtain the generalized moment recursion relation as [7]

$$2tE\langle \hat{x}^{t-1} \rangle = -\frac{1}{4}t(t-1)(t-2)\langle \hat{x}^{t-3} \rangle + \langle \hat{x}^t V'(\hat{x}) \rangle + 2t\langle \hat{x}^{t-1} V(\hat{x}) \rangle. \tag{2.4.21}$$

We note that although we called the found recursion relation to be the "generalized moment recursion relation", the found recursion relation is not applicable to all potentials $V(\hat{x})$ as some require infinitely many elements to initiate the found recursion relation. This topic will be explored further in Section 2.6.

A more generic derivation of the moment recursion relation for $\hat{\mathcal{O}} = f$ where f represents the function for any hermitian operator $\hat{\mathcal{O}}$ in configuration space, is discussed in [16].

For $t = 1$, the equation (2.4.21) becomes

$$E = \frac{1}{2}\langle \hat{x} V'(\hat{x}) \rangle + \langle V(\hat{x}) \rangle. \tag{2.4.22}$$

Notice that for potentials $V(\hat{x})$ where $V(\hat{x})$ is a homogeneous polynomial in $\hat{x}$, equation (2.4.22) becomes the virial theorem [31]. Here we show an example for this through the potential

$$V(\hat{x}) = \hat{x}^n, \tag{2.4.23}$$

where $n \in \mathbb{Z}_+$. Then the general recursion relation (2.4.21) becomes

$$2tE\langle \hat{x}^{t-1} \rangle = -\frac{1}{4}t(t-1)(t-2)\langle \hat{x}^{t-3} \rangle + (2t+n)\langle \hat{x}^{t+n-1} \rangle. \tag{2.4.24}$$

For $t = 1$ equation (2.4.24) yields

$$E = \left(1 + \frac{n}{2}\right)\langle \hat{x}^n \rangle. \tag{2.4.25}$$

2.5 Positivity Constraint Revisited

In this section, we once again show the positivity constraint of the matrix $\mathcal{M}$ through the means of quantum mechanics. We start by defining the operator $\hat{\mathcal{O}}$ to be

$$\hat{\mathcal{O}} = \sum_n c_n \hat{\mathcal{O}}_n = \sum_n c_n \hat{x}^n. \tag{2.5.1}$$

Where the coefficients $c_n \in \mathbb{C}$. Then the expectation of the products of the operators $\hat{\mathcal{O}}$ and $\hat{\mathcal{O}}^\dagger$ generate all the elements of the bootstrap matrix $\mathcal{M}$ such that

$$\begin{aligned}\langle\hat{\mathcal{O}}^\dagger\hat{\mathcal{O}}\rangle &= \sum_{ij} c_j^* c_i \langle\hat{\mathcal{O}}_j^\dagger\hat{\mathcal{O}}_i\rangle, \\ &= \sum_{ij} c_j^* c_i \mathcal{M}_{ij}, \\ &= \sum_{ij} c_j^* c_i \langle\hat{x}^{j\dagger}\hat{x}^i\rangle, \\ &= \sum_{ij} c_j^* c_i \langle\hat{x}^{i+j}\rangle,\end{aligned} \tag{2.5.2}$$

where passing from the penultimate to the last line in the identity above, we exploited the fact that $\hat{x}$ is a Hermitian operator such that; $\hat{x} = \hat{x}^\dagger$.

We now direct our focus on the expression $\langle\hat{\mathcal{O}}^\dagger\hat{\mathcal{O}}\rangle$, to explore the properties of the matrix $\mathcal{M}$. Notice that this expression is a norm in Hilbert space, then we have

$$\langle\hat{\mathcal{O}}^\dagger\hat{\mathcal{O}}\rangle \geq 0. \tag{2.5.3}$$

A simple proof for this can be given as follows. Let us suppose that $|\alpha\rangle$ denotes the eigenstates of $\hat{\mathcal{O}}$ with the eigenvalues λ,

$$\hat{\mathcal{O}}|\alpha\rangle = \lambda|\alpha\rangle. \tag{2.5.4}$$

Since the operator $\hat{\mathcal{O}}$ is not necessarily Hermitian; $\lambda \in \mathbb{C}$. Then if we evaluate the identity as the definition of an expectation value we obtain

$$\langle\alpha|\hat{\mathcal{O}}^\dagger\hat{\mathcal{O}}|\alpha\rangle = \lambda^*\lambda = |\lambda|^2 \geq 0. \tag{2.5.5}$$

Note also that

$$\hat{\mathcal{O}}|\psi\rangle \equiv |\beta\rangle, \;\; \langle\psi|\hat{\mathcal{O}}^\dagger \equiv \langle\beta|, \tag{2.5.6}$$

for some β. Then

$$\langle\psi|\hat{\mathcal{O}}^\dagger\hat{\mathcal{O}}|\psi\rangle = \langle\beta|\beta\rangle \geq 0. \tag{2.5.7}$$

Since all elements of the matrix $\mathcal{M}$ can be generated from the expression $\langle\hat{\mathcal{O}}^\dagger\hat{\mathcal{O}}\rangle$ which is a norm in Hilbert space; then $\mathcal{M}$ should be positive semidefinite, meaning that all of its eigenvalues $m_i \geq 0$.

2.6 Search Space

Our purpose is to calculate the higher order moments $\langle \hat{x}^t \rangle$, as $t \to \infty$, through the recursion relation in terms of energy E and the lower order moments $\langle \hat{x}^h \rangle$ where, $h < t$. Then, in order to initiate the recursion relation for a potential $V(\hat{x})$ where $V(\hat{x})$ is a differentiable function dependent on $\hat{x}$, we first need to define a set S which we will call the "search space". We denote the elements of the set S, as S^i where $i \in \mathbb{Z}_+$.

We seek to determine the set S with minimal number of elements that can initiate the recursion relation. The number of elements $S^i \in S$ will be called the cardinality of S and shown by $|S|$ from now on. Notice that for any function $V(\hat{x})$, the search space S should always contain the energy E as an element S^i. Then $|S|$ is defined in the domain

$$|S| \geq 1, \ \forall S. \tag{2.6.1}$$

An example of a search space S with cardinality $|S| = \Omega$ can be given as

$$S = \{S^1 \equiv E, S^2, S^3, \cdots, S^\Omega\}. \tag{2.6.2}$$

We follow the notation where; S^1 always shows the energy E for the system while $i > 1$ denote the moments $\langle \hat{x}^t \rangle$.

For a recursion relation to be initializable as $t \to \infty$, it must be self-sufficient, meaning that all of the lower order terms at each step must have been computed by the recursion relation itself. In this thesis, we are only interested in potentials in the form of a polynomial in $\hat{x}$ except the Hydrogen atom problem examined in Chapter 4. For a generic n^{th} degree polynomial potential in $\hat{x}$ defined as

$$V(\hat{x}) = \sum_{i=0}^{n} c_i \hat{x}^i, \tag{2.6.3}$$

where $c_n \neq 0$, the potential dependent identities in (2.4.21) become

$$\begin{aligned} \langle \hat{x}^t V'(\hat{x}) \rangle &= \sum_{i=0}^{n} i c_i \langle \hat{x}^{t+i-1} \rangle, \\ 2t \langle \hat{x}^{t-1} V(\hat{x}) \rangle &= 2t \sum_{i=0}^{n} c_i \langle \hat{x}^{t+i-1} \rangle. \end{aligned} \tag{2.6.4}$$

Then for a generic polynomial potential, the recursion relation becomes

$$2tE\langle\hat{x}^{t-1}\rangle = -\frac{1}{4}t(t-1)(t-2)\langle\hat{x}^{t-3}\rangle + (2t+1)\sum_{i=0}^{n}(i+1)c_i\langle\hat{x}^{t+i-1}\rangle. \quad (2.6.5)$$

In this recursion relation, the highest order term is given by the moment $\langle\hat{x}^{t+n-1}\rangle$, while the lowest order term is given by $\langle\hat{x}^{t-3}\rangle$. Starting from $t = 1$, the highest order moment is $\langle\hat{x}^{n}\rangle$. We seek the value of t when the lowest order moment $\langle\hat{x}^{t-3}\rangle$ becomes equal to the highest order moment of the initialization step. This condition is satisfied when $t-3 = n$, implying that the recursion relation becomes self-sufficient at $t = n+3$. The last value of t for which we need a predefined moment is $t = n+2$, at which point the lowest order moment becomes $\langle\hat{x}^{n-1}\rangle$. Therefore, we must know all moments $\langle\hat{x}^{h}\rangle$ for $0 \leq h \leq n-1$ in order to initialize the recursion relation. Then, at least $\langle\hat{x}^{n-1}\rangle$ moments and the energy E should be specified for us to initiate the recursion relation.

We analyze the behavior of the search space depending on the parity of the potential $V(\hat{x})$. We separate every potential $V(\hat{x})$ into an even parity part $V_{\text{even}}(\hat{x})$ and an odd parity part $V_{\text{odd}}(\hat{x})$ as

$$\begin{aligned} V(\hat{x}) &= V_{\text{even}}(\hat{x}) + V_{\text{odd}}(\hat{x}), \\ &= \frac{V(\hat{x}) + V(-\hat{x})}{2} + \frac{V(\hat{x}) - V(-\hat{x})}{2}. \end{aligned} \quad (2.6.6)$$

For potentials $V(\hat{x})$ with only even parity $V(\hat{x}) = V_{\text{even}}(\hat{x})$ ($V_{\text{odd}}(\hat{x}) = 0$), certain search space elements S^i are identically zero since

$$\langle\hat{x}^{t}\rangle = 0 \quad \text{when} \quad t = \text{odd}. \quad (2.6.7)$$

Here we present a simple proof for equation (2.6.7). When we consider potentials which are even functions of $\hat{x}$; then, all solutions $\psi(x)$ should have definite parity such that; $\psi(-x) = \pm\psi(x)$ as shown in Appendix A. Then the expectation value of $\hat{x}^t$ for any energy eigenstate is given by the integral.

$$\begin{aligned} \langle\hat{x}^{t}\rangle &= \int_{-\infty}^{\infty} \psi^*(x)\hat{x}^t\psi(x)\,dx, \\ &= \int_{-\infty}^{\infty} \hat{x}^t|\psi(x)|^2\,dx. \end{aligned} \quad (2.6.8)$$

Clearly, the term $|\psi(x)|^2$ always yields an even function of x. Then, if the operator $\hat{x}^t$ is an odd function; the total integrand $\hat{x}^t|\psi(x)|^2$ is an odd function, and should vanish under the integral

$$\begin{aligned}
\langle \hat{x}^t \rangle &= \int_{-\infty}^{\infty} \hat{x}^t |\psi(x)|^2 \, dx, \\
&= \int_{-\infty}^{0} \hat{x}^t |\psi(x)|^2 \, dx + \int_{0}^{\infty} \hat{x}^t |\psi(x)|^2 \, dx, \\
&= -\int_{0}^{\infty} \hat{x}^t |\psi(x)|^2 \, dx + \int_{0}^{\infty} \hat{x}^t |\psi(x)|^2 \, dx, \\
&= 0.
\end{aligned} \tag{2.6.9}$$

This allows us to initialize the recursion relation for even potentials with only the energy E and the even moments $\langle \hat{x}^t \rangle$ where t are even integers.

Then, the cardinality $|S|$ of the search space S can be defined for an n^{th} degree polynomial $V(\hat{x})$ in $\hat{x}$ as

$$V(\hat{x}) = \sum_{i=0}^{n} c_i \hat{x}^i \implies |S| = \begin{cases} n, & \text{if } V_{\text{odd}}(\hat{x}) \neq 0 \\ \dfrac{n}{2}, & \text{if } V_{\text{odd}}(\hat{x}) = 0 \end{cases} \tag{2.6.10}$$

where the set S is of the form;

$$S = \begin{cases} \{E, \langle \hat{x} \rangle, \langle \hat{x}^2 \rangle \cdots \langle \hat{x}^{n-1} \rangle\}, & \text{if } V_{\text{odd}}(\hat{x}) \neq 0 \\ \{E, \langle \hat{x}^2 \rangle \cdots \langle \hat{x}^{n-2} \rangle\}, & \text{if } V_{\text{odd}}(\hat{x}) = 0 \end{cases} \tag{2.6.11}$$

One can investigate potentials that are power functions containing negative values as powers, or linear combinations of such power functions, and obtain exactly the same result for a power function of degree n, as well as similar results for their linear combinations, as those obtained in this section

For some potentials $V(\hat{x})$, with the generalized moment recursion relation in (2.4.21), the required minimal search space S is an infinite set, meaning that $|S| \to \infty$, which is intractable for any practical purposes. An example of this is given in Appendix B through a periodic potential. These types of potentials can be handled through the bootstrap method with a different moment recursion relation, derived from the identities (2.4.1) and (2.4.7) with another set of operators $\hat{\mathcal{O}}_1$, $\hat{\mathcal{O}}_2$. The periodic potentials, like in our example, has been first handled through the bootstrap method in [19].

2.7 Algorithmic Structure

In this section we discuss the algorithmic structure of the bootstrap method.

2.7.1 Initialization Parameters

We first introduce the parameters for the algorithm.

I. We define the limits S_B for each of the required search space elements, $S^i \in S$. An example can be given as the following. For a search space S with cardinality $|S| = \Omega$ of the form $S = \{S^1, S^2, \cdots, S^\Omega\}$ the domain of each S^i with pre-defined start and end points are of the form

$$S_B = \{\{\chi_0^1, \chi_f^1\}, \{\chi_0^2, \chi_f^2\}, \cdots, \{\chi_0^\Omega, \chi_f^\Omega\}\}, \tag{2.7.1}$$

where $\chi_0^i \leq \chi^i \leq \chi_f^i$ and χ_0^i, χ_f^i are initial and final points of the interval of S^i with the upper index indicating the i^{th} element S^i within the set S with $0 < i < \Omega$.

II. The precision of the bootstrap, τ_a where, $\tau_a \in \mathbb{Z}_+$ which is the number of points χ_j^i each S^i should contain, with $0 \leq j \leq \tau_a - 1$. The precision τ_a can be selected independently for each search space element S^i. We follow the notation such that τ_1 always denotes the precision of the energy search space element.

III. We define the initial and final matrix sizes K_i and K_f. K_i denotes the smallest $K \times K$ matrix generated in the procedure while K_f denotes the largest $K \times K$ matrix that will be generated.

IV. We define the convergence limit of intervals ϵ where, ϵ is a very small number defined as $0 < \epsilon \ll 1$. The usage of ϵ will be discussed thoroughly while explaining the algorithmic structure in Item 4.

2.7.2 The Bootstrap Algorithm

We now elaborate about the algorithmic structure of the method which we will call the "original bootstrap" algorithm. The algorithm itself is a step by step procedure

that may be best explained as a list.

1. We start by separating each of search space elements $S^i \in S$ into τ pieces equidistantly in between the given limits $[\chi_0^i, \chi_f^i]$. An example for this procedure can be given for any S^i with the precision τ_a as

$$S^i = \{\chi_0^i, \chi_1^i, \chi_2^i, \cdots \chi_{\tau_a-2}^i, \chi_f^i\}, \tag{2.7.2}$$

   where $\chi_f^i = \chi_{\tau_a-1}^i$. The last element of the set ends with $\tau_a - 1$ since we start the count from zero.

   We then generate the search points P_μ which is formed by taking the $\chi_{\mu_{(j)}}^i \in S^i$ from each corresponding search space element S^i. An example of a search point P_μ for a search space of cardinality $|S| = \Omega$ can be given as

$$P_\mu = (\chi_{\mu_{(1)}}^1, \chi_{\mu_{(2)}}^2, \chi_{\mu_{(3)}}^3, \cdots \chi_{\mu_{(\Omega)}}^\Omega), \tag{2.7.3}$$

   where μ is defined between

$$0 < \mu \leq \prod^a \tau_a, \tag{2.7.4}$$

   and each $\mu_{(a)}$ can be any point from the search space defined in equation (2.7.2), and is defined in the respective interval, $0 < \mu_{(a)} \leq \tau_a$.

   The collection of search points P_μ over any search space element S^i forms a search line within that element. We refer to these search lines as search intervals and denote them by I.

2. Second we initiate the recursion relation for any given potential, and calculate the numerical values for the moments $\langle \hat{x}^t \rangle$ for every point P_μ generated from the search space S until $t = (2K - 2)$. During this process, we take into consideration that if the potential is even in $\hat{x}$, $\langle \hat{x}^t \rangle = 0$ for odd values of t.

   Using these numerical values, $\langle \hat{x}^t \rangle$, for each point P_μ we generate a $K \times K$ bootstrap matrix $\mathcal{M}^\mu$ in the order given in equation (2.3.12).

3. We then check if the point P_μ is inside the family of solutions for the given Hamiltonian $\hat{H}$. We do this by checking if the generated matrices $\mathcal{M}^\mu$ are positive definite or not, by performing a Cholesky decomposition on the matrix.

We digress a moment here to briefly explain the general features of this decomposition. Cholesky decomposition [32] splits a Hermitian and positive definite matrix into a lower and an upper triangular matrix, where these matrices are conjugate transpose to each other and their product generates the original matrix. For a matrix $\mathcal{M}$ the most general form of the Cholesky decomposition can therefore given by

$$\mathcal{M} = \mathbf{L}\mathbf{L}^{\dagger}, \tag{2.7.5}$$

where the matrix $\mathbf{L}$ denotes the lower triangular matrix. We only work with real matrices $\mathcal{M}^{\mu}$ meaning that $\left(\mathcal{M}^{\mu}\right)_{jk} \in \mathbb{R}$ then equation (2.7.5) becomes

$$\mathcal{M} = \mathbf{L}\mathbf{L}^{T}. \tag{2.7.6}$$

We attempt at the decomposition of $\mathcal{M}$ by using [32] Cholesky-Banachiewicz Algorithm. Cholesky-Banachiewicz Algorithm suggests that; if a matrix $\mathcal{M}$ is real, symmetric and positive definite, then the diagonal elements of the Cholesky decomposition matrices L_{jj} are given as

$$L_{jj} = \pm\sqrt{\mathcal{M}_{jj} - \sum_{\ell=1}^{j-1} L_{j\ell}^{2}}, \tag{2.7.7}$$

where ℓ is some dummy index. The off-diagonal entries L_{jk} are given as

$$L_{jk} = \frac{1}{L_{jj}}\left(\mathcal{M}_{jk} - \sum_{\ell=1}^{j-1} L_{j\ell}L_{k\ell}\right). \tag{2.7.8}$$

Calculating elements L_{jj} and L_{jk} we generate the lower and upper triangular matrices $\mathbf{L}$ and $\mathbf{L}^{T}$ and check whether if equation (2.7.6) holds for the matrix $\mathcal{M}^{\mu}$. If the equation holds we conclude that the matrix $\mathcal{M}^{\mu}$ is in fact positive definite and therefore satisfies the bootstrap constraint defined in equation (2.5.3). Then the point P_{μ} that generated the bootstrap matrix $\mathcal{M}^{\mu}$ is inside some family of possible solutions for the Hamiltonian $\hat{H}$, and accepted as a solution at the given depth K. However, if the generated matrices $\mathbf{L}$ and $\mathbf{L}^{T}$ does not satisfy the equation (2.7.6) the point P_{μ} is discarded. In this thesis we denote the accepted points with P_{μ}^{S} and the discarded points as P_{μ}^{F}.

The rejected points P_{μ}^{F} are removed from the search space. The accepted points P_{μ}^{S} either form continuous intervals denoted as I_n or single points P_n where

$n \in \mathbb{Z}_+$ labels the results in the search space. Physically n is an integer labeling the discrete spectrum of energy, which we can simply show as E_n. We refer to this occurrence as a 'split' of the interval I. An illustration of the split is provided in Figure 2.1.

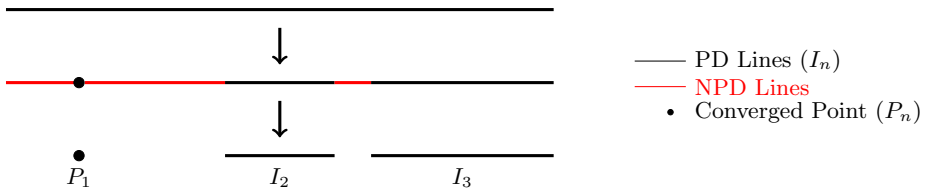

Figure 2.1: Illustration of a Split

The singular points P_n are classified as the solutions of the bootstrap and extracted from the search space as possible energy eigenvalues E_n of the Hamiltonian $\hat{H}$. The treatment of the continuous intervals I_n will be discussed in Item 4.

4. In this item we explain the treatment of continuous intervals I_n. A continuous interval I_n implies that there exists a solution E_n between the initial search point denoted as P_0^n and the final search point P_f^n in that interval I_n. However, the depth K of the bootstrap matrix was not large enough to determine the exact solution E_n. The form of an interval can be given as

$$I_n = \left(P_0^n, \cdots P_\mu^n = P_n \equiv E_n, \cdots P_f^n\right), \tag{2.7.9}$$

although we have shown the solution to be at the arbitrary point P_μ^n inside the interval, the solution can also be at the start and end points P_0^n or P_f^n.

We seek to narrow down each interval I_n to singular search points P_n in the search space through incrementing the value K. However, some intervals I_n are small enough that when $K \to (K+1)$ the interval disappears completely, or some intervals become smaller and smaller in magnitude as $K_i \to K_f$ but never converging to a single point P_n. In order to not lose a solution E_n we use the convergence limit of intervals ϵ. We consider that an interval I_n has converged to a single point P_n if the interval is smaller in magnitude then ϵ such that

$$P_f^n - P_0^n < \epsilon. \tag{2.7.10}$$

If some interval is classified as a converged point through equation (2.7.10) the possible solution point P_n is considered to be the mid value of the interval I_n which is given by

$$P_n = P_0^n + \frac{P_f^n - P_0^n}{2}. \tag{2.7.11}$$

The search points P_0^n and P_f^n of all other intervals I_n which do not converge to a point by means of ϵ convergence i.e.

$$P_f^n - P_0^n > \epsilon, \tag{2.7.12}$$

generate the new boundaries for the elements of a new search space $(S_n)^i \in S_n$. Most generally we match the same upper indices of $(\chi_0^i)^n \in P_0^n$ and $(\chi_f^i)^n \in P_f^n$ to generate the new tuples. Then the boundaries of the search space S_n with cardinality $|S_n| = \Omega$ generated from the non-convergent intervals I_n has the form

$$(S_B)_n = \{\{(\chi_0^1)^n, (\chi_f^1)^n\}, \{(\chi_0^2)^n, (\chi_f^2)^n\}, \cdots, \{(\chi_0^\Omega)^n, (\chi_f^\Omega)^n\}\}. \tag{2.7.13}$$

Each S_n goes through the same steps explained in Items 1, 2 and 3 for the next order bootstrap, with the transformation $K \to (K+1)$ until $K = K_f$.

The algorithmic structure of the original bootstrap algorithm might be better understood with the aid of a flow chart, as shown in Figure 2.2.

2.8 Problems and Optimizations in the Algorithm

The main problem in the bootstrap algorithm is numerical errors, which can be divided into two parts: floating point errors and numerical precision errors.

Floating point numbers are a representations of the fractional part of the numbers (numbers after the decimal point) in computers within finite precision due to the number of bits allocated for storing the number [33]. The fact that we can only store these numbers with finite precision leads to rounding errors, which these errors accumulate in iterative algorithms and significantly affect numerical precision. In the bootstrap algorithm, since we use a recursion relation to generate the elements of the bootstrap matrix, these rounding errors accumulate over iteration, through multiplication and

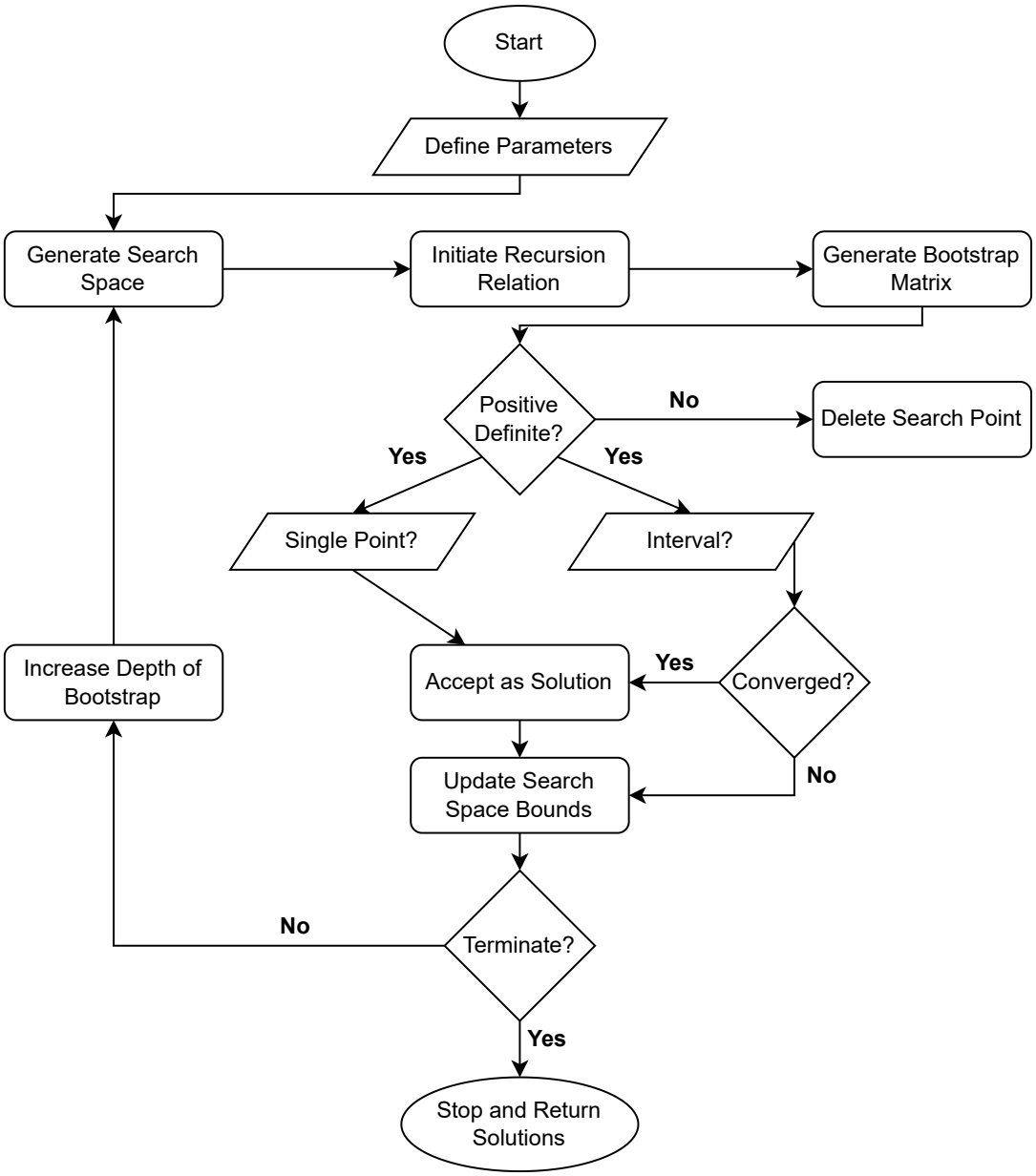

Figure 2.2: Original Bootstrap Algorithm Flowchart

division, creating serious errors for higher order moments. This leads to the generated matrix $\mathcal{M}$ to only be a numerical approximation for the theoretical Hankel matrix of the related search point P_μ. These approximated matrices, $\mathcal{M}$, do not necessarily have to contain the positive definiteness property we are expecting from the theoretical bootstrap matrices. This causes the algorithm to mistakenly remove points from the search space which should have been successful points, leading to loss of solutions or causing "multiple splitting of intervals", which is to be discussed below.

The same problems are also caused due to the numerical precision of the Cholesky-Banachiewicz algorithm that we use to determine the positive definiteness of $\mathcal{M}$. Due to the large magnitudes of the moments, the solver can incorrectly identify some positive definite matrices as non positive definite (NPD) and vice versa. However, despite testing many other solvers[1] [34], this is the best one we have found so far for the bootstrap method.

To reduce the effect of numerical errors on the algorithm, we increase the precision of the intervals τ_a as K increases such that

$$\tau_a' = \tau_a \times K \tag{2.8.1}$$

where τ_a' can be thought of the general precision of the algorithm. This enables higher precision at larger values of K, reducing the possibility of numerical errors that cause all intervals to be completely deleted losing possible solutions that could have been otherwise determined.

Another frequent problem in the algorithm is the "multiple splitting of intervals". As depth K increases, intervals I_n start to split multiple times within an iteration, which seem to be happening at random, generating many new intervals I_m. These new intervals I_m differ from I_n explained in Item 4 of Section 2.7 as they are faulty creations in the algorithm and may or may not contain solutions $P_m = E_m$. This leads to multiple problems, mainly:

1. The length of the newly generated intervals I_m can be smaller than the convergence limit ϵ, causing these intervals to converge prematurely. Since we cannot be certain whether I_m contains valid solutions or not, this premature convergence can lead to false results in the method.

2. Any interval might go through multiple splitting, so an interval I_n which only contains a single E_n may also split multiple times, generating a repeated solution E_n, differing in only (in)significant figures. This causes the same energy eigenvalue to be identified multiple times with different (in)significant figures

3. Since we generate a new S_n from each interval, each of the intervals I_m, goes through the same bootstrap procedure. As a result, these intervals encounter

[1] In our tests, we have excluded the SDPA, as it is too sophisticated for our purposes in this thesis.

the same problem of multiple splitting themselves in each iteration, potentially reaching a time complexity $\mathcal{O}(n!)$.

Although the actual reason why "multiple splitting of intervals" happen is not known to us, it is likely that this occurs due to a combination of the nature of the problem and the numerical errors explained above.

To minimize the problems caused by the multiple splitting, we implement two features to the algorithm as follows;

1. We allow each interval I_n to split only once per iteration. If there are multiple NPD intervals that are attempting to split an interval, the split is performed using the largest of the NPD intervals as illustrated in Figure 2.3.

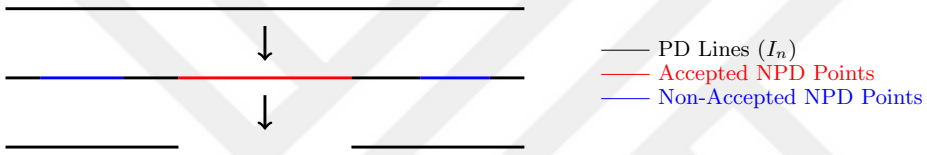

Figure 2.3: Illustration of One Split Approach

   This prevents multiple splits from one single interval occurring within the same iteration, decreasing the number of possible faulty splits. Whit this feature, an interval I_n can only split into two intervals, I_n and I_{n+1}.

2. We impose an iterative limit Γ, depending on the value of K, which is the number of minimum NPD points that can split an interval into two parts, given as

$$\Gamma(K) = \tau_a \times \left(\frac{1 + \frac{K}{10}}{100} \right). \tag{2.8.2}$$

   This feature prevents the intervals I_n from splitting for negligible numbers of NPD points. For example, a single NPD point cannot split an entire interval into two parts. The reason Γ is a function of K is to prevent smaller intervals that are already almost converged to a point from splitting.

We call the bootstrap algorithm with all these optimizations the "one split bootstrap". Although these improvements have made the bootstrap method more efficient and effective, allowing it to reach higher depths K and enabling it to find more solutions

than the original bootstrap method, numerical errors still cause loss of solutions, premature convergence, and repeated solutions problems. In the following section, we will try to handle these problems through some numerical methods we have developed.

2.9 Guided Bootstrapping

All the problems pertaining to the numerical errors we discussed in Section 2.8 can be prevented through the answers to two questions. How many energy eigenstates E exist in any interval I? For example, if we knew there is only one energy eigenstate E_n, existing in an interval I_n, we can prevent the interval from splitting, which would in turn, prevent the repeated solutions for the same energy eigenvalue. This raises the second question. What is a significant length for an interval I for not splitting? Clearly, the length of the interval should be larger than ϵ, but what is the minimum length for an interval to make physical sense? If we knew this value, we could put a length limit for the generation of new intervals, which would prevent the premature convergence of intervals problem.

We attempt at a solution to these problems through the means of numerical methods to determine a guided search space and a significant length for intervals for any given potential. One can think of this method as a "first order correction" to bootstrap while we will call this method to be the "guided bootstrap". The guided bootstrap method constitutes of three parts, an "initialization bootstrap" algorithm followed by "higher state prediction" algorithm and finalized by "no split bootstrap" algorithm.

2.9.1 Initialization Parameters

We first introduce the parameters for the guided bootstrap algorithm.

I. We define the limits for each of the required elements, $S^i \in S$ same as the original bootstrap method just as defined in Item I in Section 2.7.

II. We define the precision of the bootstrap, τ_a same as the original bootstrap method just as defined in Item II in Section 2.7.

III. We define the initial matrix size K_i which is the smallest $K \times K$ matrix generated in the procedure.

IV. We define the initial convergence limit of intervals ϵ_i where, ϵ_i is a very small number defined as $0 < \epsilon_i \ll 1$. The use of ϵ_i will be further discussed in Subsection 2.9.4.

V. We define Υ where $\Upsilon \in \mathbb{R}_+$ which is the maximum value of mean square error (MSE) for an auxiliary extrapolation function to be accepted as a valid model for the system in the algorithm.

VI. We define ρ where $\rho \in \mathbb{Z}_+$ which is the maximum number of trials for forced convergence which will be discussed thoroughly in the Subsection 2.9.4.

2.9.2 Initialization Bootstrap

The initialization bootstrap algorithm is designed to only identify and collect the first few energy intervals until multi splitting of intervals occur. Unlike the original bootstrap algorithm, it doesn't continue bootstrapping identified energy intervals after their first generation. Instead, it removes these intervals from the search space S and collects them for future use when predicting intervals for higher energy states. This process does not end at some predefined final depth K_f but instead ends when at least a minimum of three intervals are collected and multiple splitting of intervals start. We identify the multiple splitting when there are at least four distinct NPD regions within an interval, since the maximum number of NPD regions an interval can have when splitting into two separate intervals is three. We denote the number of intervals that were extracted in this process with κ. We call the longest collected interval to be the most significant interval and denote it with I_S.

2.9.3 Higher State Prediction

With the collected intervals from initialization bootstrap procedure, we want to predict the next possible energy eigenstates. This involves predicting the behavior of energy eigenvalues. The procedure may be better elucidated by listing each step.

1. We first determine whether the intervals show an increasing, decreasing, or constant distance between consecutive intervals. The procedure for determining this behaviour is as follows:

   We take 3 consecutive intervals I_1, I_2 and I_3 from the collected set of intervals. Assume that x_1 and x_3 are points inside the interval I_1 and I_3. Then in order to check if there is constant behaviour between these intervals, we assume some point in x_2 that satisfies the equation,

   $$x_2 - x_1 = x_3 - x_2 \tag{2.9.1}$$

   Solving the above equation for x_2 yields

   $$x_2 = \frac{x_1 + x_3}{2} \tag{2.9.2}$$

   We then check, if this point x_2 exists inside the interval I_2. If this condition is met, for any $x_1 \in I_1$, $x_2 \in I_2$, $x_3 \in I_3$ we classify the behaviour of the energy E_n as "equal". If the condition is not met, we check either $x_2 > \sup I_2$ or $x_2 < \inf I_2$ for all combinations of x_1, x_3 and count the occurrences of each state. If the state $x_2 < \inf I_2$ occurs more, we classify the behaviour of the energy E_n as "increasing", if the state $x_2 > \sup I_2$ occurs more, we classify the behaviour of the energy as "decreasing".

2. Second, we assign each interval to a state. In order to do this, we assume that an interval I_n contains only the eigenvalue E_n of the given system. For example, interval I_1 contains only the eigenvalue E_1 and so on. We expect that the general behavior of the eigenvalues E_n should remain consistent as n increments. For instance, if E_n is classified as increasing in previous sets of intervals, it cannot suddenly shift to equal or decreasing behavior in higher intervals. Then, we can determine if the intervals that have found by the initialization bootstrap procedure are consecutive solutions for the system by controlling the behaviour of every combination of 3 consecutive intervals I_{m-1}, I_m and I_{m+1} where $1 < m < \kappa$. If the behaviour of some set of intervals $\{I_{m-1}, I_m, I_{m+1}\}$ is different from the behaviour of the set of intervals $\{I_{m-2}, I_{m-1}, I_m\}$, we deduce that the interval I_{m+1} is not the $(n+1)^{\text{th}}$ eigenvalue of the system. This is because the general behavior of the eigenvalues should remain consistent as n increases. If we observe a different behavior for a set of three intervals

compared to previous sets, it indicates a missing or incorrect result, produced within the algorithm, meaning I_{m+1} cannot be classified as the solution $E_{(n+1)}$. We assign each I_m, its respective state n, such that $n = m$. We denote the total number of accepted intervals by k, and discard all intervals I_m, for $m > k$, in the next part.

3. Third, we attempt to find a function $A(r)$ which we will call the "auxiliary extrapolation function" over some variable r where $r \in \mathbb{R}_+$ which we will call the space of r as the auxiliary space. The function $A(r)$ is not the energy of the Hamiltonian $\hat{H}$ but yields the energy eigenvalues E_n of the system whenever $r = n$ such as

$$A(r = n) = E_n. \tag{2.9.3}$$

To find the auxiliary extrapolation function $A(r)$ we first assume that the middle point P_n of the intervals I_n defined as

$$P_n = P_0^n + \frac{P_f^n - P_0^n}{2}, \tag{2.9.4}$$

to represent the energy eigenvalue of the state n, as $P_n \equiv E_n$, and try to fit the best linear or power function to these points.

For systems which the intervals show equal behaviour, we expect the auxiliary extrapolation function to be linear, meaning the function depends only on r, so we use the model

$$A(r) = ar + b, \tag{2.9.5}$$

where $a\,, b \in \mathbb{R}$. To determine the values of a and b we use polynomial interpolation. To check how good the model fits the data we calculate the MSE value between the mid values P_n of intervals I_n and the modeled values $A(r = n)$ as [35]

$$MSE = \frac{1}{k}\sum_{n=1}^{k}(P_n - A(r = n))^2. \tag{2.9.6}$$

If the lowest returned MSE value is lower than Υ we accept the model as the auxiliary extrapolation function for that system.

For solutions that show increasing or decreasing behaviour we cannot use polynomial extrapolation, at least not immediately, since a higher order polynomial

will always fit the data better. We try to find the auxiliary extrapolation function in terms of power function models defined as

$$\begin{aligned} &\text{Increasing Behaviour :} \quad A(r) = cr^t, \\ &\text{Decreasing Behaviour :} \quad A(r) = dr^{-t}, \end{aligned} \tag{2.9.7}$$

where $c\,, d \in \mathbb{R}$ and t is an integer in the interval $2 \leq t \leq k$. We generate every power function r^t and determine the constants c and d through the identities

$$\begin{aligned} &\text{Increasing Behaviour :} \quad c = \frac{1}{k}\sum_{n=1}^{k}\frac{P_n}{n^t}, \\ &\text{Decreasing Behaviour :} \quad d = \frac{1}{k}\sum_{n=1}^{k}\frac{P_n}{n^{-t}},. \end{aligned} \tag{2.9.8}$$

Then, for each generated function, we calculate the MSE value between the mid values P_n and the modeled values $A(r = n)$ using the equation (2.9.6), and select the model with the power t that has the lowest MSE value as the best fitting model. If the lowest returned MSE value is lower than Υ and $t < k$ we accept the model as the auxiliary extrapolation function for that system. The reason we omit the $t = k$ case is because, $t = k - 1$ is the highest order power function we can try fitting with k values. This does not necessarily imply that the model fits better for some $t \geq k$.

In the systems studied in this thesis, we have never encountered an auxiliary extrapolation function with $t \geq k$ or an MSE exceeding Υ. However, for future research, if one encounters these problems, a way to come over this problem might be to fit the points to a polynomial of order t using polynomial interpolation and calculating the Akaike Information Criterion [36] and Bayesian Information Criterion [37] which can help determine if the model fits well enough to be considered the auxiliary extrapolation function of the system.

4. Finally, using the auxiliary extrapolation function we have obtained, we generate the boundaries for the guided search space S_G. We do this by generating $2k$ possible energy interval boundaries from the boundaries of the most significant interval I_S using the $A(r)$. The method works as the following:

   Assume that the end points of the interval I_S are given by P_0^S and P_F^S. We seek the values of r at P_0^S and P_F^S which are given through

$$A^{-1}(P_0^S) = r|_{\text{Lower Bound}} = l\,, \quad A^{-1}(P_f^S) = r|_{\text{Upper Bound}} = u. \tag{2.9.9}$$

Then by linear incrementation $(+1)$ for $k > S$ and linear decrementation (-1) for $k < S$ of the found l and u values we generate where all the boundaries of the $2k$ energy intervals fall in auxiliary space. For some interval I_N which is assigned to state N the boundaries are calculated through

$$A(l-S+N) = r|_{\text{Lower Bound of N}}, \quad A(u-S+N) = r|_{\text{Upper Bound of N}}. \tag{2.9.10}$$

The collection of all the boundaries of $2k$ elements generate the boundaries for the guided search space S_G.

2.9.4 No Split Bootstrap

In this Subsection we are going to present the no split bootstrap method. The main difference with the method from all other methods is that, this time we expect a single eigenvalue E_n in each of the intervals generated from the guided search space S_G. This allows us to implement two key features to prevent or at least optimize the problems encountered with the original and one split bootstrap algorithms, which are the following:

1. In no split bootstrap, we do not allow the intervals to split into two different intervals. Instead, intervals are allowed only to shrink from the sides, eventually converging to a single point. An illustration of the no split approach is given in Figure 2.4.

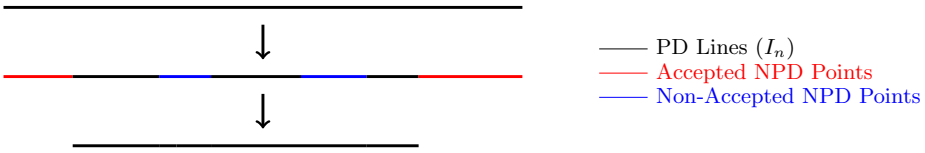

Figure 2.4: Illustration of No Split Approach

Through this, we avoid the multiple splitting problem and the problems that occur due to it.

2. Second we introduce the method of forced convergence. In the original bootstrap method due to precision or numerical errors some intervals which contain

energy eigenvalues got deleted completely. This issue couldn't be prevented because we lacked knowledge of whether any energy eigenvalues existed in those intervals. This time, since we expect that only a single energy eigenvalue to exist in every interval I_n, we can force convergence by increasing the precision of the interval through

$$\tau_a' = \tau_a \rho', \tag{2.9.11}$$

where ρ' is defined in $2 \leq \rho' \leq \rho$ and is an incremental value $(+1)$, incrementing in each consecutive time an interval I_n is deleted in the process completely. If the interval I_n does not converge through this procedure until $\rho' = \rho$, we assume the entire interval I_n to be converged.

If the auxiliary extrapolation function of a Hamiltonian changes with a power function, the numerical values of the eigenvalues will start differing in order of magnitudes. This means that a convergence limit ϵ meaningful for some state n might not be meaningful for another state m. This time, since we can assign a state value n for each of the intervals in S_G, we can also implement a state iterative convergence limit ϵ in no split bootstrap. We define epsilon to be

$$\epsilon = \epsilon_i n^{\pm t}, \tag{2.9.12}$$

where the sign of t is chosen through the behaviour of the energy eigenvalues. We choose the negative sign, if the behaviour is decreasing and positive sign if the behaviour is increasing. This allows us to find more meaningful errors in intervals through ϵ convergence.

Since we expect a solution in each of these intervals, we want each interval to ultimately converge. Hence, this bootstrap method does not terminate at a fixed depth K_f, instead, it continues until all possible intervals within the search space S_G have converged.

Here, we present a flowchart for the guided bootstrap algorithm in Figure 2.5.

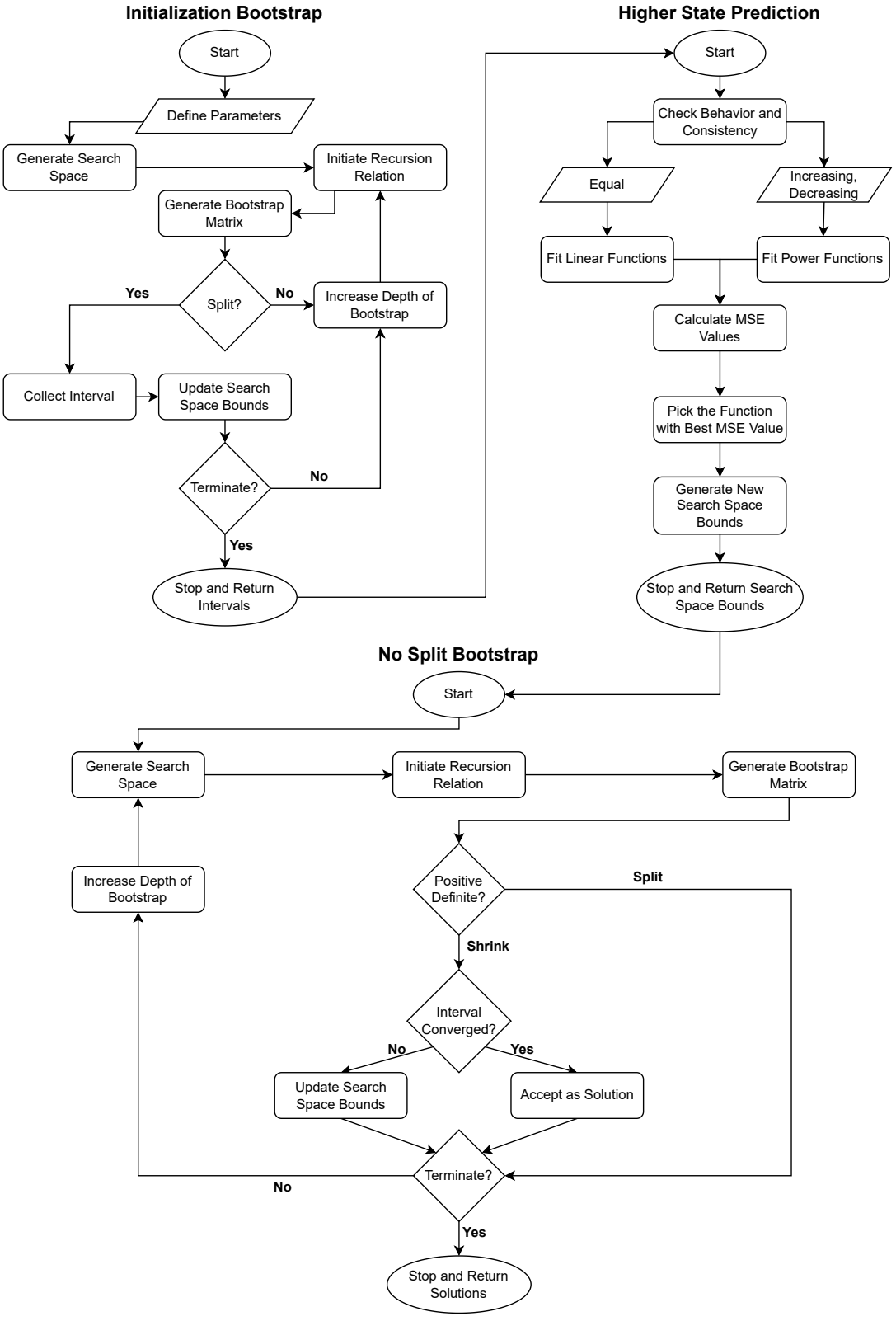

Figure 2.5: Guided Bootstrap Algorithm Flowchart

CHAPTER 3

BOOTSTRAPPING THE SIMPLE HARMONIC OSCILLATOR

3.1 The Simple Harmonic Oscillator Potential

We now start applying the bootstrap method to specific examples. We start with the SHO system which is the simplest example among the systems we study, since the system is defined in 1D Cartesian coordinates in the domain $\mathbb{R}$ with a search space containing only a single element, namely the energy.

In the most general format the SHO potential is given as

$$V(\hat{x}) = \frac{1}{2} m\omega^2 \hat{x}^2. \tag{3.1.1}$$

For simplicity in the energy eigenvalues we work with $\omega = 1$. We also implement our definition for mass $m = 1$, then the potential $V(\hat{x})$ becomes

$$V(\hat{x}) = \frac{1}{2} \hat{x}^2. \tag{3.1.2}$$

Figure 3.1 shows the graph of the function $V(\hat{x})$ in the configuration space. From the figure it is obvious that there are infinitely many bound states for the SHO system which all have an energy $E \geq 0$.

3.2 Recursion Relation, Search Space and the Bootstrap Matrix

In this section we derive the theoretical perquisites discussed in Chapter 2 for the SHO system.

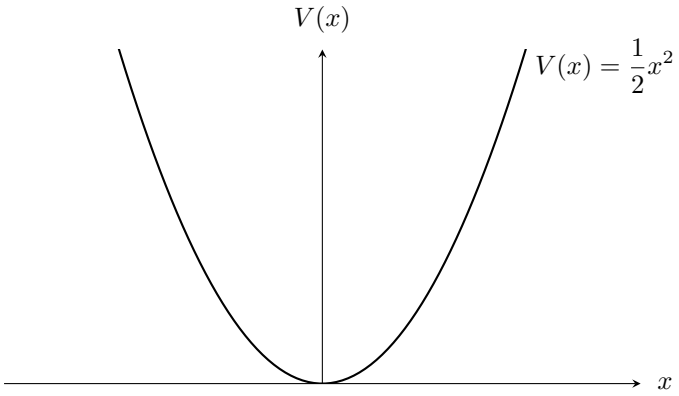

Figure 3.1: Graph of SHO Potential in the Configuration Space

3.2.1 SHO Recursion Relation

Evaluating the potential dependent identities in equation (2.4.21) for the SHO potential defined in equation (3.1.2) we obtain

$$\langle \hat{x}^t V'(\hat{x}) \rangle = \langle \hat{x}^{t+1} \rangle \,, \quad 2t \langle \hat{x}^{t-1} V(\hat{x}) \rangle = t \langle \hat{x}^{t+1} \rangle. \tag{3.2.1}$$

Implementing the identities found in equation (3.2.1) into the equation (2.4.21) we obtain the recursion relation for the SHO as

$$(t+1)\langle \hat{x}^{t+1} \rangle = 2Et \langle \hat{x}^{t-1} \rangle + \frac{1}{4} t(t-1)(t-2) \langle \hat{x}^{t-3} \rangle, \tag{3.2.2}$$

which is the moment recursion relation for the SHO system.

3.2.2 SHO Search Space

The SHO potential is a second degree polynomial which is an even function of $\hat{x}$. Then, by the methods explained in Section 2.6, the cardinality $|S|$ of the minimal search space needed to initiate the recursion relation found in equation (3.2.2) is

$$|S| = 1. \tag{3.2.3}$$

Since every search space S should contain energy E as an element, the search space element S^1 is simply E. Then the minimal search space S for the SHO system is

$$S = \{S^1 \equiv E\}, \tag{3.2.4}$$

which is the only element that should be predefined in the algorithm.

3.2.3 SHO Bootstrap Matrix and Constraints on the Search Space

We want to generate the non-zero elements of $\mathcal{M}$ using equation (3.2.2). The first non-zero element is $\langle \hat{x}^2 \rangle$ and can be generated from the recursion relation for $t = 1$ which yields

$$\langle \hat{x}^2 \rangle = E. \tag{3.2.5}$$

Clearly, we have, $\langle \hat{x}^2 \rangle \geq 0$ which enables us to put a lower bound for the energy E as $E \geq 0$ as expected from the Figure 3.1.

As an example, we also show the first four diagonal elements $\mathcal{M}_{ii}$ of the bootstrap matrix $\mathcal{M}$ which can be calculated as

$$\begin{aligned} \mathcal{M}_{00} &= \langle \hat{x}^0 \rangle = 1, \\ \mathcal{M}_{11} &= \langle \hat{x}^2 \rangle = E, \\ \mathcal{M}_{22} &= \langle \hat{x}^4 \rangle = \frac{3}{2}E^2 + \frac{3}{8}, \\ \mathcal{M}_{33} &= \langle \hat{x}^6 \rangle = \frac{5}{2}E^3 + \frac{25}{8}E, \end{aligned} \tag{3.2.6}$$

and the bootstrap matrix $\mathcal{M}$ has the form

$$\mathcal{M} = \begin{bmatrix} 1 & 0 & E & 0 & \cdots & \langle \hat{x}^{K-1} \rangle \\ 0 & E & 0 & \frac{3}{2}E^2 + \frac{3}{8} & \cdots & \langle \hat{x}^{K} \rangle \\ E & 0 & \frac{3}{2}E^2 + \frac{3}{8} & 0 & \cdots & \langle \hat{x}^{K+1} \rangle \\ 0 & \frac{3}{2}E^2 + \frac{3}{8} & 0 & \frac{5}{2}E^3 + \frac{25}{8}E & \cdots & \langle \hat{x}^{K+2} \rangle \\ \vdots & \vdots & \vdots & \vdots & \ddots & \vdots \\ \langle \hat{x}^{K-1} \rangle & \langle \hat{x}^{K} \rangle & \langle \hat{x}^{K+1} \rangle & \langle \hat{x}^{K+2} \rangle & \cdots & \langle \hat{x}^{2K-2} \rangle \end{bmatrix}. \tag{3.2.7}$$

3.3 Original Bootstrap on SHO System

We now apply the "original bootstrap" algorithm the the SHO system. We note that the exact energy levels for the system is well-known in atomic units are given by

$$E_n = \left(n + \frac{1}{2} \right), \tag{3.3.1}$$

where $n \geq 0$. For this system, we let $n \to (n+1)$ and label the states with $n \geq 1$. We write the energy levels for the systems as

$$E_n = \left(n - \frac{1}{2}\right). \tag{3.3.2}$$

We run the original bootstrap program on Python with the initialization parameters as the following:

- Search space bounds for $E \in S: \ [0, 20]$.
- Precision $\tau_1 = 200$ for search space element E.
- Initial depth $K_i = 5$ and final depth $K_f = 35$.
- Convergence limit $\epsilon = 0.01$.

Figure 3.2 shows the results of the original bootstrap algorithm for the SHO system. The horizontal axis represents the energy, and the vertical axis represents the depth of the bootstrap, K.

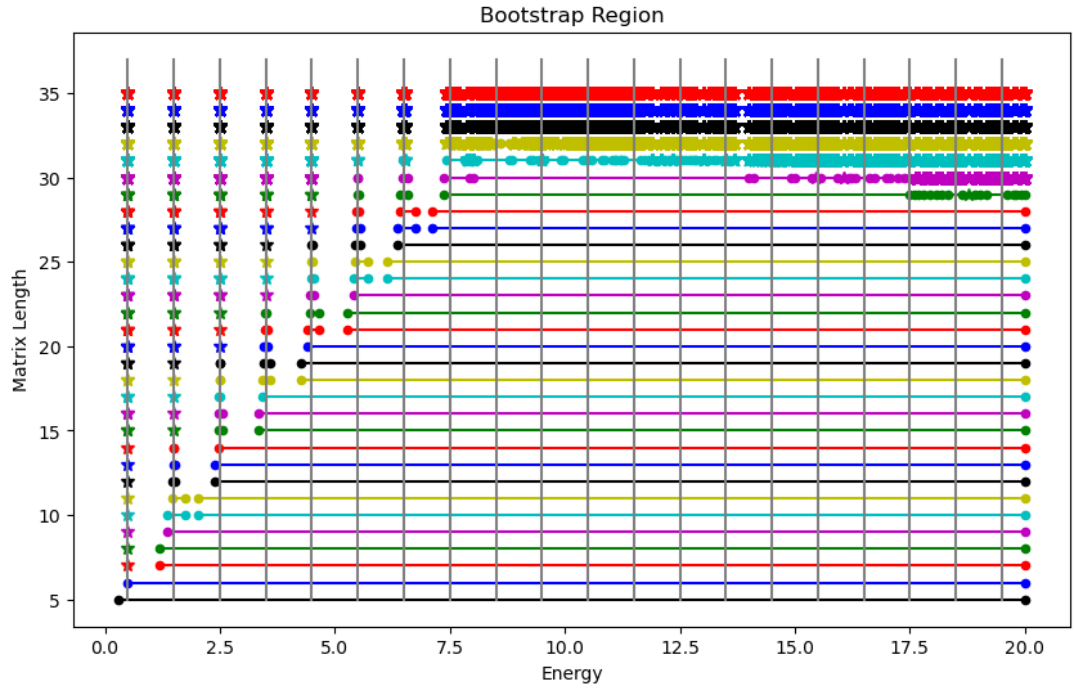

Figure 3.2: Original Bootstrap Graph for the SHO System

Unless specified otherwise, all graphs are to follow the same format throughout this thesis. Each depth K is shown with a different color. Every interval is represented

by a line, with dots indicating the start and end points of the interval. The colored stars represent the converged points of the system, which converged either through epsilon convergence or pointwise convergence. Although we stop bootstrapping the converged points, they are still plotted in higher depths K since, theoretically, they should always yield positive definite matrices. The exact energy levels for the system are indicated by gray lines in the graph.

From the graph, we can see that for smaller depths K the original bootstrap algorithm separates the main interval into smaller intervals around the exact energy levels. At depth $K = 28$ finding five converged energy levels and two possible energy intervals. However, as the depth of the bootstrap reaches $K = 29$, the multiple splitting of intervals start and the algorithm becomes unstable. For instance, when the algorithm ends at depth $K = 35$ it has identified "3471" points as possible solutions within the search space of $[0, 20]$, rather than the expected twenty solutions.

It is obvious that the original algorithm itself is not very applicable to any system. While we know the energy levels for the SHO system, for an unknown potential, it would be impossible to differentiate between actual energy eigenstates and faulty convergences in the results. This algorithm should be able to work at higher depths to determine more exact results, but for higher depths K, the original bootstrap algorithm does not yield reliable results.

3.4 One Split Bootstrap on SHO System

In this section, we seek to resolve the issues associated with the original bootstrap algorithm through the methods explained in Chapter 2 in Section 2.8.

We run the "one split bootstrap" program on Python with the initialization parameters as the following:

- Search space bounds for $E \in S: \ [0, 20]$.
- Precision $\tau_1 = 200$ for search space element E.
- Initial depth $K_i = 5$ and final depth $K_f = 45$.

- Convergence limit $\epsilon = 0.01$.

The graph in Figure 3.3 displays the results of the one split bootstrap algorithm for the SHO system.

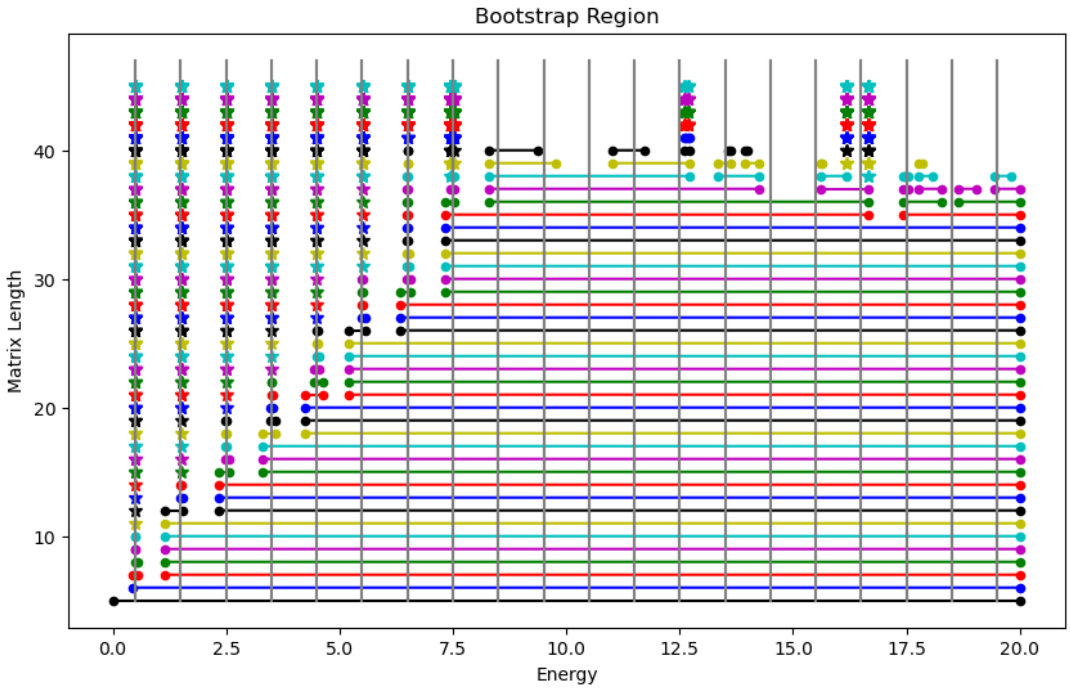

Figure 3.3: One Split Bootstrap Graph for the SHO System

As illustrated in the graph, it is clear that the one split bootstrap algorithm performs significantly better compared to the original bootstrap algorithm. At depth $K = 29$, the algorithm is still correctly splitting around the energy eigenstates without multi-splitting. This indicates that the algorithm is performing as expected at this depth.

At depth $K = 37$, the algorithm correctly splits around the eight energy level, however, it also begins to incorrectly splitting the intervals completely misses the nineteenth energy eigenstate, incorrectly identifying the point $E = 18.5$ as non-positive definite. When the algorithm reaches depth $K = 40$, it incorrectly determines that there are no positive definite intervals left in the system, hence missing all the remaining solutions. This is likely due to numerical errors generated in the recursion relation combined with the numerical sensitivity of the Cholesky-Banachiewicz algorithm.

When the program ends at $K = 45$ it has found nineteen points as solutions, which

are given in Table 3.1 in a sorted format.

Table 3.1: One Split Bootstrap Results for the SHO System

Bootstrapped Energy	Bootstrapped Energy
0.4989 ± 0.0023	7.4737 ± 0.0016
1.5022 ± 0.0046	7.4854 ± 0.0012
2.5006 ± 0.0022	7.4983 ± 0.0015
3.5017 ± 0.0047	7.5093 ± 0.0025
4.4990 ± 0.0040	7.5262 ± 0.0047
5.5010 ± 0.0035	12.6096 ± 0.0
6.4943 ± 0.0013	12.6958 ± 0.0
6.5010 ± 0.0021	16.1900 ± 0.0
7.4471 ± 0.0012	16.6475 ± 0.0044
7.4540 ± 0.0002	

The data presented in the table below shows that the algorithm correctly determined the first six energy eigenstates within some reasonable margin of error. For the seventh energy eigenstate, the interval split around the same solution twice, converging twice generating multiple results for the seventh energy eigenstate. The eighth energy eigenstate showed a similar behavior but more drastically, with the algorithm finding the same solution seven times. After that, the algorithm lost most of the solutions for the ninth through twentieth energy eigenstates, only identifying the thirteenth and seventeenth energy eigenstates with a larger margin of error. The program also found a random point $E = 16.1900 \pm 0.0$ which is not relatable to any energy eigenstate and converged through pointwise convergence.

It is evident that the one split bootstrap algorithm performs better than the original bootstrap algorithm, at least yielding examinable final results. However, it is still not reliable enough as it misses many solutions, produces the same results multiple times, and identifies random points as solutions. Therefore, it is still not applicable for systems with unknown energy eigenstates.

3.5 Guided Bootstrap on SHO System

In this section, we aim to resolve the problems of the original and one split bootstrap algorithms through the "guided bootstrap" method as explained in Section 2.9. We now investigate the SHO system with the guided bootstrap algorithm, which consists of three parts, the "initialization bootstrap", the "higher state prediction", and the "no split bootstrap". We run the guided bootstrap program on Python with the initialization parameters as the following:

- Search space bounds for $E \in S: \ [0, 20]$.
- Precision $\tau_1 = 500$[1] for search space element E.
- Initial depth $K_i = 5$.
- Initial convergence limit $\epsilon_i = 0.01$.
- Maximum value of MSE $\Upsilon = 100$ for accepting an energy model.
- Number of maximum trials $\rho = 10$ for forced convergence.

The algorithm starts with the initialization bootstrap part where we aim to only identify the initial energy intervals without further splitting or shrinking them. This method provides us a starting point for predicting a guided search space S_G.

Figure 3.4 shows the initialization bootstrap results for the SHO system.

The graph reveals that the algorithm successfully identifies the first seven energy intervals until the depth becomes $K = 28$. When the depth reaches $K = 29$, as it happened with the original bootstrap algorithm, the multi splitting of intervals start, causing the program to exit with the seven found intervals. We then sort these intervals from smallest to largest and assign each interval to a state by linear incrementation $(+1)$. These intervals and their assigned states are listed in Table 3.2.

When we look at the table, we see that all seven of the found energy intervals contain the theoretical exact energy of their respective related states. The largest interval is

[1] Initially we intended to use $\tau_1 = 200$, as we did with other sections. However, it results in a special case where all the results of the predicted states go through pointwise convergence. We wanted to avoid the impression that all the predicted intervals would undergo pointwise convergence. Hence, for this section, we use $\tau_1 = 500$

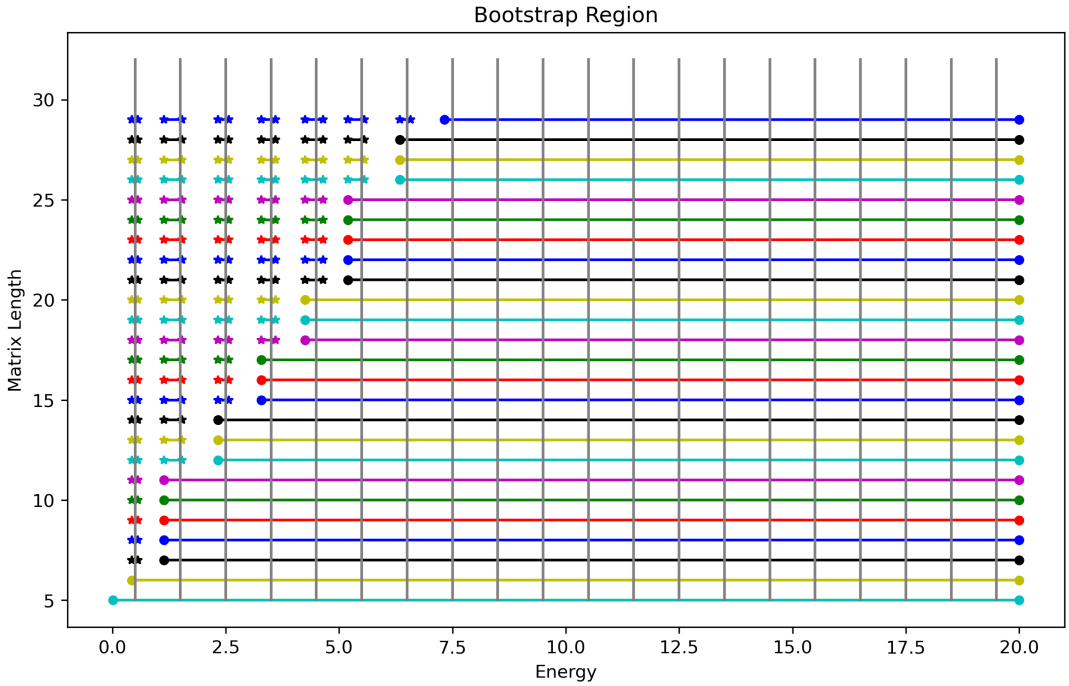

Figure 3.4: Initialization Bootstrap Graph for the SHO System

the fourth excited state, with a length of 0.4022. We assign this interval length as the significant interval length for the system and initiate the second part of the guided bootstrap.

Using the identified energy intervals, we first determine the general distance behavior between them. For the SHO system, it is apparent that the behavior should be "equal" since each interval contains the theoretical energy eigenstate, and the distance between the energy eigenstates for the system is equal, with a difference of 1 unit of energy. The algorithm determines the behavior of the energy eigenstates as "equal" and generates a linear auxiliary extrapolation function for the system. This auxiliary extrapolation function models the relationship between the identified intervals and helps estimate possible intervals for higher energy states.

Figure 3.5 shows the auxiliary extrapolation function fitted to the midpoints of the intervals found in the initialization bootstrap for the SHO system.

The best auxiliary extrapolation function that can be found for the system is

$$A(r) = r - 0.57, \tag{3.5.1}$$

Table 3.2: Initialization Bootstrap Results for the SHO System

State	Found Energy Interval
1	0.4927 ± 0.0727
2	1.3357 ± 0.1996
3	2.4455 ± 0.1178
4	3.4436 ± 0.1569
5	4.4460 ± 0.2011
6	5.3773 ± 0.1811
7	6.4560 ± 0.1187

which provides a good estimate for the energy eigenstates of the system defined in equation (3.3.2) with an MSE value of 2.42×10^{-3}. With the found intervals and the significant interval length for the system, we predict reasonable intervals for the eigenstates eight through fourteen. Since the system is linear, all the lengths for the predicted states will be equal to the significant interval length. The predicted intervals for the higher energy levels are given in Table 3.3.

Table 3.3: Guessed Energy Intervals for the SHO System

State $\rightarrow$ Guessed Energy Interval	State $\rightarrow$ Guessed Energy Interval
$1 \rightarrow 0.4498 \pm 0.2011$	$8 \rightarrow 7.4431 \pm 0.2011$
$2 \rightarrow 1.4488 \pm 0.2011$	$9 \rightarrow 8.4421 \pm 0.2011$
$3 \rightarrow 2.4479 \pm 0.2011$	$10 \rightarrow 9.4412 \pm 0.2011$
$4 \rightarrow 3.4469 \pm 0.2011$	$11 \rightarrow 10.4402 \pm 0.2011$
$5 \rightarrow 4.4460 \pm 0.2011$	$12 \rightarrow 11.4393 \pm 0.2011$
$6 \rightarrow 5.4450 \pm 0.2011$	$13 \rightarrow 12.4383 \pm 0.2011$
$7 \rightarrow 6.4440 \pm 0.2011$	$14 \rightarrow 13.4374 \pm 0.2011$

From the table of guessed energy intervals, we observe that although the theoretical expected energy levels shift from the midpoints of the intervals as the predicted state n gets higher, all predicted energy intervals contain the related theoretical energy eigenstates for the system.

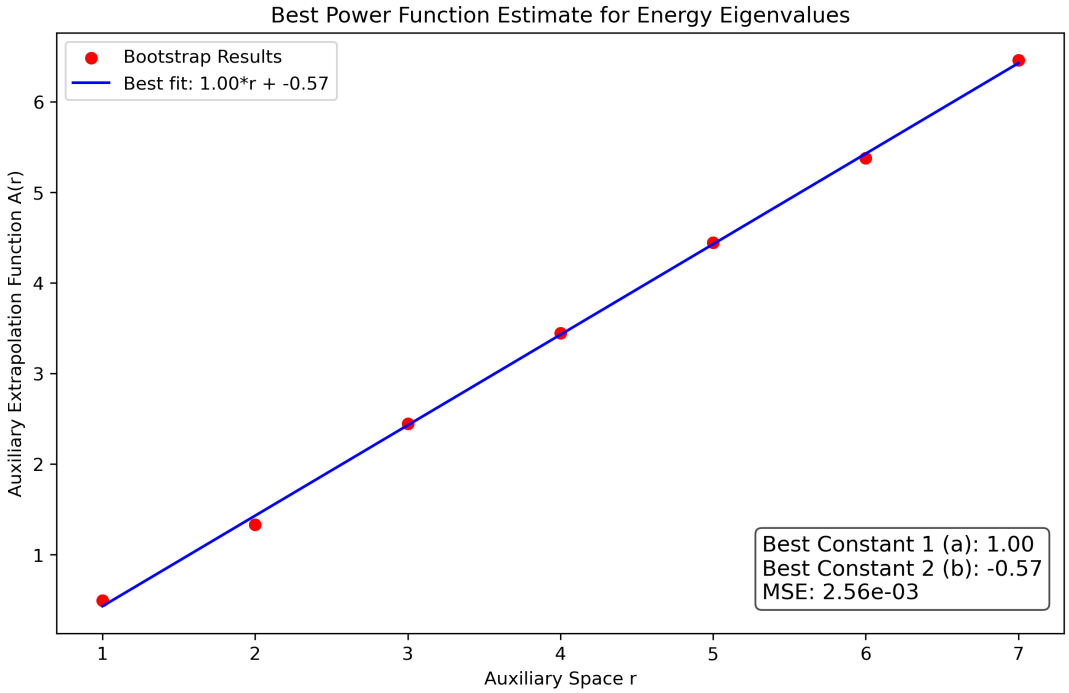

Figure 3.5: Auxiliary Extrapolation Graph for the SHO System

Finally, we apply the no split bootstrap to the SHO system. We first generate the guided search space S_G, using the boundaries of the estimated energy intervals. In the no split bootstrap method, we prevent the intervals from splitting, allowing them only to shrink from the sides. Since we expect a single solution in each interval, we force each interval to converge to a single point. Figure 3.6 shows the results of the no split bootstrap for the SHO system.

From the graph we can deduce that, as expected, the no split bootstrap algorithm converged every search space bound to a single point at depth $K = 43$. The results of the no split bootstrap algorithm are given in Table 3.4. We also show the exact energy levels and the percentage errors calculated from the midpoints of the intervals in this table.

The table indicates that, the first seven energy levels, found from the initialization bootstrap, show high precision with percentage errors below 0.2%. The higher energy levels eight through fourteen, predicted through the auxiliary equation, show slightly higher percentage errors from the theoretical values. Interestingly, for the higher states $n = 9, 10, 12, 13$, which all converged through epsilon convergence, all the

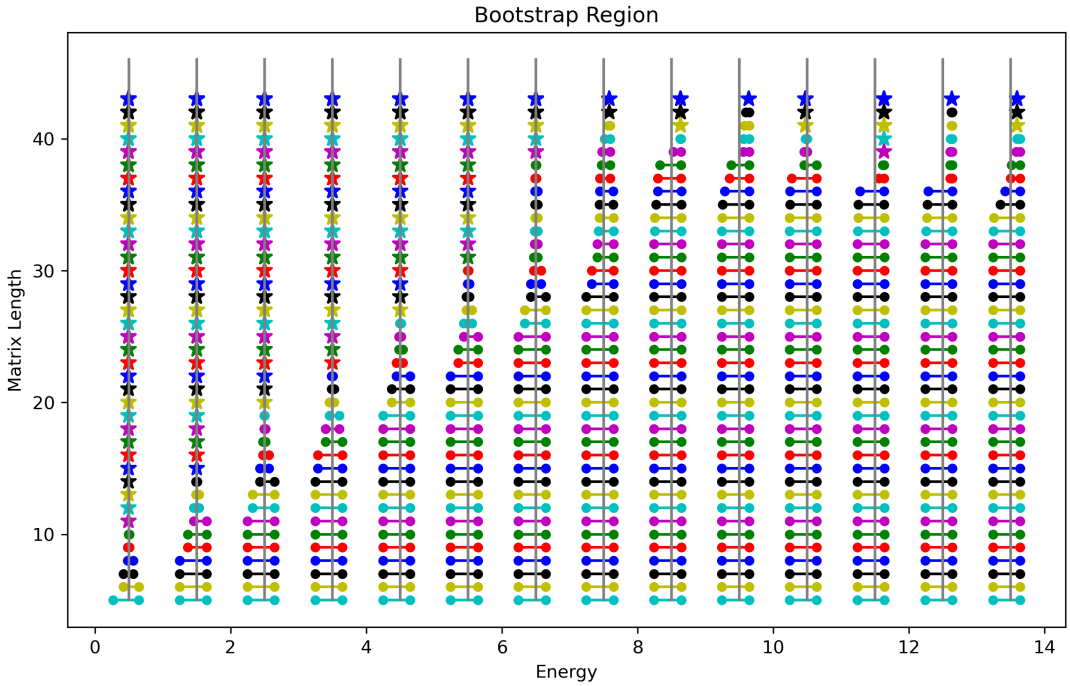

Figure 3.6: No Split Bootstrap Graph for SHO the System

midpoint values of the intervals are shifted by the same amount. We suspect that this shift is due to numerical errors in the recursion relation. These errors cause the calculations for higher moments to be slightly off, resulting in a systematic shift in the points. For instance, instead of calculating the right value $\langle \hat{x}^t \rangle$ for a moment at the correct point of 8.5, numerical errors might cause this value to be calculated at 8.63, causing a shift in the solution.

Overall, the guided bootstrap method significantly improves the reliability of the final results for the SHO system. While minor numerical errors still happen at higher energy states, the method appears to be potentially applicable to systems with unknown energy levels, though further work is needed.

Table 3.4: Guided Bootstrap Results for the SHO System

States	Bootstrapped Energy	Exact Energy	Percentage Error
1	0.4990 ± 0.0023	0.50	0.1975
2	1.5022 ± 0.0046	1.50	0.1475
3	2.5006 ± 0.0023	2.50	0.0253
4	3.5017 ± 0.0048	3.50	0.0497
5	4.4990 ± 0.0040	4.50	0.0221
6	5.5011 ± 0.0035	5.50	0.0193
7	6.5016 ± 0.0039	6.50	0.0247
8	7.5809 ± 0.0116	7.50	1.0792
9	8.6342 ± 0.0048	8.50	1.5783
10	9.6407 ± 0.0015	9.50	1.4814
11	10.4733 ± 0.0	10.50	0.2546
12	11.6305 ± 0.0021	11.50	1.1347
13	12.6336 ± 0.0058	12.50	1.0686
14	13.5918 ± 0.0	13.50	0.6797

CHAPTER 4

BOOTSTRAPPING THE HYDROGEN ATOM

4.1 Hydrogen Atom Problem

We now seek to investigate the spectrum of the Hydrogen Atom. However, due to the fundamental nature of this problem, which is also the reason why it is important for us, the methods developed in Chapter 2 cannot be directly applied, as will be discussed below.

First, Chapter 2 focused on problems defined in Cartesian coordinates, while the Hydrogen atom problem is best handled in spherical polar coordinates. Therefore, we must use the Hamiltonian defined in spherical coordinates as

$$\hat{H} = \nabla^2 + V(\hat{r}, \hat{\theta}, \hat{\phi}). \tag{4.1.1}$$

However, due to the spherical symmetric nature of the problem such that $V(\hat{r}, \hat{\theta}, \hat{\phi}) = V(\hat{r})$, the Hamiltonian in equation (4.1.1) can be separated into a radial part and an angular part where the latter does not effect the energy spectrum, while the wave functions depend on the angular quantum numbers. Therefore, we only need to solve for the eigenvalues of the radial Schrödinger equation through the method of bootstrapping to determine the spectrum of the Hydrogen atom. This change in the problem requires us to modify the chosen moment sequence $\{s_n\}$ and its associated generating polynomial operator $\hat{\mathcal{O}}$, as well as the recursion relation obtained in equation (2.4.21) which will be discussed in Sections 4.3 and 4.4 respectively.

Second, the method in Chapter 2 was applied to the entire domain $\mathbb{R}$, $(-\infty, +\infty)$, while the radial coordinate in the Hydrogen atom problem is confined to the half-line $\mathbb{R}_+$, $[0, +\infty)$. This difference in the domain of the problem requires us to use the

Stieltjes moment problem instead of the Hamburger moment problem which will be discussed in Section 4.2.

4.2 Stieltjes Moment Problem

Contrary to the Hamburger moment problem, Stieltjes moment problem searches for a positive integration measure μ on the domain $[0, +\infty)$, for a real sequence $\{s_n\}$ where $n \geq 0$, that converges and satisfies the integral [27]

$$s_n = \int_0^\infty x^n d\mu. \tag{4.2.1}$$

The Stieltjes moment problem states that if there exists a positive integration measure μ for the moment sequence $\{s_n\}$, the functional L satisfies $L(|P|^2) \geq 0$ and $L(x\,|P|^2) \geq 0, \forall P \in \mathbb{C}[x]$ [38]. Then the $(n+1) \times (n+1)$ Hankel matrices H_n and $\tilde{H}_n$ can be defined as

$$H_n(s) := (s_{i+j})\,, \quad \tilde{H}_n(s) := (s_{i+j+1}), \tag{4.2.2}$$

where $0 \leq i, j \leq n$, then, H_n and $\tilde{H}_n$ are both positive semidefinite.

In Appendix C, we discuss an interesting fact about bootstrapping even potentials on the half-line.

4.3 Bootstrapping the Hydrogen

Since we are only interested in the radial part of the Hamiltonian, we can use the radial operator $\hat{r}$ to define the Stieltjes moment problem through the operators [24]

$$\hat{\mathcal{O}} = \sum_t c_t \hat{r}^t\,, \quad \hat{\tilde{\mathcal{O}}} = \sqrt{\hat{r}} \sum_t c_t \hat{r}^t, \tag{4.3.1}$$

We note that $\hat{\tilde{\mathcal{O}}}$ is well-defined for $r > 0$. The positivity condition for the operators can be shown simply through the methods shown in equation (2.5.2).

Similar to the Hamburger moment problem, we form a real and infinite sequence $\{s_n\}$ through the expectation values of the powers of the radial operator $\hat{r}$ such that

$$s_n = \{\langle \hat{r}^n \rangle\}. \tag{4.3.2}$$

Then for the radial operator equation (4.2.1) becomes

$$\begin{aligned} s_n &= \int_0^\infty r^n d\mu, \\ &= \int_0^\infty \psi^* \hat{r}^n \psi dx, \\ &= \int_0^\infty |\psi|^2 \hat{r}^n dx = \langle \hat{r}^n \rangle, \end{aligned} \tag{4.3.3}$$

which once again yields an integration measure μ defined in equation (2.3.7) which satisfies the conditions defined in equation (2.3.8). Therefore, we conclude that the sequence $\{\langle \hat{r}^n \rangle\}$ also forms a moment sequence, which we will call the "radial moments".

Since the infinite set generated through $\langle \hat{r}^n \rangle$ form a moment sequence the Hankel matrices H_n and $\tilde{H}_n$ defined in equation (4.2.2) should be positive semidefinite. We once again call H_n as the "bootstrap matrix" and denote as $\mathcal{M}$ while $\tilde{H}_n$ as the "half-line bootstrap matrix" and denote it as $\tilde{\mathcal{M}}$. As before, the dimensions of both of these matrices are given by the depth of the bootstrap, K defined in equation (2.3.10). The elements of the bootstrap matrix $\mathcal{M}$ and half-line bootstrap matrix $\tilde{\mathcal{M}}$ are given by

$$\mathcal{M}_{ij} = \langle \hat{r}^{i+j} \rangle, \quad \tilde{\mathcal{M}}_{ij} = \langle \hat{r}^{i+j+1} \rangle, \tag{4.3.4}$$

where $0 \leq i, j \leq K-1$ and the matrix $\mathcal{M}$ at depth K is

$$\mathcal{M} := \begin{bmatrix} \langle \hat{r}^0 \rangle & \langle \hat{r}^1 \rangle & \langle \hat{r}^2 \rangle & \cdots & \langle \hat{r}^{K-1} \rangle \\ \langle \hat{r}^1 \rangle & \langle \hat{r}^2 \rangle & \langle \hat{r}^3 \rangle & \cdots & \langle \hat{r}^{K} \rangle \\ \langle \hat{r}^2 \rangle & \langle \hat{r}^3 \rangle & \langle \hat{r}^4 \rangle & \cdots & \langle \hat{r}^{K+1} \rangle \\ \vdots & \vdots & \vdots & \ddots & \vdots \\ \langle \hat{r}^{K-1} \rangle & \langle \hat{r}^{K} \rangle & \langle \hat{r}^{K+1} \rangle & \cdots & \langle \hat{r}^{2K-2} \rangle \end{bmatrix}, \tag{4.3.5}$$

while the matrix $\tilde{\mathcal{M}}$ at depth K is

$$\tilde{\mathcal{M}} := \begin{bmatrix} \langle \hat{r}^1 \rangle & \langle \hat{r}^2 \rangle & \langle \hat{r}^3 \rangle & \cdots & \langle \hat{r}^{K} \rangle \\ \langle \hat{r}^2 \rangle & \langle \hat{r}^3 \rangle & \langle \hat{r}^4 \rangle & \cdots & \langle \hat{r}^{K+1} \rangle \\ \langle \hat{r}^3 \rangle & \langle \hat{r}^4 \rangle & \langle \hat{r}^5 \rangle & \cdots & \langle \hat{r}^{K+2} \rangle \\ \vdots & \vdots & \vdots & \ddots & \vdots \\ \langle \hat{r}^{K} \rangle & \langle \hat{r}^{K+1} \rangle & \langle \hat{r}^{K+2} \rangle & \cdots & \langle \hat{r}^{2K} \rangle \end{bmatrix}, \tag{4.3.6}$$

where both matrices $\mathcal{M}$ and $\tilde{\mathcal{M}}$ are symmetric as expected from Hankel matrices.

We once again note that the radial moment $\langle \hat{r}^0 \rangle = 1$ which can be shown in a manner similar to that given in equation (2.3.13).

The bootstrap method for the Hydrogen atom closely follows the approach discussed in Chapter 2. We once again impose the stronger constraints that the matrices $\mathcal{M}$ and $\tilde{\mathcal{M}}$ must both be positive definite. The main difference is that, only the search points that yield positive definite matrices for both $\mathcal{M}$ and $\tilde{\mathcal{M}}$ are considered to be possible solutions for the system and carried forward to the higher iterations.

4.4 Radial Moment Recursion Relation

The potential for the Hydrogen atom is the Coulomb potential, which depends only on the radial coordinate $\hat{r}$. This makes the problem spherically symmetric, $V(\hat{r}, \hat{\theta}, \hat{\phi}) = V(\hat{r})$. Therefore, we only need to focus on the radial part of the spherical Hamiltonian which is [28]

$$H = \frac{1}{2}\hat{p}_r^2 + \left[\frac{\ell(\ell+1)}{2\hat{r}^2} + V(\hat{r})\right], \tag{4.4.1}$$

where ℓ is the angular momentum quantum number. Notice that this Hamiltonian has a term

$$F(\hat{r}) = \frac{\ell(\ell+1)}{2\hat{r}^2},$$

which is called the "centrifugal potential" or "centrifugal barrier" which depends on the radial operator $\hat{r}$. Then, this extra term should be treated just as any other potential function in the recursion relation (2.4.21) such that

$$\langle \hat{r}^t F'(\hat{r}) \rangle = -\ell(\ell+1)\langle \hat{r}^{t-3} \rangle, \quad 2t\langle \hat{r}^{t-1} F(\hat{r}) \rangle = \ell(\ell+1)t\langle \hat{r}^{t-3} \rangle. \tag{4.4.2}$$

If we implement equation (4.4.2) into equation (2.4.21) we obtain the general recursion relation for spherically symmetric potentials as

$$\begin{aligned} 2tE\langle \hat{r}^{t-1} \rangle = -(t-1)\left[\frac{1}{2}t(t-2) - \ell(\ell+1)\right]\langle \hat{r}^{t-3} \rangle \\ + \langle \hat{r}^t V'(\hat{r}) \rangle + 2t\langle \hat{r}^{t-1} V(\hat{r}) \rangle. \end{aligned} \tag{4.4.3}$$

4.5 Effective Potential in the Hydrogen Atom

In its usual form in SI units, the Coulomb potential is

$$V(\hat{r}) = -\frac{e^2}{4\pi\epsilon_0}\frac{1}{\hat{r}}, \tag{4.5.1}$$

while in atomic units it is

$$V(\hat{r}) = -\frac{1}{\hat{r}}. \tag{4.5.2}$$

Accounting for the centrifugal barrier term, the effective potential for the system is given as

$$V_{\text{eff}}(\hat{r}) = \frac{\ell(\ell+1)}{2\hat{r}^2} - \frac{1}{\hat{r}}. \tag{4.5.3}$$

Figure 4.1 shows the graph of the effective potential $V_{\text{eff}}(\hat{r})$ in the configuration space for $\ell = 0, 1, 2$. From the figure we conclude that there are infinitely many bound states for the Hydrogen atom which all have energy $E \leq 0$.

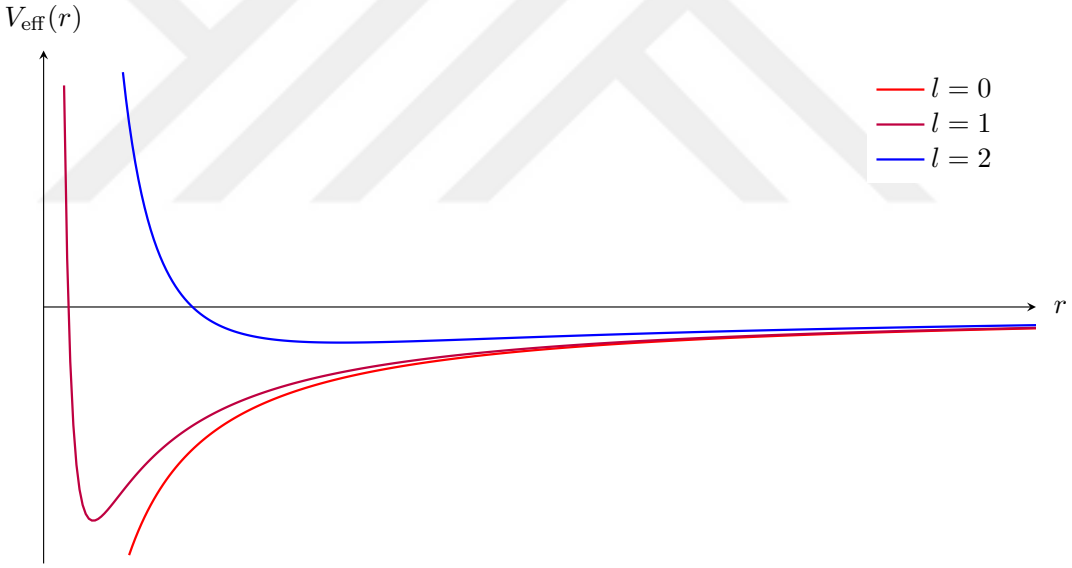

Figure 4.1: Plot of the effective potential $V_{\text{eff}}(r)$ for $l = 0, 1, 2$.

4.6 Recursion Relation, Search Space and the Bootstrap Matrix

In this section we define the theoretical perquisites discussed in Chapter 2 for the Hydrogen Atom system.

4.6.1 Hydrogen Atom Recursion Relation

Evaluating the potential dependent identities in equation (4.4.3) for the Coulomb potential we obtain

$$\langle \hat{r}^t V'(\hat{r}) \rangle = \langle \hat{r}^{t-2} \rangle \,, \quad 2t \langle \hat{r}^{t-1} V(\hat{r}) \rangle = -2t \langle \hat{r}^{t-2} \rangle. \tag{4.6.1}$$

If we implement the identities found in equation (4.6.1) into equation (4.4.3) we obtain the recursion relation for the Hydrogen atom as

$$8tE\langle \hat{r}^{t-1} \rangle = -4(2t-1)\langle \hat{r}^{t-2} \rangle - (t-1)\left[t(t-2) - 4\ell(\ell+1)\right] \langle \hat{r}^{t-3} \rangle, \tag{4.6.2}$$

which is the moment recursion relation for the Hydrogen atom.

We note that the obtained recursion relation exactly matches the Kramers–Pasternak recursion relation [39].

4.6.2 Hydrogen Atom Search Space

The search space for the Coulomb potential is a bit more tricky since the potential is a negative power function of $\hat{r}$ instead of a polynomial which, nevertheless, does not contradict the discussion given in Section 2.6. This is because the potential is defined on the half-line $\mathbb{R}_+$ such that $V(\hat{r}) > 0$ which allows us to avoid the singularity at 0.

The Coulomb potential is a first degree power function which is an odd function of $\hat{r}$ such that $V(-\hat{r}) = -V(\hat{r})$. Then as discussed in the penultimate paragraph of Section 2.6 the cardinality $|S|$ of the minimal search space needed to initiate the recursion relation found in (4.6.2) is

$$|S| = 1. \tag{4.6.3}$$

Since every search space S should contain energy E as an element, the search space element S^1 is simply E. Then the minimal search space S for the Hydrogen atom is

$$S = \{S^1 \equiv E\}, \tag{4.6.4}$$

which is the only element that should be specified in the algorithm.

4.6.3 Hydrogen Atom Matrix Terms and Constraints on the Search Space

We want to generate the non-zero elements of $\mathcal{M}$ using equation (4.6.2). Recursion can be initiated with $t = 1$. This yields,

$$\left\langle \frac{1}{\hat{r}} \right\rangle = -2E, \tag{4.6.5}$$

which is nothing but the virial theorem.

For $t = 2$, the recursion relation gives

$$\langle \hat{r} \rangle = -\frac{3}{4E} - \frac{1}{4E}\ell(\ell+1)\left\langle \frac{1}{\hat{r}} \right\rangle. \tag{4.6.6}$$

Implementing the identity in equation (4.6.5) back into equation (4.6.6) we obtain the first non-zero moment $\langle \hat{r} \rangle$, in terms of energy E as

$$\langle \hat{r} \rangle = -\frac{3}{4E} - \frac{1}{2}\ell(\ell+1). \tag{4.6.7}$$

We may note in passing that, from the virial theorem for the Hydrogen atom given in equation (4.6.5) we can put an upper bound on energy E since

$$E = -\frac{1}{2}\left\langle \frac{1}{r} \right\rangle. \tag{4.6.8}$$

All radial moments $\langle \hat{r}^n \rangle$ where $n \in \mathbb{Z}$ are defined in the domain $\langle \hat{r}^n \rangle \geq 0$ since the domain of r is the positive real line $\mathbb{R}_+$. Therefore, the upper bound on the energy E for the Hydrogen atom is given as $E \leq 0$ as expected from the Figure 4.1.

This time, we work with an odd potential so, Using equation (4.6.2), the first four moments $\langle \hat{r}^t \rangle$ can be calculated as

$$\begin{aligned}
\langle \hat{r}^0 \rangle &= 1, \\
\langle \hat{r} \rangle &= -\frac{3}{4E} - \frac{1}{2}\ell(\ell+1), \\
\langle \hat{r}^2 \rangle &= \frac{5}{8E^2} + \frac{3}{4E}\ell(\ell+1) - \frac{1}{4E}, \\
\langle \hat{r}^3 \rangle &= -\frac{7}{8E}\langle \hat{r}^2 \rangle + \left[-\frac{3}{4E} + \frac{3}{8E}\ell(\ell+1) \right] \langle \hat{r} \rangle.
\end{aligned} \tag{4.6.9}$$

4.7 Matrix Rescaling

The moments $\langle \hat{r}^n \rangle$ generated from the hydrogen recursion relation defined in equation (4.6.2) grow exponentially fast, reaching the order $\sim 10^{30}$ for $\langle \hat{r}^{25} \rangle$. This growing

cause the Cholesky-Banachiewicz algorithm to lose its numerical precision, even at relatively low values of depth K and subsequently causes the multiple splitting problem. Nevertheless, we can optimize this problem for odd potentials by implementing a matrix element transformation defined as [40]

$$\mathcal{M}_{ij} \to \frac{\mathcal{M}_{ij}}{\mathcal{M}_{i1}\mathcal{M}_{j1}}, \tag{4.7.1}$$

where, $0 \geq i\,, j \geq K-1$. This transformation preserves the signs of the eigenvalues of the matrix $\mathcal{M}$ hence also its positive definiteness property. We cannot apply this transformation to bootstrap matrices generated for even potentials, since the odd moments for even potentials are zero as we have shown in equation (2.6.7), and would involve divisions by zero which are ill-defined.

Here, we present an example for this transformation for a given matrix. Assume a 2×2 matrix A such that

$$A = \begin{bmatrix} a & b \\ c & d \end{bmatrix}, \tag{4.7.2}$$

Then, the transformed matrix B would have the form

$$B = \begin{bmatrix} \dfrac{a}{b^2} & \dfrac{1}{d} \\ \dfrac{c}{db} & \dfrac{1}{d} \end{bmatrix}. \tag{4.7.3}$$

We apply this transformation once for both of the matrices $\mathcal{M}$ and $\tilde{\mathcal{M}}$.

4.8 Original Bootstrap on Hydrogen Atom

We now apply the "original bootstrap" algorithm to the Hydrogen atom. We note that the exact energy levels for the system is well-known and in atomic units are given by

$$E_n = -\frac{1}{2n^2}. \tag{4.8.1}$$

We aim to see how well the bootstrap method captures this spectrum.

We investigate the Hydrogen atom system in two different ways. First, we look at the $\ell = 0$ case to examine the depth evolution for the algorithm. Then, we analyze the final results for various ℓ values to understand the effect of ℓ on the algorithm.

We use mostly the same initialization parameters for both cases, only changing the initial search space bounds S. As ℓ increases, the range of possible n values that the algorithm searches will change, which will be discussed further in Section 4.8.2.

We run the original bootstrap program on Python with the initialization parameters as the following:

- Precision $\tau_1 = 200$ for search space element E.
- Initial depth $K_i = 5$ and final depth $K_f = 20$.
- Convergence limit $\epsilon = 0.001$.

The initial search space bounds for the energy E will be defined in the relevant subsections.

4.8.1 $\ell = 0$ Case

For $\ell = 0$ case we use the following initial search space bounds:

- Search space bounds for $E \in S:\ [-1, -0.001]$.

Figure 4.2 presents the results of the original bootstrap algorithm for the Hydrogen atom system with $\ell = 0$.

The graph demonstrates that, for smaller depths K, the original bootstrap algorithm separates the main interval into smaller intervals around the exact energy levels. At depth $K = 13$, the algorithm identified the ground level state as a converged point and identified the intervals for the first and second excited states, close to the expected values. However, as the depth of the bootstrap reaches $K = 15$, the multiple splitting of intervals start and the algorithm begins to identify an increasing number of incorrect results. When the algorithm reaches its final depth, it has identified a total of "250" points as possible solutions within the energy search space of $[-1, -0.01]$, rather than the expected thirty solutions.

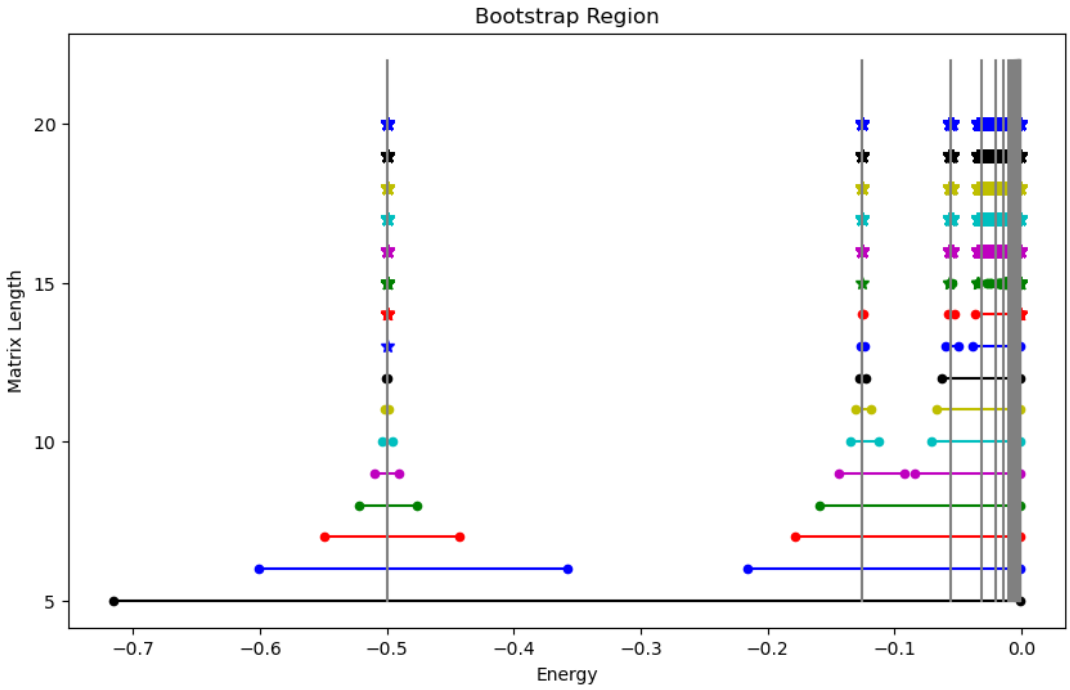

Figure 4.2: Original Bootstrap Results for Hydrogen Atom for $\ell = 0$

4.8.2 Various ℓ Cases

In the Hydrogen atom, the value of the angular momentum quantum number ℓ is constrained by the value of the principal quantum number n such that $0 \leq \ell \leq n-1$. This constraint implies that not all energy levels n are defined for each value of ℓ. If we solve the inequality for the minimum value of the principal quantum number n_{min} depending on each different ℓ value, we obtain

$$n_{\text{min}} = \ell + 1. \tag{4.8.2}$$

This can be better explained through the following examples:

i. When $\ell = 0$, we expect the bootstrap algorithm to identify the states $n = 1, 2, 3, 4, \cdots$

ii. When $\ell = 1$, we expect the bootstrap algorithm to identify the states $n = 2, 3, 4, 5, \cdots$

iii. When $\ell = 2$, we expect the bootstrap algorithm to identify the states $n = 3, 4, 5, 6, \cdots$

We will investigate the various ℓ cases for values of ℓ between $0 \leq \ell \leq 5$. This means that for $\ell = 5$ the minimum value of n will be $n = 6$ which implies that the theoretical energy for the level is $E_6 = -0.0138$. This is very close to the lower bound we have defined for the $\ell = 0$ case. Hence, for various ℓ cases, we use the following initial search space bounds:

- Search space bounds for $E \in S$: $[-1, -10^{-6}]$.

Figure 4.3 depicts the results of applying the original bootstrap algorithm to the Hydrogen atom system for various values of ℓ. In this graph, the horizontal axis represents the ℓ values, while the vertical axis represents the logarithm of the energy.

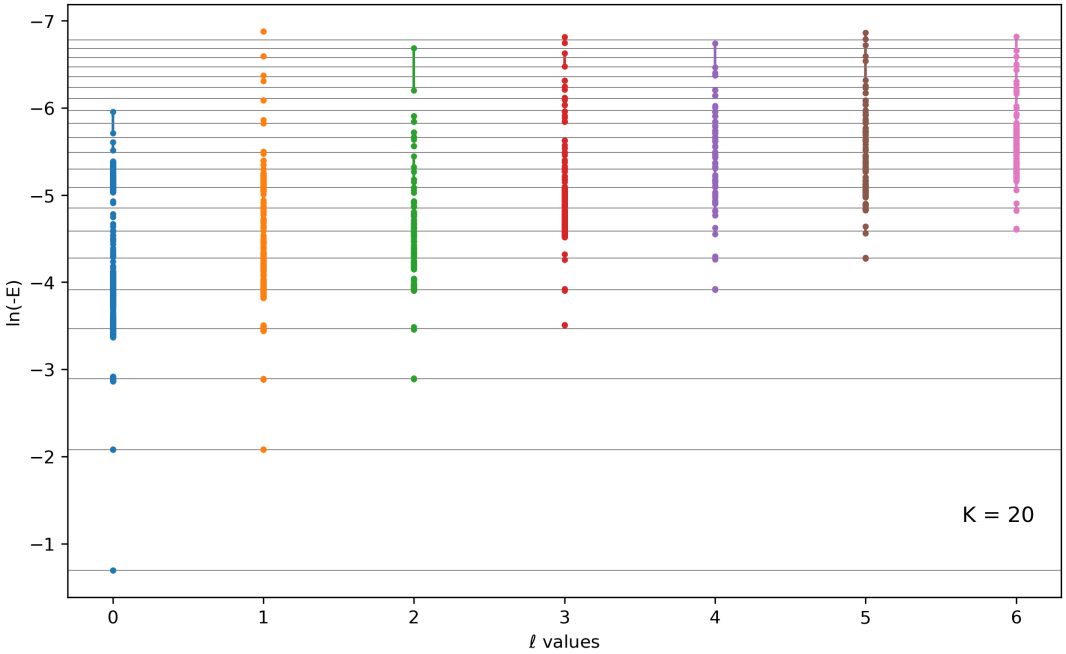

Figure 4.3: Original Bootstrap Results for Hydrogen Atom for Various ℓ

Throughout this chapter unless specified otherwise all various ℓ graphs follow the same format. All various ℓ graphs show the final results for $K = K_f$. We use the logarithm of the energy to make the graph more readable since, as the value of n gets larger, the energy levels become too close to each other, making the graph difficult to read. Each ℓ value is represented with its own color for easier readability, and the exact energy levels are shown as gray lines parallel to the horizontal axis.

It is apparent from the graph that, the algorithm can find the first three solutions for

the system within some margin of error for almost all ℓ cases, although the third solution for $\ell = 5$ is hard to notice. However, for higher energy states, the graph shows almost a continuous spectrum of faulty converged points. This indicates that while the algorithm is somewhat accurate for lower energy states for any value of ℓ, it becomes unreliable for higher energy states.

As can be seen from both $\ell = 0$ and various ℓ cases graphs the original bootstrap algorithm shows similar results to those obtained for SHO system. Initially, the algorithm correctly identifies the lower energy levels within a reasonable margin of error. However, as the depth increases, the algorithm generates a large number of incorrect results. Without knowing the exact energy levels, distinguishing true solutions from faulty results becomes impossible, reducing the algorithm's reliability and its applicability to systems with unknown energy eigenstates.

4.9 One Split Bootstrap on Hydrogen Atom

In this section, we try to resolve the problems of the original bootstrap algorithm through the methods explained in Chapter 2 in Section 2.8.

We once again use mostly the same initialization parameters for both $\ell = 0$ and various ℓ cases, only changing the initial search space bounds S. We run the "one split bootstrap" program on Python with the common initialization parameters as the following:

- Precision $\tau_1 = 200$ for search space element E.
- Initial depth $K_i = 5$ and final depth $K_f = 25$.
- Convergence limit $\epsilon = 0.001$.

The initial search space bounds for the energy E will be defined in the relevant subsections.

4.9.1 $\ell = 0$ Case

For $\ell = 0$ case we use the following initial search space bounds:

- Search space bounds for $E \in S$: $[-1, -0.001]$.

The graph in Figure 4.4 displays the results of the one split bootstrap algorithm for the Hydrogen atom system with $\ell = 0$.

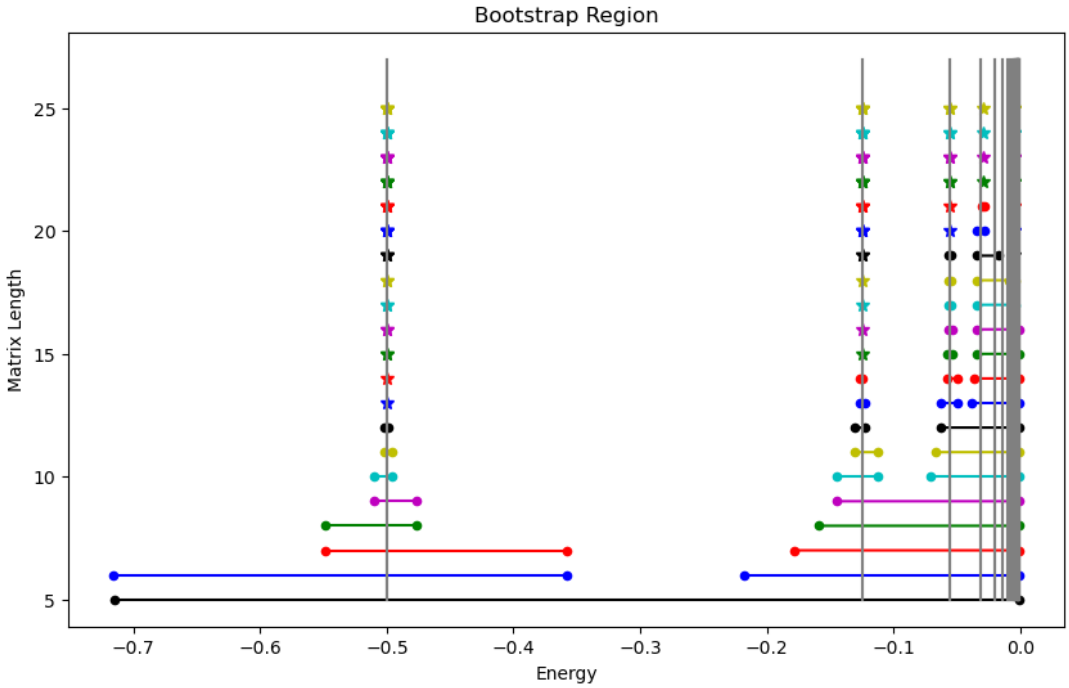

Figure 4.4: One Split Bootstrap Graph for Hydrogen Atom for $\ell = 0$

The graph makes it evident that the one split bootstrap algorithm performs significantly better compared to the original bootstrap algorithm. At depth $K = 15$, the algorithm is still correctly splitting around the energy eigenstates without multi-splitting. This indicates that the algorithm is performing as expected at this depth.

At depth $K = 20$, the algorithm correctly splits around the third excited state, converging it to a solution at $K = 22$. However, at depth $K = 22$ the algorithm incorrectly determines that there are no positive definite intervals left in the system, hence missing all remaining solutions. This is likely due to numerical errors generated in the recursion relation combined with the numerical sensitivity of the Cholesky-

Banachiewicz algorithm.

At the predetermined final depth $K = 25$, the program has identified five results given in Table 4.1 in a sorted format.

Table 4.1: One Split Bootstrap Results for Hydrogen Atom with $\ell = 0$

Bootstrapped Energy	Bootstrapped Energy
$-0.4997 \pm 4.76 \times 10^{-4}$	$-0.0296 \pm 3.32 \times 10^{-4}$
$-0.1248 \pm 4.89 \times 10^{-4}$	$-0.0053 \pm 4.47 \times 10^{-4}$
$-0.0553 \pm 4.46 \times 10^{-4}$	

The table indicates that the algorithm successfully found the ground state, the first three excited states, and the ninth excited state within an acceptable margin of error. The algorithm did not find any incorrect results. However, it failed to identify the remaining 25 possible solutions out of the 30 possible energy levels.

4.9.2 Various ℓ Cases

For various ℓ cases we use the following initial search space bounds:

- Search space bounds for $E \in S:\ [-1, -10^{-6}]$.

The graph in Figure 4.5 reveals the results of the one split bootstrap algorithm for the Hydrogen atom system with various ℓ values.

From the graph, it is obvious that the one split bootstrap algorithm performs significantly better than the original bootstrap. For all ℓ values, it correctly identifies the ground state energy and the first two excited states. For some ℓ values, it also provided a good estimation for the third excited state. However, for $\ell = 1, 3, 4, 5$ the algorithm produced some results that may or may not represent actual energy eigenstates. These results could be faulty convergences due to numerical errors, as the energy eigenvalues are very close at these points, even on a logarithmic scale.

There is also a difference in number of results between the $\ell = 0$ value in the various ℓ cases and the $\ell = 0$ case. In the $\ell = 0$ case the algorithm produces five results while

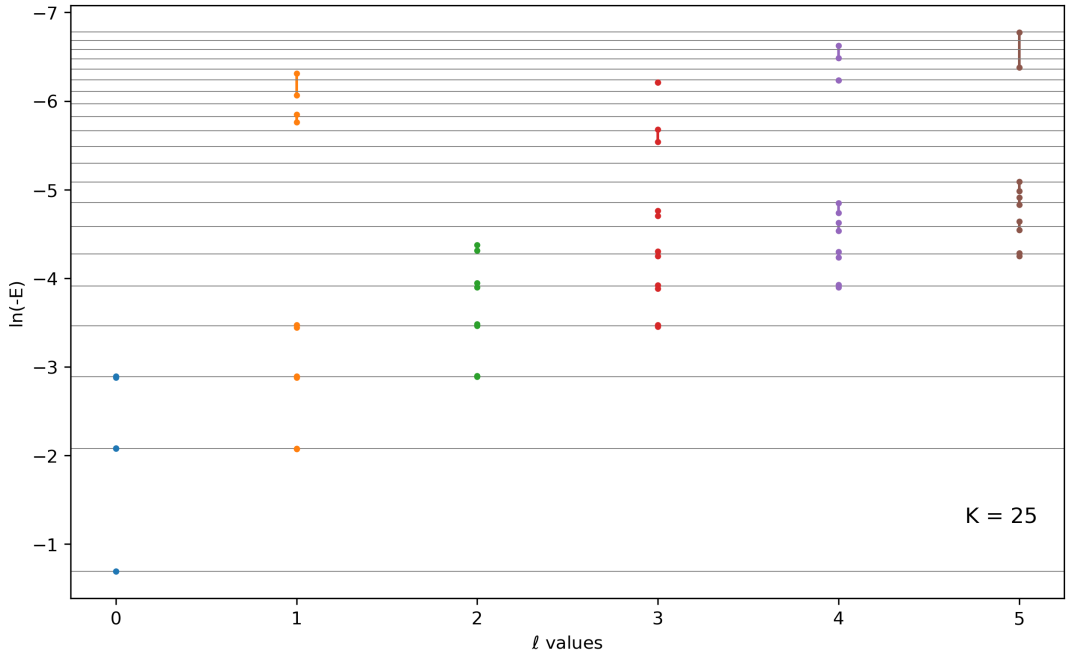

Figure 4.5: One Split Bootstrap Graph for Hydrogen Atom for Various ℓ

in various ℓcases, it only produces three. This difference in the number of results occurred because we increased the upper bound of the initial search space bounds for E while keeping the precision τ_1 the same while investigating the various ℓ cases. Therefore, we worked with much lower precision than we worked in the $\ell = 0$ case, causing the algorithm to miss the energy levels of the third and ninth excited states.

Both the $\ell = 0$ and various ℓ graphs highlight that the one split bootstrap algorithm works significantly better for the Hydrogen atom compared to the SHO system. The algorithm correctly identifies the lower energy levels without producing repeated results or random points as solutions. Additionally, it predicts some higher energy levels within some margin of error. However, it still misses most of the solutions, making it not ideal for applying to systems with unknown energy states.

4.10 Guided Bootstrap on Hydrogen Atom

In this section, we apply the "guided bootstrap" algorithm to the Hydrogen atom system at an attempt to resolve the problems of the original and one split bootstrap

algorithms. We once again use mostly the same initialization parameters for both $\ell = 0$ and various ℓ cases, only changing the initial search space bounds S. We run the one split bootstrap program on Python with the common initialization parameters as the following:

- Precision $\tau_1 = 200$ for search space element E.
- Initial depth $K_i = 5$.
- Initial convergence limit $\epsilon_i = 0.01$.
- Maximum value of MSE $\Upsilon = 100$ for accepting an energy model.
- Number of maximum trials $\rho = 10$ for forced convergence.

The initial search space bounds for the energy E will be defined in the relevant subsections.

4.10.1 $\ell = 0$ Case

For $\ell = 0$ case we use the following initial search space bounds:

- Search space bounds for $E \in S: \ [-1, -0.001]$.

We once again start with the "initialization bootstrap" part where we aim to only identify the initial energy intervals without further splitting or shrinking them. This method provides us a starting point for predicting a guided search space S_G.

Figure 4.6 shows the initialization bootstrap results for the Hydrogen atom system with $\ell = 0$.

The graph indicates that, the algorithm successfully identifies the first three energy intervals until the depth becomes $K = 14$. When the depth reaches $K = 15$, as it happened with the original bootstrap, the multi-splitting of intervals start, causing the program to exit with the three found intervals. We then sort these intervals from smallest to largest and assign each interval to a state by linear incrementation $(+1)$. These intervals and their assigned states are listed in Table 4.2.

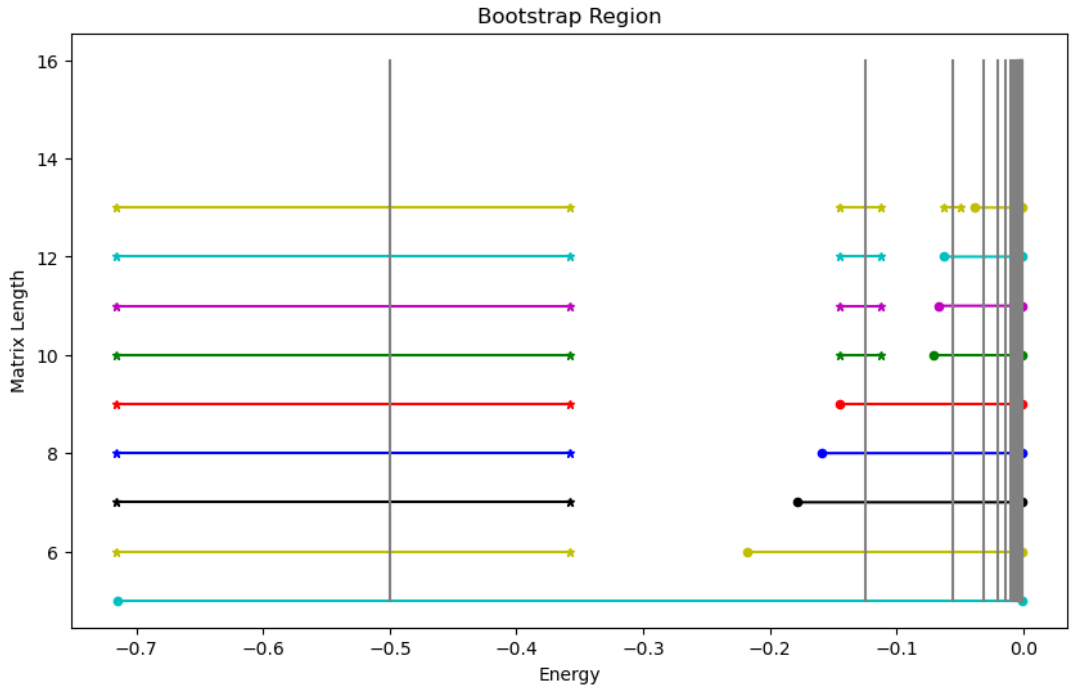

Figure 4.6: Initialization Bootstrap Graph for Hydrogen Atom for $\ell = 0$

Table 4.2: Initialization Bootstrap Results for Hydrogen Atom for $\ell = 0$

State	Found Energy Interval
1	-0.5369 ± 0.1794
2	-0.1283 ± 0.0163
3	-0.0561 ± 0.0064

The table reveals that all three of the energy intervals found contain the theoretical exact energy of their respective related states. The largest interval is the ground state, with a length of 0.3588. We assign this interval length as the significant interval length for the system and initiate the second part of the guided bootstrap.

With the energy intervals found, we first determine the general distance behavior for the intervals. For the Hydrogen atom system, it is apparent that the behavior should be "decreasing" since the theoretical energy values for the system is proportional to n^{-2}. The algorithm determines the behavior of the energy eigenstates as "decreasing" and attempts at generating the auxiliary extrapolation function of the system through power function models. The auxiliary extrapolation function models the relationship

between the identified intervals and helps estimate possible intervals for higher energy states.

Figure 4.7 illustrates the auxiliary extrapolation function fitted to the midpoints of the intervals found in the initialization bootstrap for the Hydrogen atom system with $\ell = 0$.

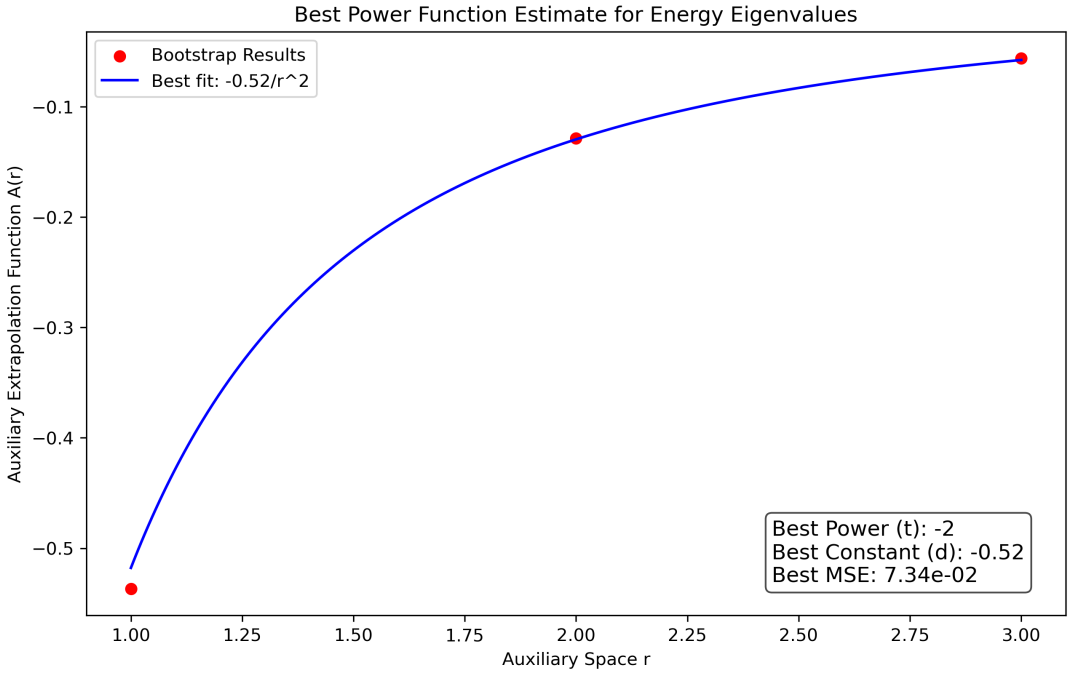

Figure 4.7: Auxiliary Extrapolation Function Graph for Hydrogen Atom for $\ell = 0$

The best auxiliary extrapolation function that can be found for the system is

$$A(r) = -\frac{0.52}{r^2}, \tag{4.10.1}$$

which provides a good estimate for the energy eigenstates of the system defined in equation (4.8.1) with an MSE value of 7.34×10^{-2}. With the found intervals and the significant interval length for the system, we predict reasonable intervals from the fourth to the sixth eigenstates. Since $A(r) \sim r^{-2}$, interval lengths for the predicted states get smaller with respect to the significant interval length. The predicted intervals for the higher energy levels are given in Table 4.3.

The table makes it clear that all related theoretical energy eigenstates of the system are in the predicted intervals.

Table 4.3: Guessed Energy Intervals for Hydrogen Atom for $\ell = 0$

State $\rightarrow$ Guessed Energy Interval	State $\rightarrow$ Guessed Energy Interval
$1 \rightarrow -0.5369 \pm 0.1794$	$4 \rightarrow -0.0321 \pm 0.0028$
$2 \rightarrow -0.1290 \pm 0.0223$	$5 \rightarrow -0.0206 \pm 0.0014$
$3 \rightarrow -0.0571 \pm 0.0066$	$6 \rightarrow -0.0143 \pm 0.0008$

Finally, we apply the "no split bootstrap" to the Hydrogen atom system. We first generate the guided search space S_G, using the boundaries of the estimated energy intervals. In the no split bootstrap method, we prevent the intervals from splitting, allowing them only to shrink from the sides. Since we expect a single solution in each interval, we force each interval to converge to a single point. Figure 4.8 shows the results of the no split bootstrap for the Hydrogen atom system with $\ell = 0$.

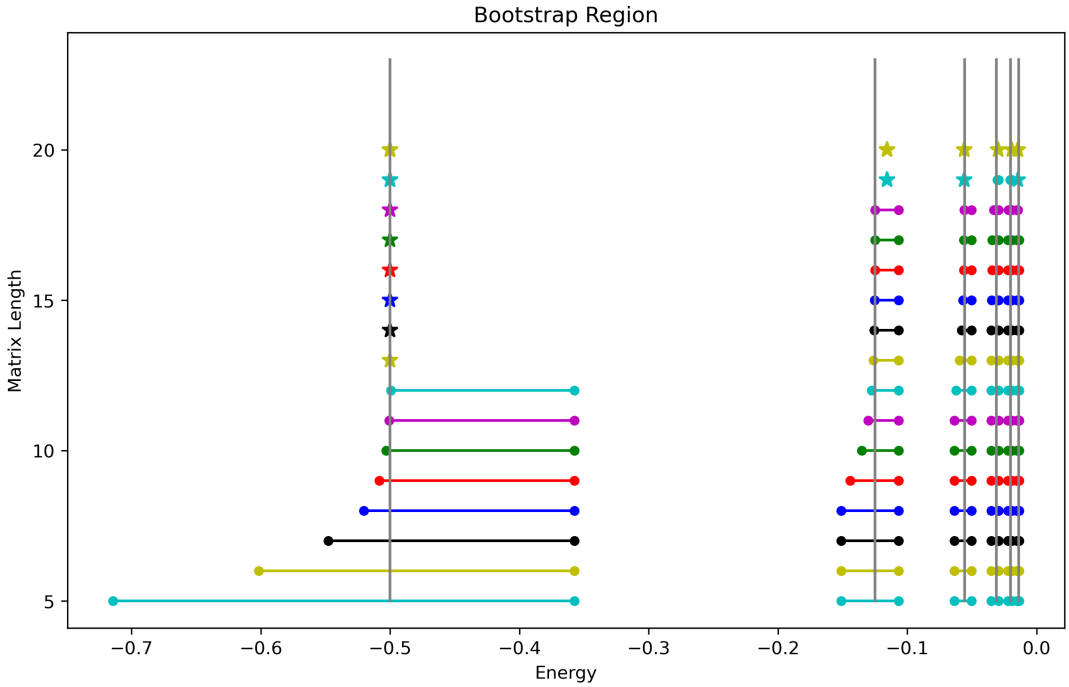

Figure 4.8: No Split Bootstrap Graph for Hydrogen Atom for $\ell = 0$

As anticipated, the graph suggests that the no split bootstrap algorithm converged every search space bound to a single point at depth $K = 20$. The results of the no split bootstrap algorithm are given in Table 4.4. We also show the exact energy levels and the percentage errors calculated from the midpoints of the intervals in this table.

Table 4.4: Guided Bootstrap Results for Hydrogen Atom for $\ell = 0$

States	Bootstrapped Energy	Exact Energy	Percentage Error
1	-0.5001 ± 0.0	-0.5000	0.0274
2	-0.1158 ± 0.0091	-0.1250	7.3673
3	-0.0559 ± 0.0	-0.0556	0.6103
4	$-0.0297 \pm 8.83 \times 10^{-5}$	-0.0312	4.9292
5	$-0.0192 \pm 2.06 \times 10^{-5}$	-0.0200	4.0438
6	$-0.0144 \pm 4.32 \times 10^{-5}$	-0.0139	3.9908

When we analyze the table, we observe that the ground state and second excited state energy intervals found from the initialization bootstrap show high precision with percentage errors below $\%0.7$. The predicted energy levels for the higher states also show good accuracy. However, there is a a problem with the first excited state, which shows a significant shift from the theoretical value, with a percentage error of $\%7.3673$. Interestingly, the one split bootstrap method found the first excited state with better accuracy.

4.10.2 Various ℓ Cases

For various ℓ cases we use the following initial search space bounds:

- Search space bounds for $E \in S: \ [-1, -10^{-6}]$.

We once again start with the initialization bootstrap algorithm. Figure 4.9 shows the initialization bootstrap results for the Hydrogen atom system for various ℓ cases.

As seen in the graph, the algorithm successfully identifies the first three energy intervals for all ℓ cases. With the found energy intervals, the algorithm once again determines the general distance behavior for all ℓ cases as "decreasing" and attempts at generating the auxiliary extrapolation function of the system through power function models.

The state assignment process is different for Hydrogen since all $n_{\text{min}} = \ell + 1$. We

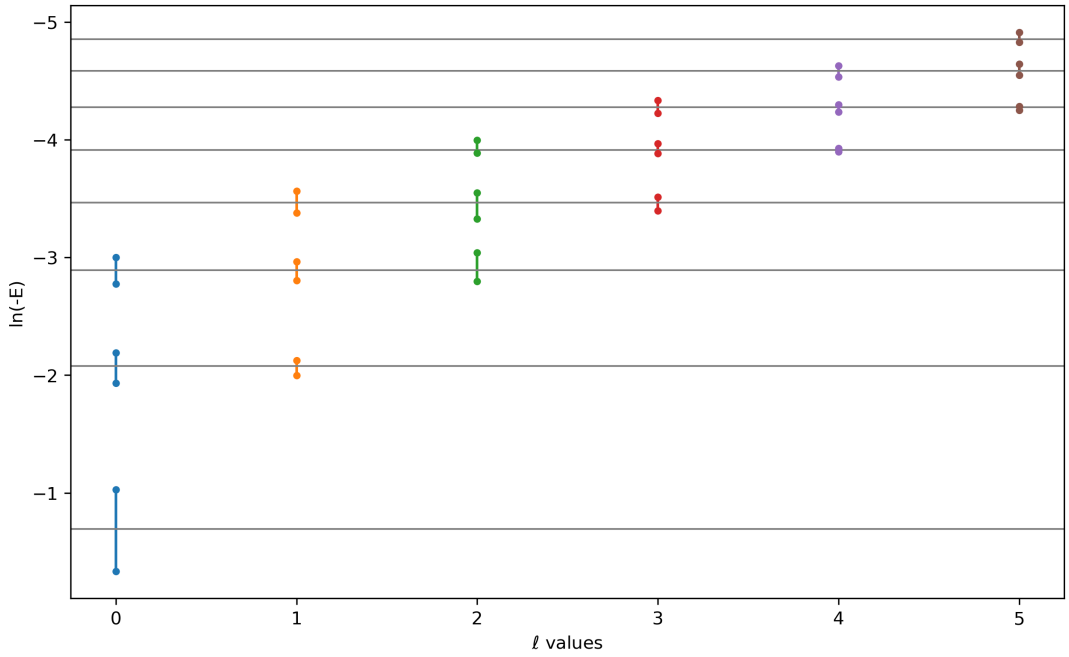

Figure 4.9: Initialization Bootstrap Graph for Hydrogen Atom for Various ℓ

generate the states n for each different ℓ value, starting from $\ell + 1$ and increment in one for each state.

Figure 4.10 presents the auxiliary extrapolation functions fitted to the midpoints of the intervals found in the initialization bootstrap for the Hydrogen atom system.

The best auxiliary extrapolation functions that can be found for the system are

$$\begin{aligned} \ell = 0 &\implies A(r) = -\frac{0.52}{r^2}, \\ \ell = 1, 2, 3, 4, 5 &\implies A(r) = -\frac{0.50}{r^2}, \end{aligned} \tag{4.10.2}$$

which provides good estimates for the energy eigenstates of the system defined in equation (4.8.1) with the highest MSE value among them is found to be 7.34×10^{-2}.

Finally, we apply the no split bootstrap to the various ℓ values of the Hydrogen atom system. Figure 4.11 shows the results of the no split bootstrap for the Hydrogen atom system.

The graph reveals that, consistent with our expectations, the no split bootstrap algorithm converged every search space bound to a single point for every ℓ value, obtaining the expected six results. The results of the no split bootstrap algorithm are given

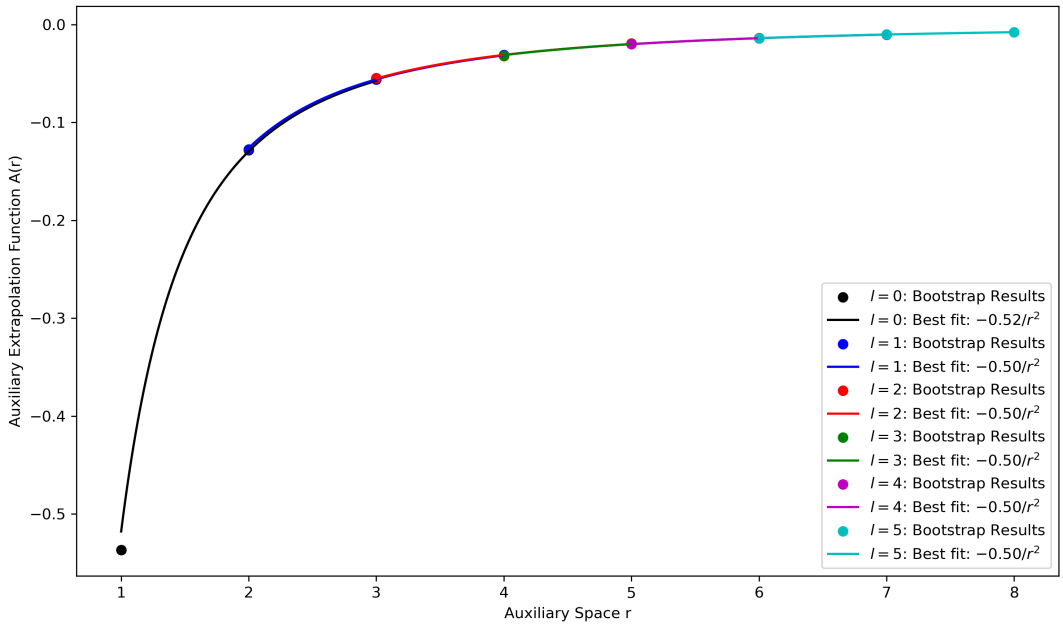

Figure 4.10: Auxiliary Extrapolation Function Graph for Hydrogen Atom for Various ℓ

in Table 4.4.

According to the table, the guided bootstrap results for the hydrogen atom for various ℓ cases show good consistency both among each other and with the theoretical values.

Overall, we once again showed that the guided bootstrap method significantly improves the reliability of the final results for the Hydrogen atom system. While minor numerical errors still happen at higher energy states, the method appears to be potentially applicable to systems with unknown energy levels, though further work is needed.

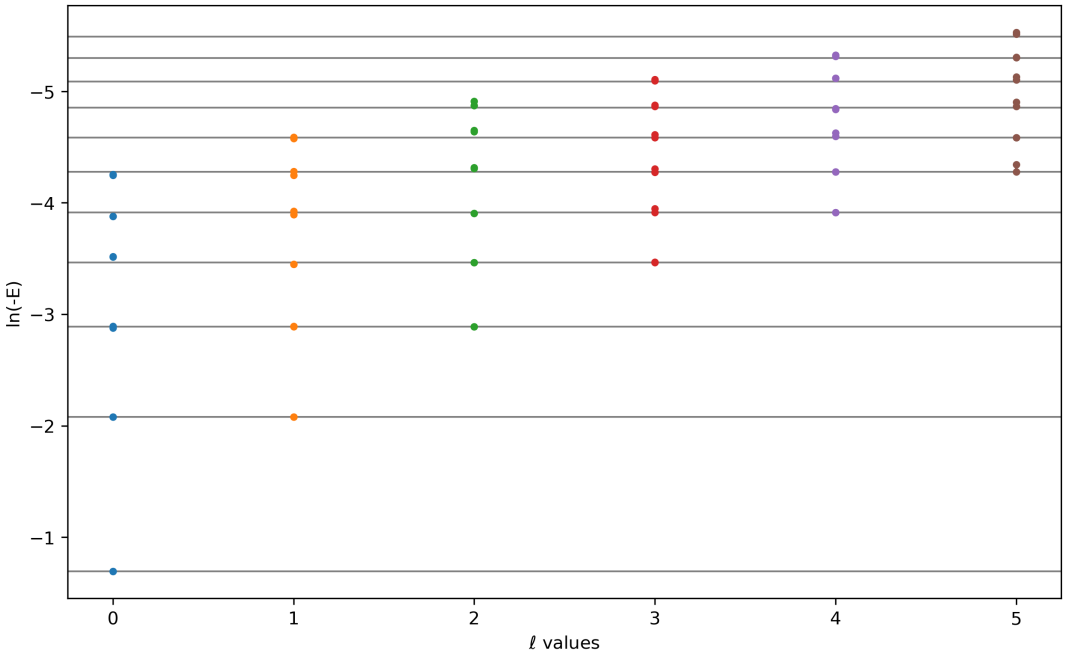

Figure 4.11: No Split Bootstrap Graph for Hydrogen Atom for Various ℓ

Table 4.5: Guided Bootstrap Results for Hydrogen Atom for Various ℓ

$\ell = 0$	$\ell = 1$	$\ell = 2$
-0.5001 ± 0.0	-0.1250 ± 0.0	-0.0556 ± 0.0
-0.1249 ± 0.0	$-0.0556 \pm 1.29 \times 10^{-4}$	$-0.0313 \pm 8.45 \times 10^{-6}$
$-0.0559 \pm 3.76 \times 10^{-4}$	-0.0317 ± 0.0	-0.0202 ± 0.0
$-0.0297 \pm 8.12 \times 10^{-5}$	$-0.0201 \pm 3.24 \times 10^{-4}$	$-0.0134 \pm 5.47 \times 10^{-5}$
-0.0206 ± 0.0	$-0.0141 \pm 2.32 \times 10^{-4}$	$-0.0096 \pm 5.62 \times 10^{-5}$
$-0.0206 \pm 4.42 \times 10^{-5}$	$-0.0102 \pm 5.99 \times 10^{-5}$	$-0.0075 \pm 1.42 \times 10^{-4}$
$\ell = 3$	$\ell = 4$	$\ell = 5$
$-0.0313 \pm 3.7 \times 10^{-5}$	-0.0200 ± 0.0	$-0.0134 \pm 4.46 \times 10^{-4}$
$-0.0196 \pm 3.56 \times 10^{-4}$	$-0.0139 \pm 5.23 \times 10^{-6}$	$-0.0102 \pm 1.04 \times 10^{-5}$
$-0.0137 \pm 2.11 \times 10^{-4}$	$-0.0099 \pm 1.49 \times 10^{-4}$	$-0.0076 \pm 1.43 \times 10^{-4}$
$-0.0101 \pm 1.30 \times 10^{-4}$	$-0.0079 \pm 2.96 \times 10^{-5}$	$-0.0060 \pm 7.79 \times 10^{-5}$
$-0.0077 \pm 3.2 \times 10^{-5}$	$-0.0060 \pm 4.79 \times 10^{-6}$	$-0.0050 \pm 4.5 \times 10^{-6}$
$-0.0061 \pm 4.17 \times 10^{-5}$	$-0.0049 \pm 2.62 \times 10^{-5}$	$-0.0040 \pm 2.93 \times 10^{-5}$

CHAPTER 5

BOOTSTRAPPING THE ANHARMONIC OSCILLATOR

5.1 The Anharmonic Oscillator Potential

We now investigate the anharmonic oscillator potential. Unlike the SHO and Hydrogen atom systems, the Anharmonic Oscillator has two elements in its search space, allowing us to examine how the method performs with search spaces with more than one element.

The anharmonic oscillator potential in its most general form is given by,

$$V(\hat{x}) = \frac{1}{2}m\omega^2\hat{x}^2 + \frac{1}{4}\lambda\hat{x}^4. \tag{5.1.1}$$

We, once again, use the parameters $m = 1$ and $\omega = 1$. However, on this occasion, in order to investigate the affect of the value of coupling constant λ in our results, we implement it into the moment recursion. Then, the potential becomes,

$$V(\hat{x}) = \frac{1}{2}\hat{x}^2 + \frac{1}{4}\lambda\hat{x}^4, \tag{5.1.2}$$

where $\lambda \in \mathbb{R}$. We also note that if $\lambda < 0$, the Hamiltonian will be unbounded from below, so we work with values $\lambda \geq 0$.

Figure 3.1 displays the graph of the function $V(\hat{x})$ in the configuration space for $\lambda = 0.1, 1, 10, 100$. From the figure, it is obvious that there are infinitely many bound states for the Anharmonic Oscillator system which all have an energy $E \geq 0$.

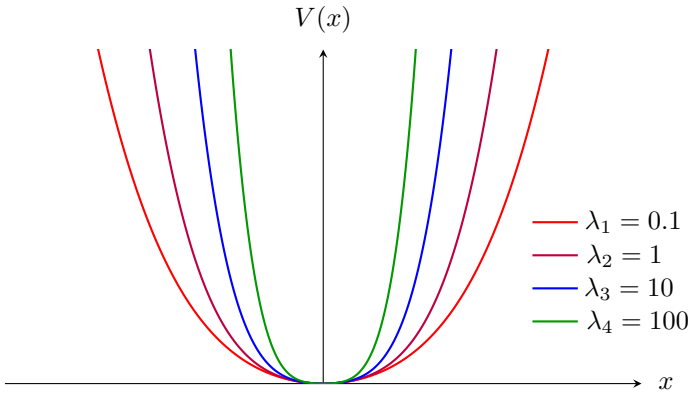

Figure 5.1: Graph of Anharmonic Oscillator Potentials for different λ values in the Configuration Space

5.2 Recursion Relation, Search Space and the Bootstrap Matrix

In this section, we define the theoretical perquisites discussed in Chapter 2 for the anharmonic oscillator system.

5.2.1 Anharmonic Recursion Relation

Evaluating the potential dependent identities in equation (2.4.21) for the anharmonic potential defined in equation (5.1.2) we obtain,

$$\langle \hat{r}^t V'(\hat{r})\rangle = \langle \hat{x}^{t+1}\rangle + \lambda\langle \hat{x}^{t+3}\rangle\,, \quad 2t\langle \hat{r}^{t-1}V(\hat{r})\rangle = t\langle \hat{x}^{t+1}\rangle + \frac{1}{2}\lambda t\langle \hat{x}^{t+3}\rangle. \tag{5.2.1}$$

Implementing the identities found in equation (5.2.1) into the equation (2.4.21), we obtain the recursion relation for the anharmonic oscillator as

$$\lambda(t+2)\langle x^{t+3}\rangle = 4tE\langle x^{t-1}\rangle + \frac{1}{2}t(t-1)(t-2)\langle x^{t-3}\rangle - 2(t+1)\langle x^{t+1}\rangle, \tag{5.2.2}$$

which is the moment recursion relation for the anharmonic oscillator system.

We note that for $\lambda = 0$ the recursion relation (5.2.2) becomes the recursion relation for the SHO system given in equation (3.2.2).

5.2.2 Anharmonic Oscillator Search Space

The anharmonic oscillator potential is a fourth degree polynomial which is an even function of $\hat{x}$. Then, by the methods explained in Section 2.6 the cardinality $|S|$ of the minimal search space needed to initiate the recursion relation found in equation (5.2.2) is

$$|S| = 2. \tag{5.2.3}$$

Then, the minimal search space S for the Anharmonic Oscillator system is

$$S = \{S^1 \equiv E, S^2 \equiv \langle \hat{x}^2 \rangle\}, \tag{5.2.4}$$

which are the elements that should be predefined in the algorithm.

5.2.3 Anharmonic Oscillator Matrix Terms and Constraints on the Search Space

We want to generate the non-zero elements of $\mathcal{M}$ using equation (5.2.2). The first non-zero element is $\langle \hat{x}^4 \rangle$ and can be generated from the recursion relation for $t = 1$ which yields

$$3\lambda \langle \hat{x}^4 \rangle = 4E + 4\langle \hat{x}^2 \rangle. \tag{5.2.5}$$

We note that since, $\langle \hat{x}^2 \rangle, \langle \hat{x}^4 \rangle \geq 0$ and also $\langle \hat{x}^4 \rangle > \langle \hat{x}^2 \rangle$ in the energy eigenstates as shown in Appendix D, we can put a lower bound constraint for the energy E as $E \geq 0$ as expected from the Figure 5.1.

As an example, we also show the first four diagonal elements $\mathcal{M}_{ii}$ of the bootstrap matrix $\mathcal{M}$ which can be calculated as

$$\begin{aligned}
\mathcal{M}_{00} &= \langle \hat{x}^0 \rangle = 1, \\
\mathcal{M}_{11} &= \langle \hat{x}^2 \rangle = \langle \hat{x}^2 \rangle, \\
\mathcal{M}_{22} &= \langle \hat{x}^4 \rangle = \frac{4}{3\lambda} E + \frac{4}{3\lambda} \langle \hat{x}^2 \rangle, \\
\mathcal{M}_{33} &= \langle \hat{x}^6 \rangle = \frac{32}{15\lambda^2} \left(\langle \hat{x}^2 \rangle - E \right) + \frac{12}{5\lambda} E \langle \hat{x}^2 \rangle + 3.
\end{aligned} \tag{5.2.6}$$

5.3 Bootstrapping the Anharmonic Oscillator

We digress a moment here to explain how the bootstrap method works for systems which involves more than one search space element. In the case of the Anharmonic Oscillator system, we have two search space elements, mainly, the energy E and the expectation value $\langle \hat{x}^2 \rangle$. However, we are only interested in determining the energy spectrum of the system, so the bootstrapping process is only applied to the energy search space element.

We use the search space element $\langle \hat{x}^2 \rangle$ to only generate search lines over the energy. At the start of the bootstrap method, we define a total number of τ_2, $\langle \hat{x}^2 \rangle$ lines, in between the lower and upper bounds pre-defined in S^2. These lines remain fixed throughout the bootstrapping process and do not get redefined as the depth increases. We call the collection of these search lines a "search area" and denote this area by A. These search lines may either split into separate energy intervals or be entirely eliminated from the search space.[1] In each iteration, only the energy boundaries of these search lines are bootstrapped, getting closer to the actual energy values.

The main difference of bootstrapping process between systems that has a single search space element and a two search space element is the the process of splitting. In the latter case, we're dealing with areas instead of lines. A split can occur in an area, in two different ways,

- Every search line within a given area A_n can split into m lines over the energy element, thereby creating m distinct areas $A_{(n-m+1)}, A_{(n-m+2)} ... A_n, A_{n+1}$. We call this type of splitting an "energy split".[2] Figure 5.2 provides an illustration of how an energy split occurs.

- A continuous set of search lines within an area A_n may vanish entirely during an iteration, dividing the area into two parts, A_n and A_{n+1}. We call this type of splitting an "vanishing split". Figure 5.3 provides an illustration of how a vanishing split occurs.

[1] We have made an interesting observation during our studies that these $\langle \hat{x}^2 \rangle$ lines do not split into different energy intervals for the Anharmonic Oscillator system. Instead, they consistently shrink from the boundaries, similar to the no split bootstrap algorithm we introduced for systems with a single search space element.

[2] In our implementation of Anharmonic Oscillator, we have never encountered this way of splitting. This if

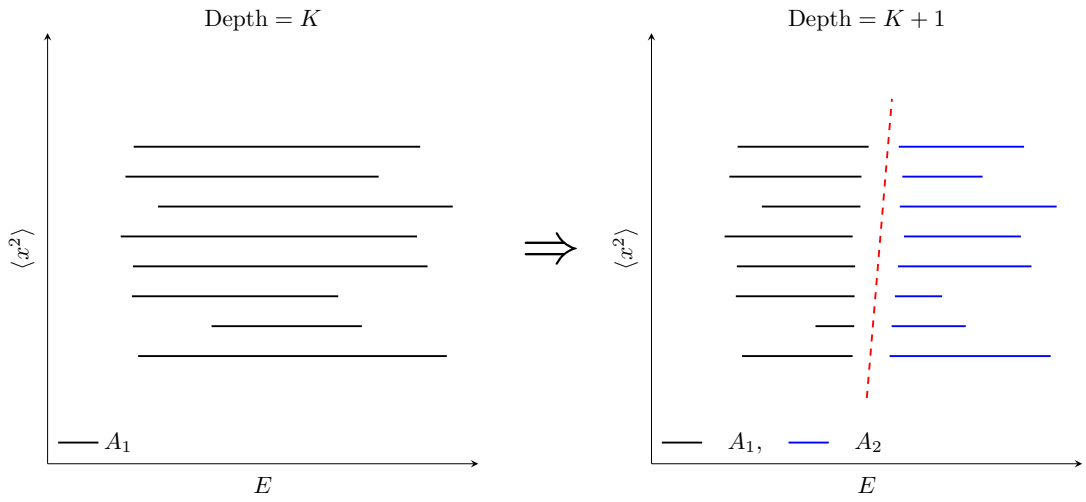

Figure 5.2: Illustration of Energy Split

In our implementation of the Anharmonic Oscillator, we never encountered an energy split, which is likely due to the behavior of the search lines as mentioned in footnote 1. This renders the application of the one split bootstrap algorithm unnecessary, as the energy elements do not multi split, thereby avoiding the issues caused by multiple interval splitting.

However, we have frequently encountered multiple vanishing splits even at low values of depth K. As K increases, these small areas created by the multiple vanishing splits completely disappear without causing issues with the algorithm. However, this makes the guided bootstrap method inapplicable to the system, as the initialization bootstrap process will collect many energy areas that do not contain actual energy eigenstates, which will prevent us from obtaining a sensible extrapolation function. Therefore, we only apply the original bootstrap algorithm to the Anharmonic Oscillator system.

We also need to handle areas that have become small enough to be considered as a point through epsilon convergence. We define the area convergence for an area A, such that when the number of search lines, call τ, satisfies $\tau \leq 0.01\tau_2$, the area starts to be examined for convergence. This process is similar to the one described in Section 2.7, with the difference being that the operation defined in equation (2.7.10) is applied to the longest line (the largest energy interval) within the area A. If an area is classified as converged through epsilon convergence, the energy eigenvalue is

likely due to the behavior of the search lines as mentioned earlier.

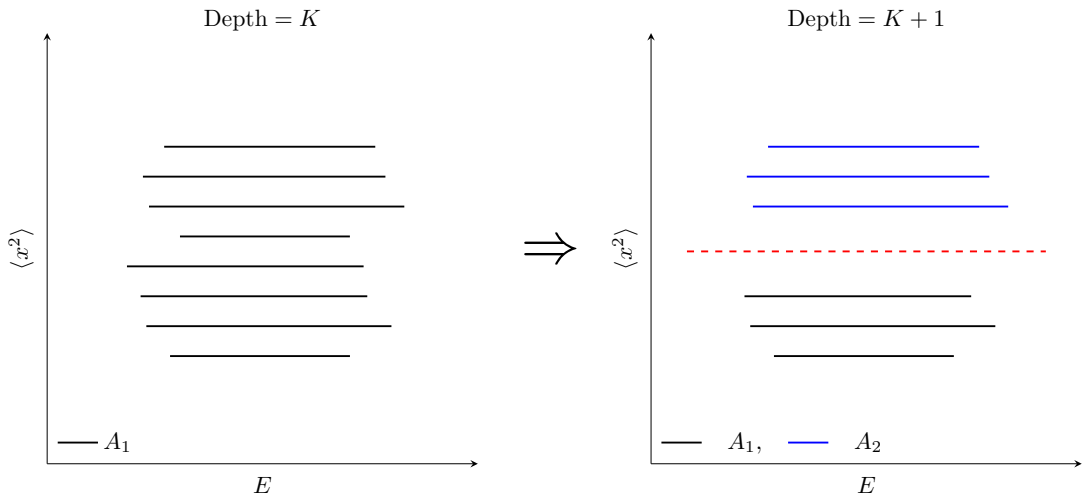

Figure 5.3: Illustration of Vanishing Split

determined as the geometric midpoint of the area. [3]

Although, we have only discussed the bootstrapping method for systems with two search space elements, the principle ideas we mentioned in this section can be extended to systems with more search space elements. In such cases, every element other than the energy can be treated in a similar way to how we treated $\langle \hat{x}^2 \rangle$ in the Anharmonic Oscillator system, generating search lines, search areas, search volumes, and so on as needed.

5.4 Original Bootstrap on Anharmonic Oscillator System

We now apply the "original bootstrap" algorithm the the Anharmonic Oscillator system. We note that there is no analytic formula for the exact energy levels for this problem. Thus, to compare the obtained results, we utilize two different methods. The first method of comparison is the first order energy correction to the perturbed Harmonic Oscillator given as [41]

$$\begin{aligned} E_n &= E_n + E_n^{(1)}, \\ &= \left(n - \frac{1}{2}\right) + \frac{3\lambda}{16}(2(n-1)^2 + 2n - 1), \end{aligned} \tag{5.4.1}$$

[3] We note that although we have not attempted, using the centroid of the area might increase precision for the area convergence.

where we once again let $n \to (n+1)$ and label the states with $n \geq 1$.

We will only compare the $\lambda = 0.1, 1$ cases through the first order energy correction, as for larger values of λ, the $\hat{x}^4$ term becomes the dominant term in the potential and the perturbation approach is no longer applicable.

For a second comparison, we also solve the Schrödinger equation numerically, in the boundary $x \in (-5, 5)$, using the MATHEMATICA package NDEigensystem for all values of λ.

Throughout this chapter, unless specified otherwise, all graphs follow the same format. Since we have two elements in the search space, we plot the graphs accordingly, meaning that the horizontal axis represents the energy, and the vertical axis represents the expectation value $\langle \hat{x}^2 \rangle$. Each depth K is represented by a different color, starting with transparent shades for lower depths and becoming more opaque as the depth increases. Although the algorithm linearly increments $(+1)$ the depth K at each iteration, within the range specified in the initial parameter list, we only plot the results at depths that are multiples of five for better readability. Every positive definite space is depicted as an area, with bold lines indicating the contours. Red dots represent the converged points of the system, which are determined through epsilon convergence.

5.4.1 $\lambda = 0.1$ Case

We use this case to investigate the low values of λ, such that the term containing $\hat{x}^4$ can be considered as a perturbation from the SHO system.

We run the original bootstrap algorithm on Python with the initialization parameters as the following:

- Search space bounds for $E \in S: \ [0, 6], \ \ \langle \hat{x}^2 \rangle \in S: \ [0, 4]$.
- Precision $\tau_1 = 1000$ for search space element E, precision $\tau_2 = 1300$ for search space element $\langle \hat{x}^2 \rangle$.
- Initial depth $K_i = 4$ and final depth $K_f = 22$.
- Convergence limit $\epsilon = 10^{-9}$.

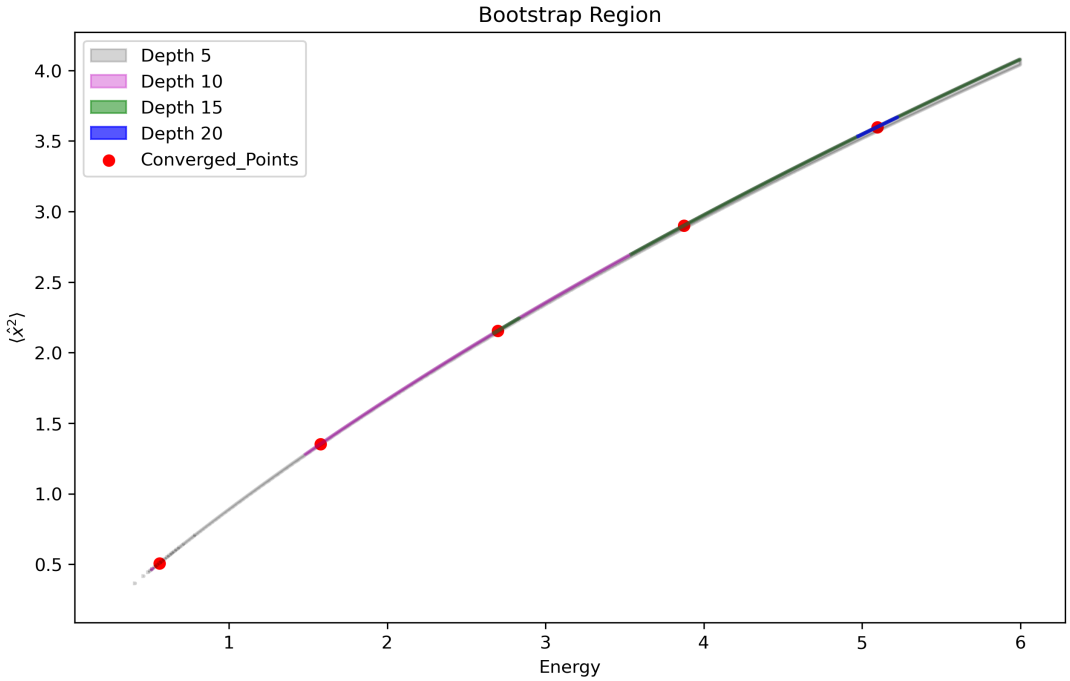

Figure 5.4: Original Bootstrap Graph for Anharmonic Oscillator System for $\lambda = 0.1$

Figure 5.4 demonstrates the results of the original bootstrap algorithm for the Anharmonic Oscillator system with a coupling constant $\lambda = 0.1$. The results of the algorithm are given in Table 5.1 alongside with the first order correction to the energy of the perturbed SHO system and the numerical results of the NDEigensystem.

The results indicate that all three numerical methods agree with each other within a small margin of error. This indicates that the original bootstrap algorithm has successfully identified the first five energy eigenstates of the Anharmonic Oscillator system with a small coupling constant $\lambda = 0.1$.

This success is due to the fact that positive definite areas of the system being split by the vanishing of search lines rather than by multiple splits in energy, which prevents faulty convergences. However, achieving these results required extreme precision lowering the epsilon convergence limit to 10^{-9}. This was necessary because the system is highly susceptible to numerical errors, especially since the higher terms in the recursion relation are divided by λ, causing them to grow rapidly and leading the algorithm to lose numerical precision rather quickly. As $\lambda \to 0$, the system will increasingly encounter larger numerical errors, eventually facing the same issues ob-

Table 5.1: Original Bootstrap Results for Anharmonic Oscillator System for $\lambda = 0.1$

States	Bootstrap Method	First Order Correction to Energy	MATHEMATICA NDEigensystem
1	0.5606 ± 0.0	0.51875	0.5174
2	$1.5780 \pm 4.3017 \times 10^{-10}$	1.59375	1.5843
3	$2.7135 \pm 1.2978 \times 10^{-12}$	2.74375	2.7113
4	$3.8905 \pm 1.8207 \times 10^{-14}$	3.96875	3.8924
5	$5.0969 \pm 8.881 \times 10^{-16}$	5.26875	5.1237

served in the SHO and Hydrogen Atom systems. This numerical limitation prevents us from exploring whether, as $\lambda \to 0$, the system would behave similarly to the SHO system, as one would expect.

5.4.2 $\lambda = 1$ Case

This is the most extensively studied case in the literature [9–12]. At this value of the coupling constant, the $\hat{x}^4$ term begins to dominate the system. We investigate this case to verify that our algorithm produces results consistent with those in the literature. Additionally, the first order correction to the energy of the perturbed SHO system still remains comparable at this value of λ, allowing for a reasonably significant comparison.

We run the program on Python with the initialization parameters as the following:

- Search space bounds for $E \in S: \ [0, 10], \ \langle \hat{x}^2 \rangle \in S: \ [0, 3]$.
- Precision $\tau_1 = 300$ for search space element E, precision $\tau_2 = 500$ for search space element $\langle \hat{x}^2 \rangle$.
- Initial depth $K_i = 4$ and final depth $K_f = 22$.
- Convergence limit $\epsilon = 0.001$.

Figure 5.5 illustrates the results of the original bootstrap algorithm for the Anharmonic Oscillator system with a coupling constant $\lambda = 1$. The results of the algorithm

are given in Table 5.2 alongside with the first order correction to the energy of the perturbed SHO system and the numerical results of the NDEigensystem.

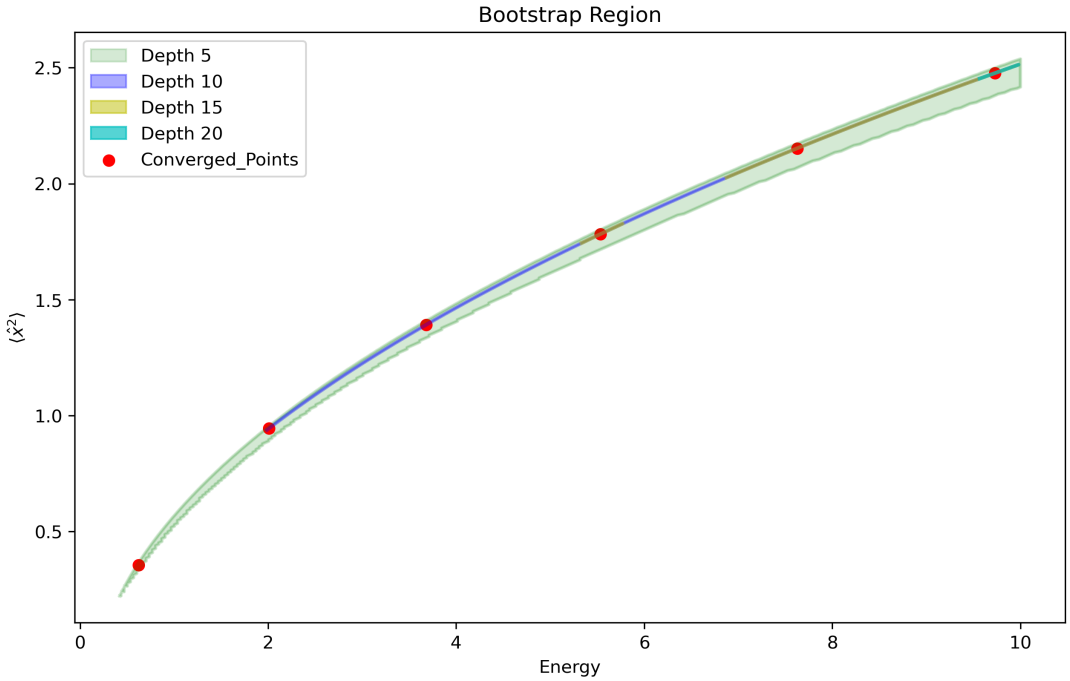

Figure 5.5: Original Bootstrap Graph for Anharmonic Oscillator System for $\lambda = 1$

The results indicate that the numerical solution methods agree closely with each other within a small margin of error, while the first order correction to the energy began to show significant deviations from the other methods in the higher energy states.

Table 5.2: Original Bootstrap Results for Anharmonic Oscillator System for $\lambda = 1$

States	Bootstrap Method	First Order Correction to Energy	MATHEMATICA NDEigensystem
1	$0.6208 \pm 1.812 \times 10^{-4}$	0.6875	0.6211
2	$2.0079 \pm 1.935 \times 10^{-4}$	2.4375	2.0278
3	$3.6829 \pm 7.864 \times 10^{-6}$	4.9375	3.7071
4	$5.5350 \pm 2.217 \times 10^{-7}$	8.1875	5.5836
5	$7.6254 \pm 1.895 \times 10^{-8}$	12.1875	7.6297
6	$9.7314 \pm 7.094 \times 10^{-10}$	12.1875	9.8313

Our result align closely with the results obtained in [9–12].

5.4.3 $\lambda = 10$ Case

We use this case to investigate how the bootstrap method performs with large values of the coupling constant λ.

We run the program on Python with the initialization parameters as the following:

- Search space bounds for $E \in S: \ [0, 15], \ \langle \hat{x}^2 \rangle \in S: \ [0, 5]$.
- Precision $\tau_1 = 1500$ for search space element E, precision $\tau_2 = 1500$ for search space element $\langle \hat{x}^2 \rangle$.
- Initial depth $K_i = 4$ and final depth $K_f = 17$.
- Convergence limit $\epsilon = 0.01$.

Since, we need to cover higher values of energy and $\langle \hat{x}^2 \rangle$ to determine the energy eigenstates, we have also adjusted the precision for the search space elements accordingly.

Figure 5.6 depicts the results of the original bootstrap algorithm for the Anharmonic Oscillator system with a coupling constant $\lambda = 10$.

The results of the algorithm are given in Table 5.3 alongside with the the numerical results of the NDEigensystem. After this point, it is meaningless to compare the results with the first order correction, since the dominant term in the potential is $\hat{x}^4$.

Table 5.3: Original Bootstrap Results for Anharmonic Oscillator System for $\lambda = 10$

States	Bootstrap Method	MATHEMATICA NDEigensystem
1	0.9955 ± 0.0049	1.0103
2	3.5042 ± 0.0032	3.5184
3	$6.6622 \pm 9.392 \times 10^{-4}$	6.7876
4	$10.2908 \pm 4.433 \times 10^{-5}$	10.5954
5	$14.5856 \pm 3.187 \times 10^{-6}$	14.9449

The results indicate that the numerical solution methods still agree closely with each

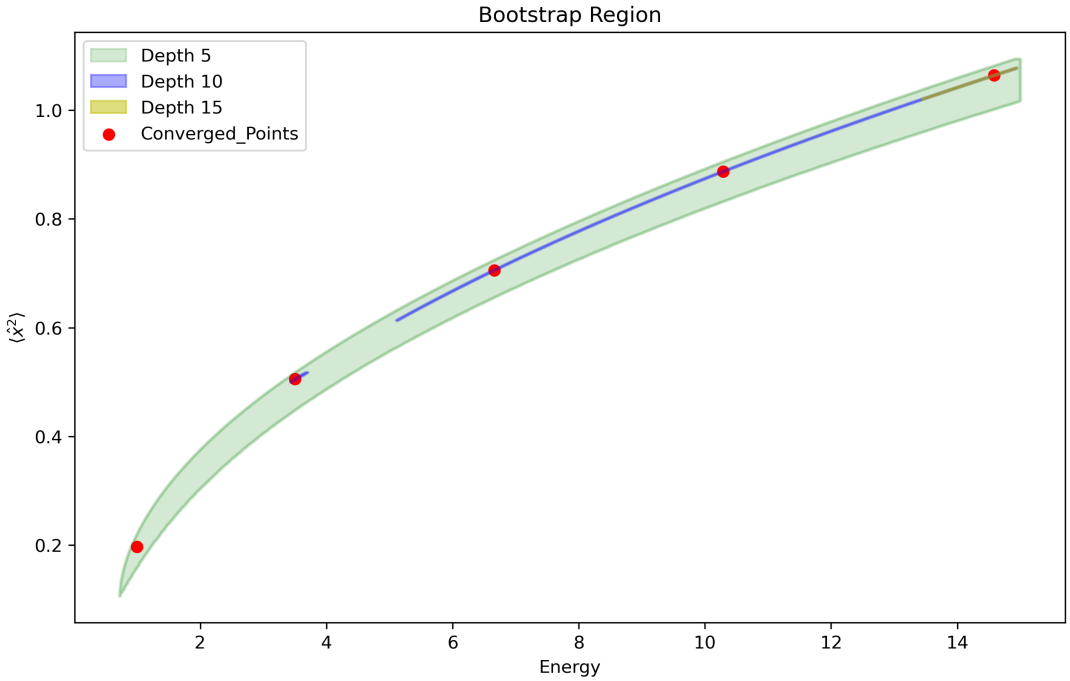

Figure 5.6: Original Bootstrap Graph for Anharmonic Oscillator System for $\lambda = 10$

other within some margin of error proving the methods reliability for large values of the coupling constant λ.

5.4.4 $\lambda = 100$ Case

We use this case to explore how the bootstrap method behaves with very large values of the coupling constant λ.

We run the program on Python with the initialization parameters as the following:

- Search space bounds for $E \in S: \ [0, 50], \ \ \langle \hat{x}^2 \rangle \in S: \ [0, 1]$.
- Precision $\tau_1 = 1500$ for search space element E, precision $\tau_2 = 1500$ for search space element $\langle \hat{x}^2 \rangle$.
- Initial depth $K_i = 4$ and final depth $K_f = 22$.
- Convergence limit $\epsilon = 0.01$.

Figure 5.7 reveals the results of the original bootstrap algorithm for the Anharmonic

Oscillator system with a coupling constant $\lambda = 100$. The results of the algorithm are given in Table 5.3 alongside with the the numerical results of the NDEigensystem.

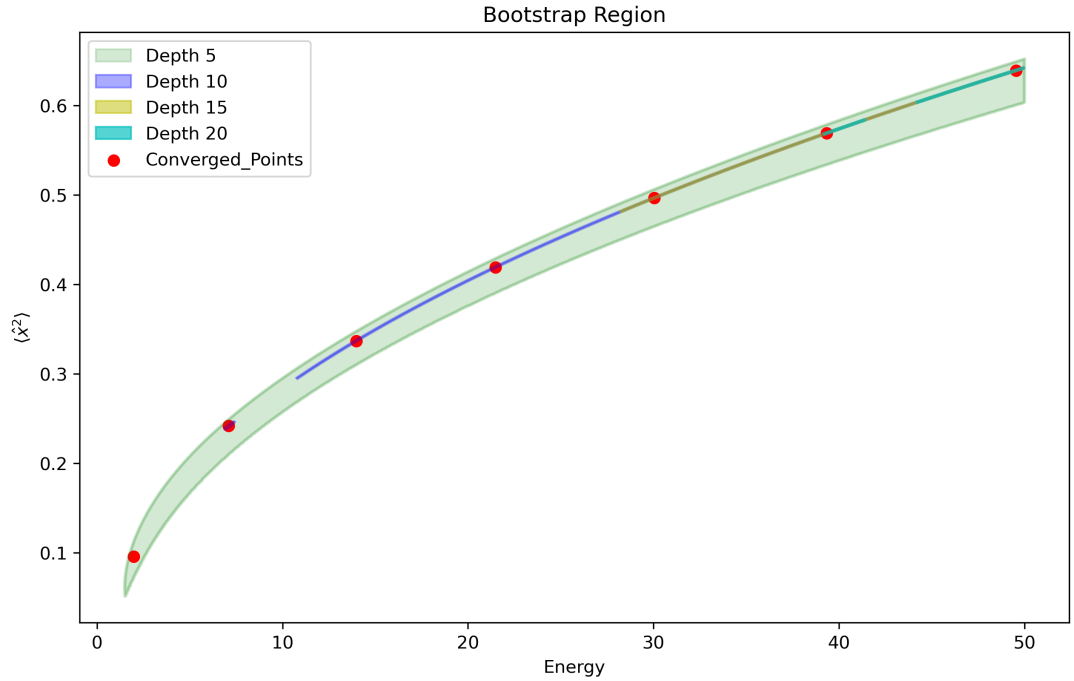

Figure 5.7: Original Bootstrap Graph for Anharmonic Oscillator System for $\lambda = 100$

From the results, it can be observed that for very large values of λ, both numerical methods yield similar results for the lower energy eigenstates. However, for higher states, the results start to differ significantly.

It is important to note that for large values of λ, the precision of the NDEigensystem may decrease, potentially leading to missed or faulty results. Therefore, the comparison between these two methods is not entirely reliable and cannot be considered a definitive verification of the bootstrap method's failiure.

Table 5.4: Original Bootstrap Results for Anharmonic Oscillator System for $\lambda = 100$

States	Bootstrap Method	MATHEMATICA NDEigensystem
1	1.9710 ± 0.0132	2.0081
2	7.0821 ± 0.0034	7.2262
3	13.9718 ± 0.0031	14.6822
4	$21.4857 \pm 1.989 \times 10^{-4}$	21.9273
5	$30.0417 \pm 9.655 \times 10^{-6}$	34.7209
6	$39.3419 \pm 4.943 \times 10^{-7}$	46.5715
7	$49.5374 \pm 2.313 \times 10^{-8}$	59.6702

CHAPTER 6

CONCLUSION

In this thesis, we examined the bootstrap method for 1D quantum mechanical systems, a numerical technique originally proposed by Han, Hartnoll, and Kruthoff [6] for determining the energy eigenvalues in these systems. We provided the theoretical and computational background of the method and then applied it to three different quantum systems: the SHO, the Hydrogen atom, and the Anharmonic Oscillator. We also explored various optimizations of the bootstrap method to improve its reliability and applicability to other quantum systems with unknown energy spectra.

In Chapter 2, we discussed the theoretical background and the algorithmic structure of the bootstrap method. We started out by reviewing the moment problems, specifically focusing on the Hamburger moment problem, which forms the basis for the bootstrap method. We discussed the necessary conditions for a sequence to be called a moment sequence and then explored the positivity constraints over the Hankel matrices generated through these moment sequences. We followed this review by relating the moment problem to quantum mechanics and showed that for the Hermitian operator $\hat{\mathcal{O}} \sim \hat{x}^n$ the sequence generated through the expectation values of powers of $\hat{\mathcal{O}}$ is in fact a moment sequence and the Hankel matrices which we called the bootstrap matrices generated from this moment sequence, satisfy the positivity constraints. We then derived a generalized moment recursion relation that generates the expectation values of powers of the Hermitian operator $\hat{x}$ which depend on the energy eigenvalues E of any given Hamiltonian and discussed the minimum requirements to initialize this recursion relation. We provided a detailed structure of the "original bootstrap" algorithm, discussed the problems that can be addressed with it and suggested an optimized version of the algorithm which we called the "one split bootstrap" algorithm.

Finally, we introduced a new algorithm which we called the "guided bootstrap" algorithm, that works with the bootstrapping method and uses numerical methods to improve the reliability of the final results.

In Chapter 3, we applied the bootstrap method to the SHO system. We started by discussing the theoretical requirements of the system, deriving the moment recursion relation and defining the search space for it. We have shown that the recursion relation can be initiated only using the search space element E. Finally, we applied the original bootstrap algorithm, one split bootstrap algorithm and guided bootstrap algorithm to the SHO system and successfully determined the first seven energy eigenstates from each of these algorithms within some margin of error. The results of this chapter may be observed in Figure 6.1 and in Table 3.4.

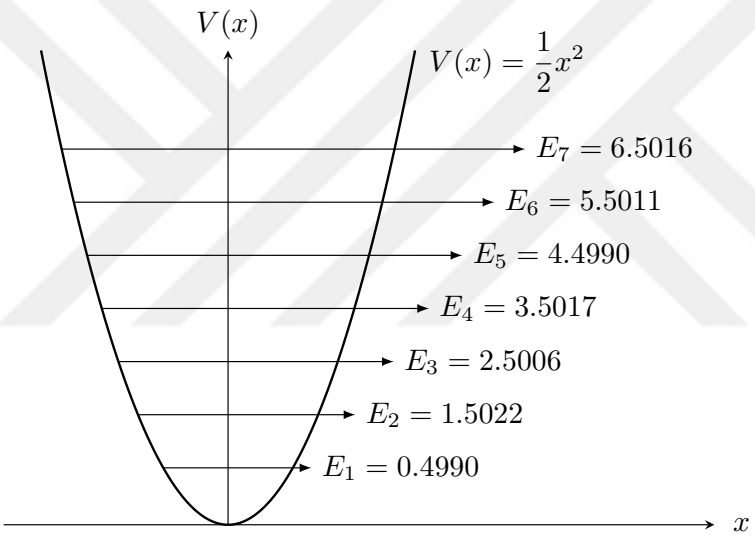

Figure 6.1: Bootstrap Results for SHO Potential

In Chapter 4, we focused on the Hydrogen atom. Since the problem is defined in the half-line $\mathbb{R}_+$, we introduced bootstrapping on the half-line. We first reviewed the Stieltjes moment problem which is defined on $\mathbb{R}_+$. We have discussed the necessary conditions for a sequence to be called a moment sequence in $\mathbb{R}_+$ and then discussed the positivity constraints over the Hankel matrices generated through these moment sequences. We then derived a generalized moment recursion relation that generates the expectation values of powers of the Hermitian operator $\hat{r}$ for any Hamiltonian defined in spherical polar coordinates with angular symmetry. We followed up by

developing the theoretical requirements of the Hydrogen atom system, deriving the moment recursion relation and defining the search space for it. We have shown that the recursion relation can be initiated only using the search space element E. Finally, we applied the original bootstrap algorithm, one split bootstrap algorithm and guided bootstrap algorithm to the Hydrogen Atom system. We investigated how different values of angular momentum quantum number ℓ effected each independent algorithm. We successfully determined the first three energy eigenstates from each of these algorithms within some margin of error. Our main results can be accessed from the Figure 6.2 and Table 4.5.

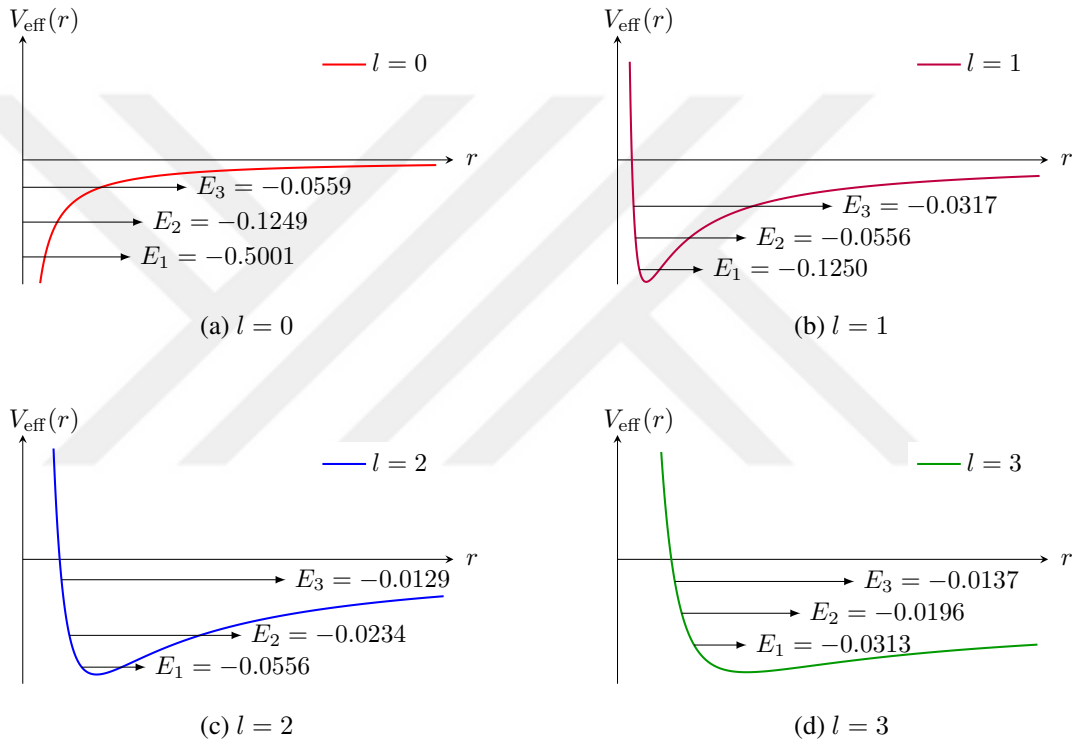

(a) $l = 0$ (b) $l = 1$ (c) $l = 2$ (d) $l = 3$

Figure 6.2: Bootstrap Results for the Hydrogen Potential $V_{\text{eff}}(\hat{r})$ for $l = 0, 1, 2, 3$

In Chapter 5, we applied the bootstrap method to the Anharmonic Oscillator system. We started by discussing the theoretical requirements of the system, deriving the moment recursion relation and defining the search space for it. We have shown that the recursion relation can be initiated using the search space elements E and $\langle \hat{x}^2 \rangle$. Finally, we applied the original bootstrap algorithm to the Anharmonic Oscillator system. We investigated how different values of the coupling constant λ effected

the bootstrap method. We successfully determined the first five energy eigenstates for each of the different coupling constants, within some margin of error. The first three of our results may be seen from the Figure 6.3 and the full results can be observed from Tables 5.1, 5.2, 5.3, 5.4

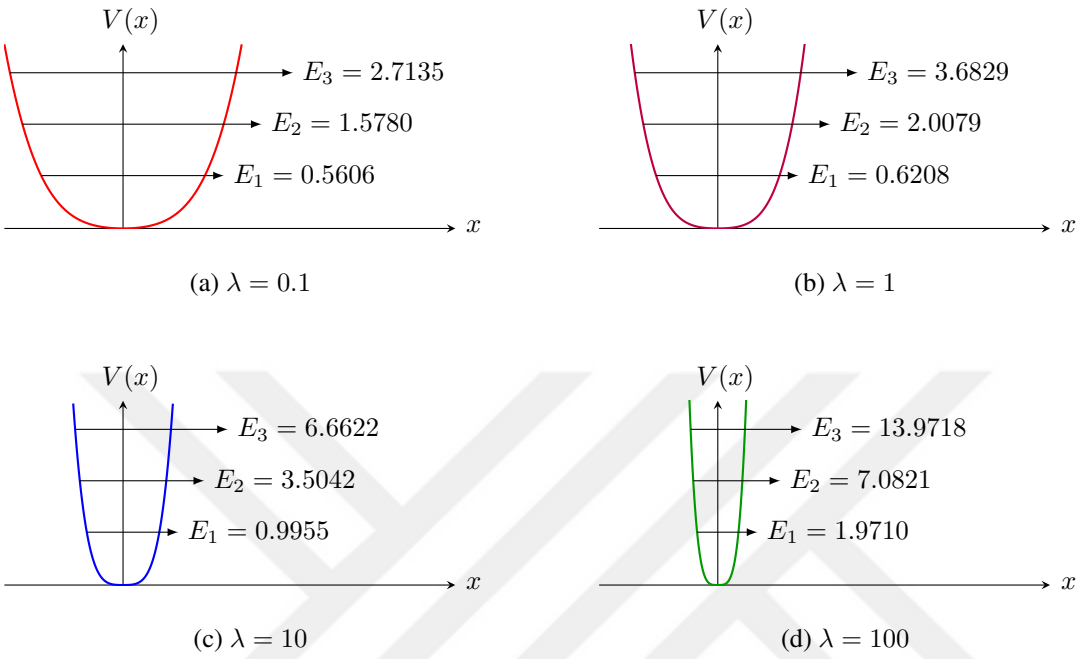

(a) $\lambda = 0.1$ (b) $\lambda = 1$

(c) $\lambda = 10$ (d) $\lambda = 100$

Figure 6.3: Bootstrap Results for Anharmonic Oscillator for $\lambda = 0.1, 1, 10, 100$

In this thesis, we have analyzed three different types of problems, mainly a problem with a single search space element (SHO), a problem in a different domain (Hydrogen atom) and a problem with two search space elements (Anharmonic Oscillator) via different algorithms that use the bootstrap method, in order to test its reliability and effectiveness in providing accurate results for lower level energy eigenstates within 1D quantum mechanical systems.

We have applied the original bootstrap algorithm to all of the systems. For the SHO and Hydrogen atom systems, we observed that while the algorithm could identify lower energy states accurately at low depths, at higher depths due to interval multi splitting it found a large number of incorrect results, reducing the method's reliability.

To resolve this issue with the bootstrapping process for these systems (SHO and Hydrogen atom), we introduced the one split bootstrap algorithm. This method improved

the accuracy of the results enabling the algorithm to reach higher depths and reducing the number of incorrect results. However, the algorithm eventually began splitting intervals incorrectly, leading to repeated results for the same eigenvalue and missed some eigenvalues. These problems show that numerical errors still affect the algorithm's reliability.

We finally applied the guided bootstrap algorithm to SHO and Hydrogen atom systems. This method identified the first energy intervals for both of the systems. Using these intervals, we estimated energy intervals for higher states, generating a guided search space. We treated the guided search space with a no split approach, which prevented intervals from splitting and ensured that every interval in the guided search space converged to a single point. The guided bootstrap algorithm, accurately found the low lying energy levels, though numerical errors still affected the higher levels decreasing the algorithms reliability for higher energy eigenstates.

Unlike the SHO and Hydrogen Atom systems, the Anharmonic Oscillator did not encounter interval multi splitting issue due to the nature of its search space, with the latter consisting of two elements. All the area splittings in this system occurred through vanishing splits, preventing multi splitting in the energy. This allowed the original bootstrap algorithm to be applied effectively to the system. However, this also caused the application of one split bootstrap algorithm to become unnecessary due to the absence of multi splitting, and the guided bootstrap algorithm was inapplicable because the initialization bootstrap process would have gathered energy areas which do not contain actual energy eigenstates, leading to wrong extrapolation of energy. The original bootstrap method produced accurate results across different values of the coupling constant, particularly for lower energy states.

In summary, the bootstrap algorithms applied to the systems, consistently identified the lower energy levels. We obtained similar results for all systems with each of the algorithms, proving the methods success. This shows that the bootstrap method works well for finding low lying energy eigenvalues of 1D Hamiltonian problems.

REFERENCES

[1] G. F. Chew, S. C. Frautschi, and S. Mandelstam, Regge poles in $\pi-\pi$ scattering, Phys. Rev. **126**, 1202 (1962).

[2] A. M. Polyakov, Nonhamiltonian approach to conformal quantum field theory, Zh. Eksp. Teor. Fiz. **66**, 23 (1974).

[3] S. El-Showk *et al.*, Solving the 3D Ising model with the conformal bootstrap, Phys. Rev. D **86**, 025022 (2012).

[4] H. W. Lin, Bootstraps to strings: solving random matrix models with positivity, JHEP **2020**, 090 (2020).

[5] F. Kos, D. Poland, and D. Simmons-Duffin, Bootstrapping the $O(N)$ vector models, JHEP **06**, 091 (2014).

[6] X. Han, S. A. Hartnoll, and J. Kruthoff, Bootstrapping matrix quantum mechanics, Phys. Rev. Lett. **125**, 041601 (2020).

[7] D. Berenstein and G. Hulsey, Bootstrapping simple QM systems, 2021, arXiv:2108.08757.

[8] Y. Aikawa, T. Morita, and K. Yoshimura, Bootstrap method in harmonic oscillator, Phys. Lett. B **833**, 137305 (2022).

[9] T. Morita, Universal bounds on quantum mechanics through energy conservation and the bootstrap method, Prog. Theor. Exp. Phys. **2023**, 023A01 (2023).

[10] Y. Nakayama, Bootstrapping microcanonical ensemble in classical system, Mod. Phys. Lett. A **37**, 2250054 (2022).

[11] J. Bhattacharya, D. Das, S. K. Das, A. K. Jha, and M. Kundu, Numerical bootstrap in quantum mechanics, Phys. Lett. B **823**, 136785 (2021).

[12] W. Fan, H. Zhang, and Z. Li, Unify the effect of anharmonicity in double-wells and anharmonic oscillators, 2023, arXiv:2309.09269.

[13] W. Fan and H. Zhang, Non-perturbative instanton effects in the quartic and the sextic double-well potential by the numerical bootstrap approach, 2023, arXiv:2308.11516.

[14] D. Berenstein and G. Hulsey, Bootstrapping more QM systems, J. Phys. A-Math **55**, 275304 (2021).

[15] S. Tchoumakov and S. Florens, Bootstrapping bloch bands, J. Phys. A-Math **55**, 015203 (2021).

[16] M. J. Blacker, A. Bhattacharyya, and A. Banerjee, Bootstrapping the Kronig-Penney model, Phys. Rev. D **106**, 116008 (2022).

[17] B.-N. Du, M.-X. Huang, and P.-X. Zeng, Bootstrapping Calabi–Yau quantum mechanics, Comm. Theo. Phys. **74**, 095801 (2022).

[18] S. Khan, Y. Agarwal, D. Tripathy, and S. Jain, Bootstrapping PT symmetric quantum mechanics, Phys. Lett. B **834**, 137445 (2022).

[19] Y. Aikawa, T. Morita, and K. Yoshimura, Application of bootstrap to a θ term, Phys. Rev. D **105**, 085017 (2022).

[20] X. Han, Quantum many-body bootstrap, 2020, arXiv:2006.06002.

[21] C. O. Nancarrow and Y. Xin, Bootstrapping the gap in quantum spin systems, JHEP **08**, 052 (2023).

[22] W. Li, The ϕ^n trajectory bootstrap, 2024, arXiv:2402.05778.

[23] V. Kazakov and Z. Zheng, Analytic and numerical bootstrap for one-matrix model and "unsolvable" two-matrix model, JHEP **06**, 030 (2022).

[24] D. Berenstein and G. Hulsey, Anomalous bootstrap on the half-line, Phys. Rev. D **106**, 045029 (2022).

[25] D. Berenstein and G. Hulsey, Semidefinite programming algorithm for the quantum mechanical bootstrap, Phys. Rev. E **107**, L053301 (2023).

[26] D. Berenstein and G. Hulsey, One-dimensional reflection in the quantum mechanical bootstrap, Phys. Rev. D **109**, 025013 (2024).

[27] J. A. Shohat and J. D. Tamarkin, *The Problem of Moments* (American Mathematical Society, Rhode Island, 2021).

[28] R. Shankar, *Principles of Quantum Mechanics* (Kluwer Academic/Plenum Publishers, New York, 1994).

[29] K. Schmüdgen, *The Moment Problem* (Springer, Switerland, 2017).

[30] F. Zhang, *The SCHUR Complement and its Applications* (Springer Science & Business Media, New York, 2005).

[31] J. J. Sakurai and J. Napolitano, *Modern Quantum Mechanics* (Addison-Wesley, San Francisco, 2020).

[32] L. Das, A. Keswani, A. Babbar, and K. Ahuja, Application of square matrix decomposition in the prospectus of cholesky algorithm, in *Proceedings of the 2021 4th International Conference on Mathematics and Statistics*, ICoMS '21, p. 22–26, New York, NY, USA, 2021, Association for Computing Machinery.

[33] R. L. Burden and J. D. Faires, *Numerical Analysis* (Cengage Learning, Boston, 2010).

[34] J. Izaac and J. Wang, *Computational Quantum Mechanics* (Springer, Switzerland, 2018).

[35] T. Hastie, R. Tibshirani, and J. Friedman, *The Elements of Statistical Learning* (Springer, New York, 2009).

[36] H. Akaike, A new look at the statistical model identification, IEEE Transactions on Automatic Control **19**, 716 (1974).

[37] G. Schwarz, Estimating the dimension of a model, The Annals of Statistics **6**, 461 (1978).

[38] K. Schmüdgen, Ten lectures on the moment problem, 2020, arXiv:2008.12698.

[39] T. Szymanski and J. K. Freericks, Algebraic derivation of Kramers–Pasternack relations based on the Schrödinger factorization method, Eur. J. Phys. **42**, 025409 (2021).

[40] A. Berman, D. Hershkowitz, and C. R. Johnson, Linear transformations that preserve certain positivity classes of matrices, Linear Algebra and its Applications **68**, 9 (1985).

[41] S. Blinder, *Introduction to Quantum Mechanics* (Academic Press, London, 2021).

APPENDICES

A Even Potential Wave Function

Starting from the Time Independent Schrödinger Equation

$$\begin{aligned}\hat{H}\psi(x) &= -\frac{1}{2m}\frac{d^2\psi(x)}{dx^2} + V(\hat{x})\psi(x), \\ &= E\psi(x).\end{aligned} \tag{A.1}$$

Under a transformation $x \to -x$, the potential transforms as $V(\hat{x}) \to V(-\hat{x})$ and the solutions transform as; $\psi(x) \to \psi(-x)$.

Then for an even potential $V(\hat{x}) = V(-\hat{x})$, the Time Independent Schrödinger Equation under the transformation $x \to -x$ reads

$$\begin{aligned}\hat{H}\psi(-x) &= -\frac{1}{2m}\frac{d^2\psi(-x)}{dx^2} + V(-\hat{x})\psi(-x), \\ &= -\frac{1}{2m}\frac{d^2\psi(-x)}{dx^2} + V(\hat{x})\psi(-x), \\ &= E\psi(-x).\end{aligned} \tag{A.2}$$

Since both $\psi(x)$ & $\psi(-x)$ should satisfy the same equation then the solutions $\psi(x)$ should have definite parity such that

$$\psi(-x) = \pm\psi(x). \tag{A.3}$$

B Search Space of a Periodic Potential

Starting with the periodic potential

$$V(\hat{x}) = \sin\hat{x}, \tag{B.1}$$

For which the recursion relation found in equation (2.4.21) becomes

$$2tE\langle\hat{x}^{t-1}\rangle = -\frac{1}{4}t(t-1)(t-2)\langle\hat{x}^{t-3}\rangle + \langle\hat{x}^t\cos\hat{x}\rangle + 2t\langle\hat{x}^{t-1}\sin\hat{x}\rangle. \tag{B.2}$$

We can relate the last two identities $\langle \hat{x}^t \cos \hat{x} \rangle$ and $\langle \hat{x}^{t-1} \sin \hat{x} \rangle$ to moments $\langle \hat{x}^t \rangle$ if we expand the trigonometric functions in a power series as

$$\begin{aligned} \sin \hat{x} &= \sum_{n \geq 0} (-1)^n \frac{1}{(2n+1)!} \hat{x}^{2n+1}, \\ \cos \hat{x} &= \sum_{n \geq 0} (-1)^n \frac{1}{(2n)!} \hat{x}^{2n}. \end{aligned} \tag{B.3}$$

Then equation (B.2) becomes

$$2tE\langle \hat{x}^{t-1} \rangle = -\frac{1}{4} t(t-1)(t-2) \langle \hat{x}^{t-3} \rangle + \sum_{n \geq 0} (-1)^n \frac{1}{(2n)!} \frac{2(n+1)}{2n+1} \langle \hat{x}^{t+2n} \rangle. \tag{B.4}$$

Notice that in equation (B.4) the highest order moment is $\langle \hat{x}^{t+2n} \rangle$ where $n \to \infty$. Then, in order to initiate this recursion relation we need all the smaller order moments, which also approach to infinity. Hence the the required minimal search space S is an infinite set, meaning that $|S| \to \infty$.

C Bootstrapping Even Potentials on the Half-Line

If we bootstrap on the half-line $[0, +\infty)$ we have two bootstrap matrices $\mathcal{M}$ and $\tilde{\mathcal{M}}$ which the elements are given by

$$\mathcal{M}_{ij} = \langle \hat{x}^{i+j} \rangle \,, \quad \tilde{\mathcal{M}}_{ij} = \langle \hat{x}^{i+j+1} \rangle, \tag{C.1}$$

where $0 \leq i \,, j \leq K$. Then a $K \times K$ matrix $\tilde{\mathcal{M}}$ has the form

$$\tilde{\mathcal{M}} = \begin{bmatrix} \langle \hat{x}^1 \rangle & & & & \\ & \langle \hat{x}^3 \rangle & & & \\ & & \langle \hat{x}^5 \rangle & & \\ & & & \ddots & \\ & & & & \langle \hat{x}^{2K} \rangle \end{bmatrix}, \tag{C.2}$$

where all diagonal elements are odd powers of $\langle \hat{x}^t \rangle$. For even potentials, all $\langle \hat{x}^t \rangle$ should be zero for odd values of t. Then for even potentials all diagonal elements of the matrix $\tilde{\mathcal{M}}$ are zero. This implies that the trace of a $K \times K$ matrix $\tilde{\mathcal{M}}$ generated

from an even potential is given by

$$\begin{aligned} \mathrm{Tr}(\tilde{\mathcal{M}}) &= \sum_{i=0}^{K} = \tilde{\mathcal{M}}_{ii} \\ &= \sum_{j=1}^{K+1} \lambda_j \\ &= 0 \end{aligned} \tag{C.3}$$

There are only two possible ways for the last two lines in the equation above to hold. Either λ_j has both positive and negative values, or all $\lambda_j = 0$. Therefore the matrix $\tilde{\mathcal{M}}$ can never be positive definite. In fact it can only be positive semidefinite if and only if all of its eigenvalues λ_j are zero.

When bootstrapping even potentials on the half-line, we cannot implement our stronger condition that all the half-line bootstrap matrix $\tilde{\mathcal{M}}$ should be positive definite. However, this fact implies a stricter condition such that all eigenvalues of λ_j of matrix $\tilde{\mathcal{M}}$, generated from points close to the true observables of the system, are zero.

We can use this fact to speed up the bootstrapping process since the characteristic polynomial of the matrix $\tilde{\mathcal{M}}$ with all $\lambda_j = 0$ is given as

$$\left|\tilde{\mathcal{M}} - \lambda I\right| = \left|\tilde{\mathcal{M}}\right| = 0. \tag{C.4}$$

This implies that the determinant of all matrices $\tilde{\mathcal{M}}$, generated from points close to the true observables of the system, is zero. Therefore, the matrix $\tilde{\mathcal{M}}$ is non-invertible, such that $\nexists \tilde{\mathcal{M}}^{-1}$. The algorithm can be sped up by checking whether $\tilde{\mathcal{M}}$ has an inverse. If $\tilde{\mathcal{M}}$ is not invertible, we then check whether both $\mathcal{M}$ and $\tilde{\mathcal{M}}$ are positive semidefinite.

D Higher Order Moment Value Comparison

We seek to compare the values of $\langle \hat{x}^t \rangle$. However since $\langle \hat{x}^t \rangle = 0$ for odd values of t for even potentials, we make the comparison through the first two consecutive even powers of t as $\langle \hat{x}^t \rangle, \langle \hat{x}^{t+2} \rangle$. For this we compare $\langle \hat{x}^2 \rangle$ and $\langle \hat{x}^4 \rangle$ for any polynomial Hamiltonian $\hat{H}$.

Assume the creation and annihilation operators $\hat{a}_+$ and $\hat{a}_-$, where the action of the operators on any fock space element $|n\rangle$ where $n \in \mathbb{Z}_0$ is given by

$$\begin{aligned} \hat{a}_+|n\rangle &= \sqrt{n+1}|n+1\rangle, \\ \hat{a}_-|n\rangle &= \sqrt{n}|n-1\rangle. \end{aligned} \tag{D.1}$$

The energy eigenstate $|\psi\rangle$ is expressed as a linear combination of the Fock space elements $|n\rangle$

Any Hamiltonian $\hat{H}$ with a polynomial potential depending only on the operators of $\hat{x}^k$ and $\hat{p}^l$ where $k, l \geq 0$, can be written in terms of annihilation and creation operators $\hat{a}_-$ and $\hat{a}_+$ using the identities

$$\hat{x} = \sqrt{\frac{\hbar}{2m\omega}}(\hat{a}_+ + \hat{a}_-), \qquad \hat{p} = i\sqrt{\frac{\hbar}{2m\omega}}(\hat{a}_+ - \hat{a}_-). \tag{D.2}$$

We are only interested in the expectation values of $\langle \hat{x}^k \rangle$ so we focus on the $\hat{a}_+, \hat{a}_-$ representation of $\hat{x}$. In atomic units and our definitions $m = 1$, $\omega = 1$, $\hat{x}$ reduces to

$$\hat{x} = \sqrt{\frac{1}{2}}(\hat{a}_+ + \hat{a}_-). \tag{D.3}$$

We can express the energy eigenstates $|\psi\rangle$ of the Hamiltonian $\hat{H}$ as a linear combination of the Fock space elements $|n\rangle$ as

$$|\psi\rangle = \sum_n c_n |n\rangle, \tag{D.4}$$

where $c_n \in \mathbb{C}$. We seek to calculate $\langle \psi|\hat{x}^2|\psi\rangle$ and $\langle \psi|\hat{x}^4|\psi\rangle$ to compare the results.

The operator $\hat{x}^2$ is defined in terms of annihilation creation operators as

$$\hat{x}^2 = \frac{1}{2}(\hat{a}_+\hat{a}_+ + \hat{a}_-\hat{a}_- + \hat{a}_+\hat{a}_- + \hat{a}_-\hat{a}_+). \tag{D.5}$$

Then the expectation value of $\hat{x}^2$ in the energy eigenkets $|\psi\rangle$ is given by

$$\begin{aligned} \langle \psi|x^2|\psi\rangle = \frac{\hbar}{2m\omega} \Bigg(&\sum_{n,m} c_n^* c_m \langle n|\hat{a}_+\hat{a}_+|m\rangle + \sum_{n,m} c_n^* c_m \langle n|\hat{a}_-\hat{a}_-|m\rangle \\ &+ \sum_{n,m} c_n^* c_m \langle n|\hat{a}_+\hat{a}_-|m\rangle + \sum_{n,m} c_n^* c_m \langle n|\hat{a}_-\hat{a}_+|m\rangle \Bigg) \end{aligned} \tag{D.6}$$

We calculate each term one by one,

$$\begin{aligned}
\langle\psi|\hat{a}_+\hat{a}_+|\psi\rangle &= \sum_{n,m} c_n^* c_m \langle n|\hat{a}_+\hat{a}_+|m\rangle, \\
&= \sum_{n,m} c_n^* c_m \sqrt{(n+1)(n+2)}\delta_{n+2,m}, \\
&= \sum_{n} c_n^* c_{n+2} \sqrt{(n+1)(n+2)}, \qquad \text{(D.7)} \\
\langle\psi|\hat{a}_-\hat{a}_-|\psi\rangle &= \sum_{n,m} c_n^* c_m \langle n|\hat{a}_-\hat{a}_-|m\rangle, \\
&= \sum_{n,m} c_n^* c_m \sqrt{n(n-1)}\delta_{n-2,m}, \\
&= \sum_{n} c_{n+2}^* c_n \sqrt{(n+2)(n+1)}, \qquad \text{(D.8)} \\
\langle\psi|\hat{a}_+\hat{a}_-|\psi\rangle &= \sum_{n,m} c_n^* c_m \langle n|\hat{a}_+\hat{a}_-|m\rangle, \\
&= \sum_{n,m} c_n^* c_m n\delta_{n,m}, \\
&= \sum_{n} |c_n|^2 n, \qquad \text{(D.9)} \\
\langle\psi|\hat{a}_-\hat{a}_+|\psi\rangle &= \sum_{n,m} c_n^* c_m \langle n|\hat{a}_-\hat{a}_+|m\rangle, \\
&= \sum_{n,m} c_n^* c_m \sqrt{n+1}\sqrt{n+1}\delta_{n,m}, \\
&= \sum_{n} |c_n|^2 (n+1). \qquad \text{(D.10)}
\end{aligned}$$

Combining these results, we get

$$\langle\psi|\hat{x}^2|\psi\rangle = \frac{1}{2}\left(\sum_n \sqrt{(n+1)(n+2)}(c_n^* c_{n+2} + c_{n+2}^* c_n) + (2n+1)|c_n|^2\right) \qquad \text{(D.11)}$$

The operator $\hat{x}^4$ is defined in terms of annihilation creation operators as

$$\begin{aligned}
\hat{x}^4 = \frac{1}{4}\,(&\hat{a}_+\hat{a}_+\hat{a}_+\hat{a}_+ + \hat{a}_+\hat{a}_+\hat{a}_+\hat{a}_- + \hat{a}_+\hat{a}_+\hat{a}_-\hat{a}_+ + \hat{a}_+\hat{a}_+\hat{a}_-\hat{a}_- \\
&+\hat{a}_+\hat{a}_-\hat{a}_+\hat{a}_+ + \hat{a}_+\hat{a}_-\hat{a}_+\hat{a}_- + \hat{a}_+\hat{a}_-\hat{a}_-\hat{a}_+ + \hat{a}_+\hat{a}_-\hat{a}_-\hat{a}_- \\
&+\hat{a}_-\hat{a}_+\hat{a}_+\hat{a}_+ + \hat{a}_-\hat{a}_+\hat{a}_+\hat{a}_- + \hat{a}_-\hat{a}_+\hat{a}_-\hat{a}_+ + \hat{a}_-\hat{a}_+\hat{a}_-\hat{a}_- \\
&+\hat{a}_-\hat{a}_-\hat{a}_+\hat{a}_+ + \hat{a}_-\hat{a}_-\hat{a}_+\hat{a}_- + \hat{a}_-\hat{a}_-\hat{a}_-\hat{a}_+ + \hat{a}_-\hat{a}_-\hat{a}_-\hat{a}_-)\,.
\end{aligned} \qquad \text{(D.12)}$$

Then the expectation value of $\hat{x}^4$ in the energy eigenkets $|\psi\rangle$ is given by

$$\begin{aligned}
\langle\psi|\hat{a}_+\hat{a}_+\hat{a}_+\hat{a}_+|\psi\rangle &= \sum_{n,m} c_m^* c_n \langle m|\hat{a}_+\hat{a}_+\hat{a}_+\hat{a}_+|n\rangle, \\
&= \sum_{n,m} c_m^* c_n \sqrt{(n+1)(n+2)(n+3)(n+4)}\delta_{m,n+4}, \\
&= \sum_{n} c_{n+4}^* c_n \sqrt{(n+1)(n+2)(n+3)(n+4)}, \qquad \text{(D.13)} \\
\langle\psi|\hat{a}_+\hat{a}_+\hat{a}_+\hat{a}_-|\psi\rangle &= \sum_{n,m} c_m^* c_n \langle m|\hat{a}_+\hat{a}_+\hat{a}_+\hat{a}_-|n\rangle, \\
&= \sum_{n,m} c_m^* c_n n\sqrt{(n+1)(n+2)}\delta_{m,n+2}, \\
&= \sum_{n} c_{n+2}^* c_n n\sqrt{(n+1)(n+2)}, \qquad \text{(D.14)} \\
\langle\psi|\hat{a}_+\hat{a}_+\hat{a}_-\hat{a}_+|\psi\rangle &= \sum_{n,m} c_m^* c_n \langle m|\hat{a}_+\hat{a}_+\hat{a}_-\hat{a}_+|n\rangle, \\
&= \sum_{n,m} c_m^* c_n (n+1)\sqrt{(n+1)(n+2)}\delta_{m,n+2}, \\
&= \sum_{n} c_{n+2}^* c_n (n+1)\sqrt{(n+1)(n+2)}, \qquad \text{(D.15)} \\
\langle\psi|\hat{a}_+\hat{a}_+\hat{a}_-\hat{a}_-|\psi\rangle &= \sum_{n,m} c_m^* c_n \langle m|\hat{a}_+\hat{a}_+\hat{a}_-\hat{a}_-|n\rangle, \\
&= \sum_{n,m} c_m^* c_n n(n-1)\delta_{m,n}, \\
&= \sum_{n} |c_n|^2 n(n+1), \qquad \text{(D.16)} \\
\langle\psi|\hat{a}_+\hat{a}_-\hat{a}_+\hat{a}_+|\psi\rangle &= \sum_{n,m} c_m^* c_n \langle m|\hat{a}_+\hat{a}_-\hat{a}_+\hat{a}_+|n\rangle, \\
&= \sum_{n,m} c_m^* c_n (n+2)\sqrt{(n+1)(n+2)}\delta_{m,n+2}, \\
&= \sum_{n} c_{n+2}^* c_n (n+2)\sqrt{(n+1)(n+2)}, \qquad \text{(D.17)} \\
\langle\psi|\hat{a}_+\hat{a}_-\hat{a}_+\hat{a}_-|\psi\rangle &= \sum_{n,m} c_m^* c_n \langle m|\hat{a}_+\hat{a}_-\hat{a}_+\hat{a}_-|n\rangle, \\
&= \sum_{n,m} c_m^* c_n n^2\delta_{m,n}, \\
&= \sum_{n} |c_n|^2 n^2, \qquad \text{(D.18)}
\end{aligned}$$

$$\begin{aligned}
\langle\psi|\hat{a}_+\hat{a}_-\hat{a}_-\hat{a}_+|\psi\rangle &= \sum_{n,m} c_m^* c_n \langle m|\hat{a}_+\hat{a}_-\hat{a}_-\hat{a}_+|n\rangle, \\
&= \sum_{n,m} c_m^* c_n n(n+1)\delta_{m,n}, \\
&= \sum_{n} |c_n|^2 n(n+1), \qquad \text{(D.19)} \\
\langle\psi|\hat{a}_+\hat{a}_-\hat{a}_-\hat{a}_-|\psi\rangle &= \sum_{n,m} c_m^* c_n \langle m|\hat{a}_+\hat{a}_-\hat{a}_-\hat{a}_-|n\rangle, \\
&= \sum_{n,m} c_m^* c_n (n-2)\sqrt{n(n-1)}\delta_{m,n-2}, \\
&= \sum_{n} c_n^* c_{n+2} n\sqrt{(n+1)(n+2)}, \qquad \text{(D.20)} \\
\langle\psi|\hat{a}_-\hat{a}_+\hat{a}_+\hat{a}_+|\psi\rangle &= \sum_{n,m} c_m^* c_n \langle m|\hat{a}_-\hat{a}_+\hat{a}_+\hat{a}_+|n\rangle, \\
&= \sum_{n,m} c_m^* c_n (n+3)\sqrt{(n+1)(n+2)}\delta_{m,n+2}, \\
&= \sum_{n} c_{n+2}^* c_n (n+3)\sqrt{(n+1)(n+2)}, \qquad \text{(D.21)} \\
\langle\psi|\hat{a}_-\hat{a}_+\hat{a}_+\hat{a}_-|\psi\rangle &= \sum_{n,m} c_m^* c_n \langle m|\hat{a}_-\hat{a}_+\hat{a}_+\hat{a}_-|n\rangle, \\
&= \sum_{n,m} c_m^* c_n n(n+1)\delta_{m,n}, \\
&= \sum_{n} |c_n|^2 n(n+1), \qquad \text{(D.22)} \\
\langle\psi|\hat{a}_-\hat{a}_+\hat{a}_-\hat{a}_+|\psi\rangle &= \sum_{n,m} c_m^* c_n \langle m|\hat{a}_-\hat{a}_+\hat{a}_-\hat{a}_+|n\rangle, \\
&= \sum_{n,m} c_m^* c_n (n+1)^2\delta_{m,n}, \\
&= \sum_{n} |c_n|^2 (n+1)^2, \qquad \text{(D.23)} \\
\langle\psi|\hat{a}_-\hat{a}_+\hat{a}_-\hat{a}_-|\psi\rangle &= \sum_{n,m} c_m^* c_n \langle m|\hat{a}_-\hat{a}_+\hat{a}_-\hat{a}_-|n\rangle, \\
&= \sum_{n,m} c_m^* c_n (n-1)\sqrt{n(n-1)}\delta_{m,n-2}, \\
&= \sum_{n} c_n^* c_{n+2} (n+1)\sqrt{(n+2)(n+1)}, \qquad \text{(D.24)}
\end{aligned}$$

$$\begin{aligned}
\langle\psi|\hat{a}_-\hat{a}_-\hat{a}_+\hat{a}_+|\psi\rangle &= \sum_{n,m} c_m^* c_n \langle m|\hat{a}_-\hat{a}_-\hat{a}_+\hat{a}_+|n\rangle, \\
&= \sum_{n,m} c_m^* c_n (n+1)(n+2)\delta m, n, \\
&= \sum_{n} |c_n|^2 (n+1)(n+2), \qquad \text{(D.25)} \\
\langle\psi|\hat{a}_-\hat{a}_-\hat{a}_+\hat{a}_-|\psi\rangle &= \sum_{n,m} c_m^* c_n \langle m|\hat{a}_-\hat{a}_-\hat{a}_+\hat{a}_-|n\rangle, \\
&= \sum_{n,m} c_m^* c_n n\sqrt{n(n-1)}\delta_{m,n-2}, \\
&= \sum_{n} c_n^* c_{n+2}(n+2)\sqrt{(n+2)(n+1)}, \qquad \text{(D.26)} \\
\langle\psi|\hat{a}_-\hat{a}_-\hat{a}_-\hat{a}_+|\psi\rangle &= \sum_{n,m} c_m^* c_n \langle m|\hat{a}_-\hat{a}_-\hat{a}_-\hat{a}_+|n\rangle, \\
&= \sum_{n,m} c_m^* c_n (n+1)\sqrt{n(n-1)}\delta_{m,n-2}, \\
&= \sum_{n} c_n^* c_{n+2}(n+3)\sqrt{(n+2)(n+1)}, \qquad \text{(D.27)} \\
\langle\psi|\hat{a}_-\hat{a}_-\hat{a}_-\hat{a}_-|\psi\rangle &= \sum_{n,m} c_m^* c_n \langle m|\hat{a}_-\hat{a}_-\hat{a}_-\hat{a}_-|n\rangle, \\
&= \sum_{n,m} c_m^* c_n \sqrt{n(n-1)(n-2)(n-3)}\delta_{m,n-4}, \\
&= \sum_{n} c_n^* c_{n+4}\sqrt{(n+1)(n+2)(n+3)(n+4)}. \qquad \text{(D.28)}
\end{aligned}$$

Combining these results, we get

$$\begin{aligned}
\langle\psi|\hat{x}^4|\psi\rangle = \frac{1}{4}\Bigg(&\sum_n \sqrt{(n+1)(n+2)(n+3)(n+4)}(c_{n+4}^* c_n + c_n^* c_{n+4}) \\
&+ (4n+6)\sqrt{(n+2)(n+1)}(c_n^* c_{n+2} + c_{n+2}^* c_n) \qquad \text{(D.29)} \\
&+ (7n^2+9n+3)|c_n|^2\Bigg)
\end{aligned}$$

From equation (D.11) and (D.29) it is clear that, $\langle\hat{x}^4\rangle$ includes all the terms of $\langle\hat{x}^2\rangle$, but with coefficients involving higher orders of n, leading to larger values. Additionally, the remaining terms introduce positive contributions since $n \geq 0$. Therefore, we conclude that for any energy eigenket $|\psi\rangle$, we have

$$\langle\hat{x}^4\rangle > \langle\hat{x}^2\rangle. \qquad \text{(D.30)}$$